

# Pacific Northwest National Laboratory

Operated by Battelle for the  
U.S. Department of Energy

## Organic Tanks Safety Program Waste Aging Studies Final Report

D. M. Camaioni

W. D. Samuels

J. C. Linehan

A. K. Sharma

S. T. Autrey

M. A. Lilga

M. O. Hogan

S. A. Clauss

K. L. Wahl

J. A. Campbell

September 1998

RECEIVED  
SEP 28 1998  
OSTI

Prepared for the U.S. Department of Energy  
under Contract DE-AC06-76RLO 1830

PNNL-11909

MASTER *NOT*

DISTRIBUTION OF THIS DOCUMENT IS UNLIMITED

## DISCLAIMER

This report was prepared as an account of work sponsored by an agency of the United States Government. Neither the United States Government nor any agency thereof, nor Battelle Memorial Institute, nor any of their employees, makes any warranty, express or implied, or assumes any legal liability or responsibility for the accuracy, completeness, or usefulness of any information, apparatus, product, or process disclosed, or represents that its use would not infringe privately owned rights. Reference herein to any specific commercial product, process, or service by trade name, trademark, manufacturer, or otherwise does not necessarily constitute or imply its endorsement, recommendation, or favoring by the United States Government or any agency thereof, or Battelle Memorial Institute. The views and opinions of authors expressed herein do not necessarily state or reflect those of the United States Government or any agency thereof.

PACIFIC NORTHWEST NATIONAL LABORATORY

*operated by*

BATTELLE

*for the*

UNITED STATES DEPARTMENT OF ENERGY

*under Contract DE-AC06-76RLO 1830*

Printed in the United States of America

Available to DOE and DOE contractors from the  
Office of Scientific and Technical Information, P.O. Box 62, Oak Ridge, TN 37831;  
prices available from (615) 576-8401.

Available to the public from the National Technical Information Service,  
U.S. Department of Commerce, 5285 Port Royal Rd., Springfield, VA 22161



This document was printed on recycled paper.

## **DISCLAIMER**

**Portions of this document may be illegible in electronic image products. Images are produced from the best available original document.**

## **Organic Tanks Safety Program Waste Aging Studies Final Report**

D. M. Camaioni  
W. D. Samuels  
J. C. Linehan  
A. K. Sharma  
S. T. Autrey  
M. A. Lilga  
M. O. Hogan  
S. A. Clauss  
K. L. Wahl  
J. A. Campbell

September 1998

Prepared for  
the U. S. Department of Energy  
under Contract DE-AC06-76RLO 1830

Pacific Northwest National Laboratory  
Richland, Washington 99352

## Summary

Uranium and plutonium production at the Hanford Site produced large quantities of radioactive byproducts and contaminated process chemicals that are stored in underground tanks awaiting treatment and disposal. Aging of the organic compounds used in the extraction processes has a direct bearing on several safety issues, including gas generation and chemical behavior hazards associated with fuel-nitrate combustion accidents. The purpose of this project was to determine the fate of organic species added to the tank wastes. We were interested specifically in learning the extent to which waste aging changes the energy content of organic species. Our approach included subjecting nonradioactive waste simulants to a range of temperatures and doses of  $\gamma$ -radiation and then performing chemical analyses for inorganic and organic species. We correlated the results with literature insights, inferred mechanisms, and developed fundamental kinetic models for complex reaction sequences. We also transformed the species data to carbon and energy content to obtain a quantitative description of the effects of temperature, radiation dose, and radiation flux on the indexes that are key to assessing the safety of stored wastes.

The results show that radiation and heat promote redox reactions between organic compounds (reducing agents) and nitrates/nitrites (precursors to oxidizing agents) in the wastes. We find that production of  $H_2$ ,  $N_2$ , and  $N_2O$  by radiolysis is significant and that it occurs concurrently with the disappearance of organic species and appearance of oxidized fragments of the original species. The observations are consistent with progressive degradation to species with more C-O bonds and fewer C-H and C-C bonds, resulting in an overall lower energy content of the organic inventory. The results of studies using both simple and complex waste simulants show quantitatively that the energy content of the wastes should decrease due to aging. However, the lifetimes and aging rates of organic complexants are strongly dependent on radiolytic and thermal exposure, and therefore the degree of aging will vary from tank to tank.

The modeling effort provides the first measurements of rate constants for reactions of  $NO_2$  with carboxylate salts and complexants. The absolute rate constant for formate is  $\sim 10 M^{-1}s^{-1}$  and  $\sim 70 M^{-1}s^{-1}$  for glycine. The ratios of these rate constants agree well with reactivities measured by competition kinetic experiments. Reactivities of other complexants relative to formate were also measured. Thus, rate constants may be estimated.

The studies corroborate the hypothesis (Meisel et al. 1991, 1993, 1997) that  $NO_2$  is radical dominates the radiolytic oxidation of complexants. Under laboratory conditions of high concentrations of nitrite and hydroxide and high dose rates (to accelerate aging), kinetic models show that  $NO_2$  and  $O^-$  are the primary oxidizing species. However, under conditions likely to be encountered in actual wastes, e.g., low dose rates, the models predict that  $NO_2$  is dominantly responsible.

Generation of  $NO$  is also shown to be important. Modeling results suggest that  $NO$  mainly disproportionates with  $NO_2$ , making nitrite ions. However, other reactions leading to generation of  $N_2O$ ,  $N_2$ , and  $NH_3$  must also occur. But information reactions is not sufficient to support quantitative models.

The multiple roles that nitrite ion plays are noteworthy. First, it reduces radiolysis radicals,  $\text{OH}/\text{O}^-$  and forms  $\text{NO}_2$ . Second, it oxidizes  $\text{NO}_3^{2-}$  radicals that form by reaction of electrons with nitrate. To the extent that this reaction occurs, it reduces the efficiency of radiolytic aging by converting  $\text{NO}_2$  to  $\text{NO}$ , a much less powerful oxidizing radical. The reaction is relatively slow and requires high nitrite ion concentrations for it to scavenge a significant fraction of  $\text{NO}_3^{2-}$  radicals. Third, nitrite ion reacts with organic radicals generated from complexants, and thereby promotes organic reactions that yield simple innocuous products such as oxalate, formate, and carbonate. Without this step, the products from complexants would be complicated and perhaps more troublesome issues for storage, retrieval, and pretreatment activities. And finally, nitrite is required for thermal degradation of complexants.

Although the safety issue surrounding safe storage of organic wastes is nearing closure, we suggest directions that continued studies could follow. We note that the product identifications and subsequent modeling of the reactions of higher complexants are incomplete. We suggest that continued work to expand the model is worthwhile, especially if the effort also leads to the addition of thermal and thermal plus radiolytic reaction mechanisms so that the combined processes can be modeled and understood. Steps for reactions that lead to gaseous products may also be added so that the model yields information about generation rates and distributions of gaseous products. Developing such capabilities could facilitate resolution of flammable gas safety issues and answer questions about reactions that may be induced by retrieval and pretreatment activities.

## References

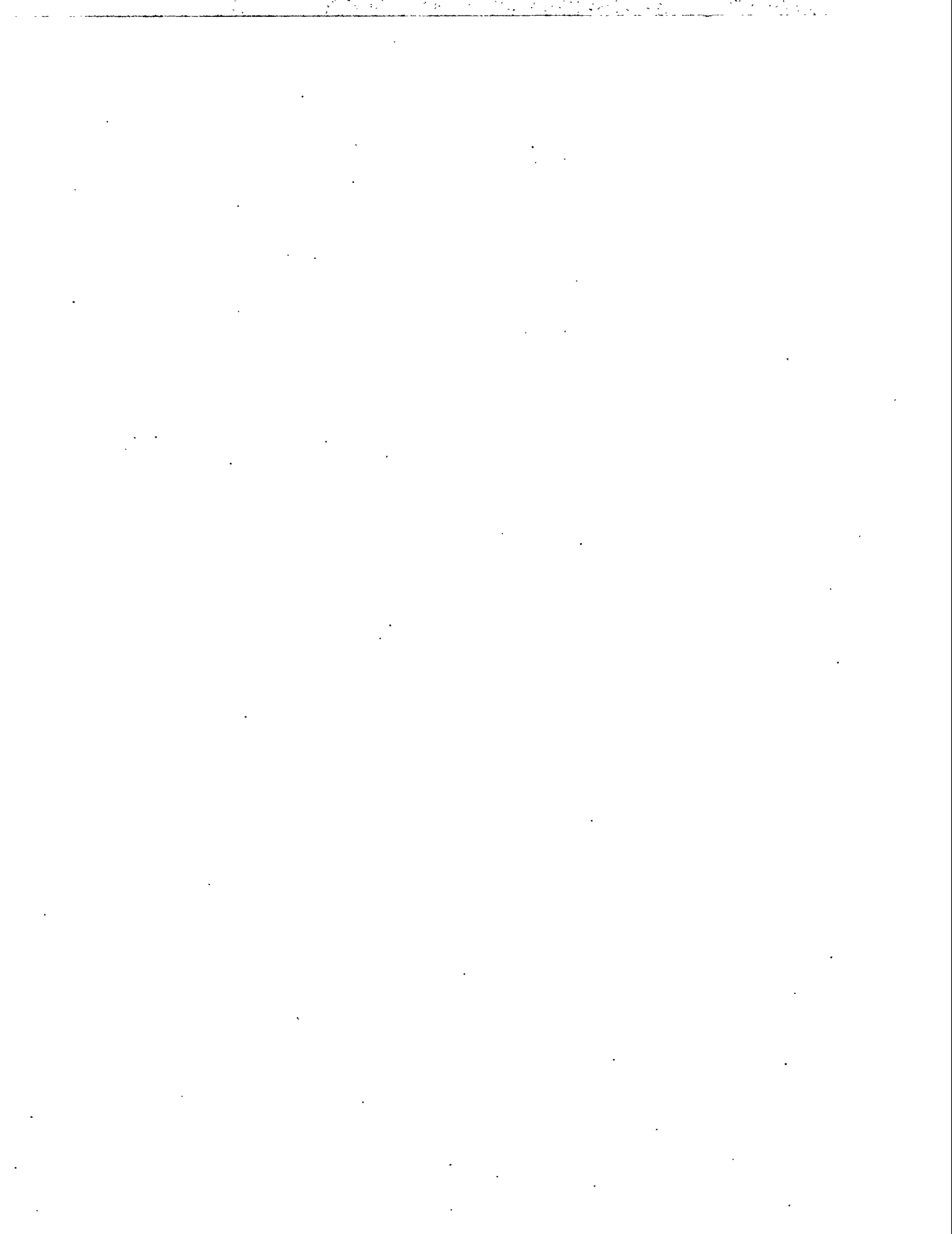
- Meisel D, H Diamond, EP Horwitz, MS Matheson, MC Sauer Jr, and JC Sulliyon. 1991. *Radiation Chemistry of Synthetic Waste*. ANL-91/40, Argonne National Laboratory, Argonne, Illinois.
- Meisel D, CD Jonah, S Kapoor, MS Matheson, and MC Sauer Jr. 1993. *Radiolytic and Radiolytically Induced Generation of Gases from Synthetic Wastes*. ANL-93/43, Argonne National Laboratory, Argonne, Illinois.
- Meisel D, A Cook, D Camaioni, and T Orlando. 1997. "Chemistry, Radiation, and Interfaces in Suspensions of Nuclear Waste Simulants." *Photoelectrochemistry*, K Rajeshwar, LM Peter, A Fujishima, D Meissner, M Tomkiewicz, eds. The Electrochemical Society, 97-20:350-7.

## Acknowledgments

This work progressed in collaboration with projects on “The NO<sub>x</sub> System in Nuclear Waste” at Argonne National Laboratory (ANL) and “Interfacial Radiolysis Effects in Tank Waste Speciation” at Pacific Northwest National Laboratory. These projects are funded by the DOE Environmental Management Science Program (EMSP).

We thank Phil Cappe, Associated Western Universities Summer Undergraduate Research Participant, and Dr. Sarah Burton (PNNL) for recording NMR spectra. We thank Dr. Leon Stock, consultant to Organic Tanks Safety Program, for helpful discussion and for contributing Appendix C. And we thank Dr. Harry Babad, formerly of Westinghouse Hanford Co., for guidance and unwavering enthusiasm for these studies.

Dr. William D. Samuels led the simulatant aging studies Task (Section 4). Amit Sharma, Scott Clauss, Dr. Karen Wahl, and Dr. James A. Campbell provided analytical support for this task. Dr. John Linehan led the task to measure relative reactivities of organic species (Section 3). He developed the NMR analytical methods and collected and reduced much of the data. Dr. Tom Autrey performed the mechanistic kinetic modeling of formate and glycine and extrapolated the results to low dose rates representative of actual tank wastes. Michael O. Hogan and Dr. Michael A. Lilga provided technical support for work in Section 3 by handling the preparation of samples and scheduling them in and out of the  $\gamma$  facilities. Dr. Donald M. Camaioni led the Waste Aging Studies project at PNNL. Inquiries about and comments on this report or the Waste Aging Studies Task should be directed to him at 509-375-2739 or e-mail: Donald.Camaioni@pnnl.gov.



## Abbreviations

DBP	dibutyl phosphate
EDMA	ethylenediaminemonoacetate
EDTA	ethylenediaminetetraacetate
EDDA	ethylenediaminediacetate
ED3A	ethylenediaminetriacetate
EMSP	Environmental Management Science Program
GC	gas chromatography
FAI	Fauske & Associates, Inc.
FY	fiscal year
HEDTA	hydroxyethylethylenediaminetriacetate
hexone	methyl isobutyl ketone
HPLC	high performance liquid chromatography
IDA	iminodiacetate
IC	ion chromatography
IPC	ion-pair chromatography
MS	mass spectrometry
NMR	nuclear magnetic resonance
NPH	normal paraffinic hydrocarbons
NTA	nitrilotriacetate
PUREX	Plutonium-Uranium Extraction (Plant)
REDOX	Reduction-Oxidation (Plant)
RSST	Reactive Systems Screening Tool
SST	single-shell storage tank
TBP	tributyl phosphate
TOC	total organic carbon



# Contents

Summary .....	iii
Acknowledgments .....	v
Abbreviations .....	vii
1.0 Introduction .....	1.1
1.1 Objective .....	1.1
1.2 Approach .....	1.1
1.3 Background .....	1.2
2.0 Mechanisms of Organic Aging .....	2.1
2.1 Mechanism and Kinetics of Radiolytically Induced Organic Aging .....	2.1
2.1.1 Oxidizing Radicals Generated by Radiolysis of Wastes .....	2.1
2.1.2 Reactions of O <sup>-</sup> Radicals with Organic Species .....	2.2
2.1.3 Reactions of NO <sub>x</sub> Radicals .....	2.3
2.2 Mechanisms and Kinetic Parameters for Thermal Aging .....	2.5
2.2.1 Mechanisms for Thermal Aging of Complexants .....	2.5
2.2.2 Activation Barriers for Thermal Aging of HEDTA and Glycolate .....	2.7
2.3 Synergistic Effects of Radiation on Thermal Reactions .....	2.8
3.0 Relative Rate Constants for Radiolytic Aging of Organic Species .....	3.1
3.1 Reactivities of Organic Complexants Relative to Formate .....	3.1
3.2 Kinetic Model for Radiolytic Oxidation .....	3.4
3.2.1 Oxidation of Formate .....	3.6
3.2.2 Oxidation of Glycine .....	3.10
3.3 Products of Degradation .....	3.16
3.4 Experimental Section .....	3.20
3.4.1 Sample Preparation .....	3.20
3.4.2 NMR Analysis .....	3.21
3.4.3 Fricke Dosimetry .....	3.21
3.4.4 Calculation of Radiolytic Yields .....	3.22
3.4.5 Mechanistic Kinetic Modeling .....	3.22
3.4.6 Calculation of Fractions of Formate and Glycine Oxidized by O <sup>-</sup> , OH, H, and NO <sub>2</sub> .....	3.23
4.0 Organic Aging Studies Using Waste Simulants .....	4.1
4.1 Results .....	4.2
4.1.1 Effect of Radiation Dose on Aging .....	4.2
4.1.2 Effect of Temperature on Radiolytic Aging .....	4.3
4.1.3 Results for Thermal Aging of the Simulant .....	4.5

4.1.4 Effects of O <sub>2</sub> and Fe on Aging .....	4.7
4.2 Radiolytic Effects on TOC and Nitrate Oxidation Enthalpies of Organic Species .....	4.9
4.3 Experimental Section .....	4.12
4.3.1 Simulant Preparation and Irradiation .....	4.12
4.3.2 Solution Phase Analyses .....	4.13
5.0 Organic Aging in Tank Wastes .....	5.1
5.1 Organic Species Found in Tank Wastes .....	5.1
5.2 Radiolytic Aging in Wastes .....	5.2
5.2.1 Effects of Dose Rate, Nitrite, and Hydroxide on Radiolytic Yields .....	5.2
5.2.2 Radiolytic Contribution to Organic Aging in Tank Wastes .....	5.5
5.3 Thermally Activated Organic Aging .....	5.8
5.4 Rates of Aging in High Heat-Load Waste Tanks .....	5.8
6.0 Conclusions .....	6.1
6.1 Effects of Aging on Organic Nitrate Reaction Enthalpies .....	6.1
6.2 Mechanistic Understanding of Organic Aging .....	6.2
6.3 Recommendations .....	6.2
7.0 References .....	7.1
Appendix A: Data for Relative Rate Determinations .....	A.1
Appendix B: Data for SIM-PAS-95-1 Aging Studies .....	B.1
Appendix C: Energy Content of Intermediate Organic Compounds .....	C.1

## Figures

2.1	Pathways for Oxidation of Aminocarboxylates .....	2.3
2.2	Electron Transfer and Combination Reactions of Organic Radicals with NO <sub>2</sub> and NO <sub>2</sub> <sup>-</sup> .....	2.5
2.3	Mechanism for Base-Catalyzed Decomposition of Citrate Ion .....	2.5
2.4	Potential Energy Surface for Nitrosation of Primary Alcohols by Nitrite Ion .....	2.7
3.1	<sup>13</sup> C NMR Spectra of 0.024 M Sodium Formate in a 3.75 M NaNO <sub>3</sub> , 1.25 M NaNO <sub>2</sub> , and 2 M NaOH Solution before and after γ Radiolysis .....	3.2
3.2	<sup>1</sup> H NMR Spectra of Unirradiated and Irradiated EDTA/Formate- <sup>13</sup> C Solutions ....	3.2
3.3	Dependence of Radiolytic Yield of Carbonate from Formate versus Initial EDTA Concentration in a 3.75 M NaNO <sub>3</sub> , 1.25 M NaNO <sub>2</sub> , and 2 M NaOH Solution .....	3.3
3.4	Reactivity of EDTA Relative to Formate Correlates with Average EDTA and Conversion of EDTA .....	3.4
3.5	Measured and Modeled Radiolytic Yield of Carbonate Versus Formate Concentration .....	3.6
3.6	Time Dependence of NO and NO <sub>2</sub> Radicals Predicted by Kinetic Model for Radiolytic Oxidation of Formate in NaNO <sub>2</sub> , NaNO <sub>3</sub> , 2 M NaOH Solutions .....	3.8
3.7	<sup>13</sup> C NMR Spectrum of Equal Parts 1- <sup>13</sup> C-Glycine and 2- <sup>13</sup> C-Glycine in 2 M NaNO <sub>3</sub> , 2 M NaNO <sub>2</sub> , 2 M NaOH Solutions After γ Radiolysis at 22°C .....	3.11
3.8	<sup>13</sup> C-NMR Spectrum of a 2- <sup>13</sup> C-Glycine in a 2 M NaNO <sub>3</sub> , 2 M NaOH Solution after a 29 Mrad Dose at 25°C .....	3.12
3.9	Results of Kinetic Model and Experiments for Radiolytic Degradation of Glycine .....	3.14
3.10	<sup>1</sup> H NMR Spectra Showing that NTA Degrades to IDA and Glycine During γ Radiolysis in Nitrate/Nitrite/Hydroxide Solution .....	3.18

3.11	<sup>1</sup> H NMR Spectra of EDTA before and after $\gamma$ Radiolysis in 2 M NaNO <sub>2</sub> , 2 M NaNO <sub>3</sub> , 2 M NaOH Solution .....	3.18
3.12	<sup>1</sup> H NMR Spectra of HEDTA before and after $\gamma$ Radiolysis in Nitrate/Nitrite/Hydroxide Solution .....	3.19
3.13	Structures Consistent with Hydroxyethylene Resonances in <sup>1</sup> H NMR Spectra of $\gamma$ Irradiated HEDTA Solutions .....	3.19
4.1	Disappearance of Complexants and Appearance of Products in a Radiation Field of $\sim 3 \times 10^5$ rad hr <sup>-1</sup> at 70°C .....	4.3
4.2	Plots of Carbon Content Versus Dose for 70 and 90°C Irradiations .....	4.4
4.3	Effects of Temperature and Initial O <sub>2</sub> Concentration in Headspace Gas on Radiolytic Yields of Gases .....	4.5
4.4	Disappearance of Starting Organic Compounds and Appearance of Products Versus Time at 90°C in the Absence of $\gamma$ Radiation .....	4.6
4.5	Effects of Initial Concentration of O <sub>2</sub> in Headspace Gas on Distribution of Gases Produced at 90°C .....	4.9
4.6	Nitrate Reaction Enthalpy and TOC of Simulants Versus Dose at 40, 70, and 90°C .....	4.11
5.1	Effects of Dose Rate, Nitrite, and Hydroxide on the Radiolytic Yield of CO <sub>3</sub> <sup>2-</sup> from Formate .....	5.4

## Tables

3.1	Relative Rate Constants for Disappearance of Organic Species in Nitrate/Nitrite/Hydroxide Solutions during $\gamma$ Radiolysis .....	3.5
3.2	Kinetic Model for Radiolytic Aging of Formate in Solutions Containing Nitrite, Nitrate and Hydroxide .....	3.7
3.3	Total Yield and Fractions of Carbonate Produced from Radiolytically Generated Species .....	3.10
3.4	Kinetic Reaction Steps Added to Formate Kinetic Model to Model Glycine Oxidation in Solutions of Nitrate, Nitrite, and Hydroxide .....	3.13
3.5	Radiolytic Yields of Glycine in Solutions Containing Nitrite, Nitrate, and Hydroxide .....	3.15
3.6	Products Identified by NMR from Radiolytic Oxidation of Complexants in Nitrate/Nitrite/Hydroxide Solutions .....	3.17
4.1	Target Composition of SIM-PAS-95-1c and -1d Simulants .....	4.1
4.2	Effects of Temperature on Radiolytic Aging of SIM-PAS-95-1d .....	4.4
4.3	Effects of O <sub>2</sub> on Radiolytic Aging of SIM-PAS-95-1d at 70°C .....	4.7
4.4	Nitrate Reaction Enthalpies ( $\Delta H_r$ ) for Organic Species .....	4.10
4.5	Effect of Dose on Organic Carbon Content and Average $-\Delta H_r$ of SIM-PAS-95-1 Simulants .....	4.11
5.1	Fractions of TOC that are Oxalate in Tank Wastes .....	5.2
5.2	Analyses of Organic Species in Tank Waste Samples .....	5.3
5.3	Summary of Radiolytic Aging Model Showing Effects of Dose Rate, Nitrite, and Hydroxide on Radiolytic Yield and Distribution of Oxidizing Species .....	5.4
5.4	Changes in Nitrate Reaction Enthalpies Due to Aging Reactions .....	5.7
5.5	Radiolytic Yield and Thermal Rates of Formation of Aging Products from PAS-95 Simulants at 90°C .....	5.9

5.6 AZ-101 and AZ-102 Characterization Data ..... 5.10

5.7 Estimated Rates of Organic Aging to Carbonate, Formate, and Oxalate Ions  
at 120°C in AZ Tank Wastes ..... 5.10

## 1.0 Introduction

Uranium and plutonium production at the Hanford Site produced large quantities of radioactive byproducts and contaminated process chemicals that are stored in underground tanks awaiting treatment and disposal. Having been made strongly alkaline and then subjected to successive water evaporation campaigns to increase storage capacity, the wastes now exist in the physical forms of saltcakes, metal oxide sludges, and aqueous brine solutions. Tanks that contain organic process chemicals mixed with nitrate/nitrite salt wastes might be at risk for fuel-nitrate combustion accidents. This project started in fiscal year (FY) 1993 to provide information on the chemical fate of stored organic wastes. While historical records (Klem 1990; Sederburg and Reddick 1994) had identified the organic compounds originally purchased and potentially present in wastes, aging experiments were needed to identify the probable degradation products and evaluate the current hazard. The determination of the rates and pathways of degradation have facilitated prediction of how the hazard changes with time and altered storage conditions. Also, the work with aged simulated waste contributed to the development of analytical methods for characterizing actual wastes. Finally, the results for simulants provide a baseline for comparing and interpreting tank characterization data.

### 1.1 Objective

The purpose of the Waste Aging Studies project is to elucidate how chemical and radiological processes have transformed the organic compounds stored in the tanks. Ultimately, the project has developed quantitative measures of how aging changes the energetic properties of the wastes. This information directly supports efforts to evaluate the hazard as well as to develop potential control and mitigation strategies.

### 1.2 Approach

Hazards posed by uncontrolled exothermic oxidation of organic compounds by nitrate and nitrite relate directly to the energy content and oxidation kinetics of the various organic compounds in the waste. Because sampling and analysis of the tank wastes for aging characteristics were not routine procedures, our approach to assessing the probable current organic content of the tanks was to simulate the chemical conditions of the tanks and elucidate mechanistic pathways that would reveal whether the hazards have increased, decreased, or remained constant. Accordingly, this project has used simulants in its studies of chemical aging. The effects of radiation were simulated by irradiating simulants with an external  $^{60}\text{Co}$   $\gamma$  source rather than including radioactive isotopes in the simulant. The major radiation sources in tank wastes are  $^{137}\text{Cs}$  and  $^{90}\text{Sr}$ , which emit  $\gamma$  and  $\beta$  radiation. Because "there are no significant differences in the chemical effects of  $\gamma$  and  $\beta$  irradiation" (Meisel et al. 1991a), using an external  $\gamma$  source is a reasonable, cost-efficient, and safe alternative to using radioactive simulants. The dose rates used were 100 to 1000 times greater than tank waste dose rates so that tests could be performed over periods of days or weeks rather than years. After irradiation, the disappearance and appearance of detectable organic species in the simulant and evolved gases were determined.

### 1.3 Background

Waste aging is an integral part of the effort to understand and assess the organic-nitrate hazard. Each of the 177 waste tanks on the Hanford Site has a unique and uncertain composition of organic, inorganic, and radioactive elements (Agnew 1996a,b,c). Organic-containing wastes have been stored in underground storage tanks at Hanford for nearly half a century, during which time they have been constantly exposed to radiation and heated to temperatures of up to 140°C (284°F). The wastes contain hydroxide, nitrate, nitrite, aluminate, oxides of transition metals including noble metals, radioactive elements (e.g., uranium, plutonium, cesium, strontium), and many other substances that may catalyze or promote degradation of the original compounds. Many of the single-shell tanks have been sampled and total organic carbon (TOC) contents measured. However, knowledge of the TOC in a particular storage tank is insufficient to bound the safety risk because the organic species in the wastes have different energy content and the heats of oxidation vary widely.

The organic compounds that were added to the tanks are divided into two main classes: complexants and solvents. The major organic complexants believed to have been added to the tanks are glycolate, citrate, hydroxyethylethylenediaminetriacetate (HEDTA), and ethylenediaminetetraacetate (EDTA). Allen (1976) estimated the approximate quantities that were used at Hanford

- glycolic acid,  $8.8 \times 10^5$  kg
- citric acid,  $8.5 \times 10^5$  kg
- hydroxyethylethylenediaminetriacetic acid,  $8.3 \times 10^5$  kg
- ethylenediaminetetraacetic acid,  $2.2 \times 10^5$  kg.

Lesser amounts of other complexants such as nitrilotriacetate and oxalate were used, but amounts that actually were discharged to the tanks are not known.

Process solvents of concern that were used in chemical processes and stored in the tanks are tributyl phosphate (TBP), normal paraffin hydrocarbons (NPHs), and methyl isobutyl ketone (hexone). Sederburg and Reddick (1994) examined material balances at the Plutonium-Uranium Extraction (PUREX) Plant from 1955 to 1991;<sup>(a)</sup> their findings indicate that  $7.22 \times 10^5$  and  $1.31 \times 10^6$  kg of TBP and NPH, respectively, went to the storage tanks. Other processes also used organic solvents and organic phosphate extractants, but less is known about the quantities that were added to the tanks. Di(2-ethylhexyl)phosphoric acid diluted with hydrocarbon solvent was used in the waste fractionation and encapsulation process. The reflux solvent extraction process used TBP/carbon tetrachloride (Cleveland 1967) and dibutyl butyl phosphonate/carbon tetrachloride for extraction solvents (Kingsley 1965). Considerable quantities of hexone were

---

(a) The amount of organic entrained in PUREX wash waste discharged to the tanks was estimated to be 2,479 m<sup>3</sup> (655,000 gal). Assuming the composition of this waste was similar to the PUREX solvent (nominally 30 vol% TBP and 70 vol% NPH), then approximately  $7.22 \times 10^5$  and  $1.31 \times 10^6$  kg of the respective solvents would have been discharged to the waste tanks.

used in the Reduction-Oxidation (REDOX) Plant as both extractant and solvent. For example, 65,000 kg (65 metric tons) of hexone were retrieved from one storage tank, treated, and sent offsite (Gerber et al. 1992).

The evidence suggests that the quantities of organic solvents added to the tanks rival the quantities of complexants. However, the volatile organic solvents have escaped the wastes through evaporation, and the phosphate esters have saponified in the alkaline wastes. Although the amounts remaining are not known precisely, a recent topical report by Meacham et al. (1998) points out that during early PUREX operations, the organic wash waste was combined with high-level wastes that generated enough thermal heat to boil the tank wastes.

At the start of this project in FY 1994, little work had been performed on aging of organic solvent components. Therefore, an extensive series of aging experiments was begun on simulants that contained organic solvent compounds and complexants. One simulant, designated SY1-SIM-94C (Camaioni et al. 1995, 1996), contained equimolar amounts of dodecane, EDTA, TBP, dibutyl phosphate (DBP), methyl isobutyl ketone (hexone), stearate, and citrate in an inorganic matrix containing hydroxide, nitrate, nitrite, aluminum hydroxide, and a variety of alkali, alkaline earth, and transition metal cations. Radiolytic yields (G, molecules/100 eV) of gases at 70°C were measured for hydrogen (0.11), nitrous oxide (0.17), and nitrogen (0.08). Ammonia was also produced, but its yield was not measured. Concurrent with gas generation, the organic compounds disappeared. Identified products included dodecanones, heptadecane, isobutyrate, succinate, oxalate, formate, and glycolate. The TBP was totally consumed in almost every run; its rapid consumption was attributed to alkaline hydrolysis to DBP and butanol. Disappearances of EDTA and citrate were fit to a first-order kinetic rate law,  $A=A_0e^{-kD}$ , where D is the radiolytic dose. The radiation doses necessary to reduce the concentration of EDTA in the simulant by half were 63 Mrad at 50°C, 51 Mrad at 70°C, and 41 Mrad at 90°C. Citrate was less reactive, requiring about five times more radiation to reduce its concentration by half. Analyses for hexone, stearate, and dodecane showed significant scatter due to sample variability caused by their low solubility in the inorganic matrix of the simulant.

Studies were also performed to learn the possible fates of TBP hydrolysis products: sodium dibutyl phosphate (DBP) and butanol (Camaioni et al. 1996). Aging of sodium butyrate was also examined because butanol may oxidize to butyrate in the PUREX process. The disappearance of the subject compounds and appearance of products during radiolysis were consistent with radiolytically induced oxidation reactions. Radiolytic doses in excess of 60 Mrad completely consumed butanol and sodium butyrate, producing formate, oxalate, acetate, glycolate, malonate (propan-1,3-dioate), malate (2-hydroxysuccinate), and possibly fumarate ions. These products accounted for about 25 and 40%, respectively, of the initial carbon in butyrate and butanol simulants that had received 100 Mrad doses. A review of the literature found that alkaline hydrolysis of DBP and MBP is probably only a minor pathway for aging of DBP in tank wastes. Radiolysis experiments showed that DBP and MBP degrade by oxidation of the butyl groups.

While the above studies were in progress, energetics and reactivity tests performed by Fauske & Associates, Inc. (Fauske 1995, 1996; Webb et al. 1995; Fauske and Epstein 1995) showed that

complexants and organic salts pose the greatest risk of propagating reactions. Attempts to ignite sodium nitrate-organic solvent mixtures (Fauske 1995, Webb et al. 1995) in either a Reactive Systems Screening Tool (RSST) (Creed and Fauske 1990) or in a tube propagation device (Webb et al. 1995) did not lead to propagating reactions, despite the high potential energy content of test compounds such as dodecane, mineral oil, tributyl phosphate and sodium di-2-ethylhexyl phosphate, calcium dibutyl phosphate and sodium stearate. Instead, the solvent components vaporized away from the ignition source. Although tributyl phosphate and dibutyl phosphate ion have low or negligible vapor pressures, they tend to decompose, liberating hydrocarbon gases, before ignition temperatures are attained. Presumably, the amounts of the complexants and low molecular weight carboxylic acid salts (e.g., acetate, butyrate, and succinate) have sufficiently high thermal stability to keep them in contact with an ignition source until melt temperatures (~200 to 250°C) are attained and propagating reactions ensue. Accordingly, these findings focused our concern on how aging affects the organic complexants that can sustain propagating reactions.

In FY 1996, we initiated a study of a neutralized PUREX Acid Sludge (PAS) simulant that contained HEDTA, EDTA, glycolate and citrate. Radiolytic aging was studied at 70°C. The change in distribution of organic carbon and average energy content was determined as a function of radiolytic dose. In FY 1997, we did similar experiments at 90°C in the absence of radiation to assess susceptibilities of organic species to thermal degradation, and we extended radiolytic aging studies to 40 and 90°C with and without O<sub>2</sub> gas in contact with the simulant. Section 3 of this report describes these results.

In FY 1997, aging studies of the PAS simulant were completed, and new work was started measuring relative reactivities of organic species and their reaction paths as a first step toward developing chemical kinetic models of organic aging. Although an aggressive campaign to speciate a large number of representative tank wastes is underway to better determine the organic species that are now present, many tanks remain unsampled, and few tanks will be extensively sampled. Consequently, this targeted investigation was designed to elaborate on the behavior of the many different chemical complexants under the diverse storage conditions (temperature and dose rate) to provide the information necessary for the establishment of models enabling quantitative predictions of future aging and to assess the safety of long-term storage. For example, although much of the current waste inventory is too wet to sustain propagating reactions regardless of its energy content, unsafe conditions could develop as the wastes dry out. Thermally activated aging reactions have significant activation barriers and much of the waste is at relatively low temperatures (~25-60°C). Therefore, this investigation focused on the evaluation of the rate of the ongoing, temperature independent, radiolytic process.

## 2.0 Mechanisms of Organic Aging

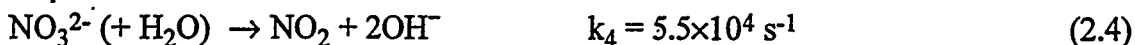
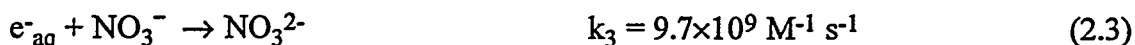
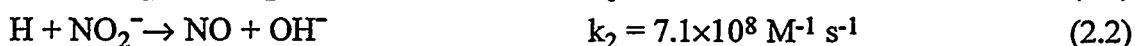
Complex mechanisms are involved in the degradation of organic chemicals in tank wastes. This section summarizes some pertinent literature on radiolytically and thermally induced reactions. For a primer on the wide range of chemistry organic reactions that may occur, the report by Stock and Pederson (1997) is recommended.

### 2.1 Mechanism and Kinetics of Radiolytically Induced Organic Aging

Passage of ionizing radiation through the wastes generates highly reactive radicals that either oxidize the organic species directly or induce production of other radicals that subsequently oxidize the organic species. Little temperature dependence is observed because the oxidizing radicals react with relatively low energies of activation. Reaction rates are controlled by the rate of generation of radicals, which is controlled by the radiation dose rate, and the selectivity of the radicals for various organic functionalities. Products depend on how the radicals attack the organic species and on how the resulting organic radicals convert to products, e.g., combination with NO, NO<sub>2</sub>, O<sub>2</sub>, or oxidation by NO<sub>2</sub><sup>-</sup>.

#### 2.1.1 Oxidizing Radicals Generated by Radiolysis of Wastes

Pathways for radiolytic aging are expected to involve generation of O<sup>-</sup>, and NO<sub>x</sub> radicals that, in turn, attack and oxidize the organic complexants (Meisel et al. 1991a, 1991b, 1993, 1997). Although primary intermediates of water radiolysis are e<sup>-</sup>, H, and OH, Equations 2.1–2.4 show that these species will convert to NO<sub>x</sub> radicals in wastes that are high in nitrate and nitrite ions.<sup>(a)</sup>



Essentially all of the electrons are scavenged by nitrate to make the reducing radical, NO<sub>3</sub><sup>2-</sup>. It is short-lived, dissociating to NO<sub>2</sub> in less than 15 μsec (Meisel et al. 1997). The pK<sub>a</sub> for HO is 11.8. In highly alkaline solutions, HO may convert to O<sup>-</sup>, which also reacts with nitrite to produce NO<sub>2</sub> but at a rate that is significantly below the diffusion limit.



The tank wastes are heterogeneous mixtures consisting of considerable solids and colloidal particles in contact with solution phases. The possible role that interfacial radiolysis may play is just starting to be explored (Orlando et al. 1998; Meisel et al. 1998). Fundamental studies of electron beams interacting with NaNO<sub>3</sub> crystal surfaces in vacuum show that species that desorb

---

(a) All rate constants from Buxton et al. (1988).

from the surface are NO, O, O<sub>2</sub>, and NO<sub>2</sub> (Knutsen and Orlando 1997). The dominant species are NO and O. The O atoms react in part with NO<sub>3</sub><sup>-</sup> to form O<sub>2</sub> and NO<sub>2</sub>. Extrapolating to NaNO<sub>3</sub> interfaces with tank waste aqueous supernatants, we expect that O atom would be scavenged by NO<sub>2</sub><sup>-</sup> and NO<sub>3</sub><sup>-</sup> (Warneck and Worzinger 1988). Therefore, radiolysis of wastes containing solid NaNO<sub>3</sub> is expected to generate the same oxidants as solution phase radiolysis, with perhaps greater yields of NO. NO is not a good oxidant of organic species; however, it is a ready scavenger of organic radicals, the products of which subsequently react to produce organic carbonyl compounds and hydroxylamine. Hydroxylamine decomposes rather rapidly in alkaline solutions to form NH<sub>3</sub>, N<sub>2</sub> and N<sub>2</sub>O in varying ratios depending on temperature and presence of other reactive species, e.g., nitrite ion (Meisel et al 1993; Ashby et al. 1994). To understand radiation chemical effects in solutions containing colloidal oxide particles, Meisel and coworkers (Schatz et al. 1998; Orlando et al. 1998a, 1998b) have studied the radiolysis of silica-loaded aqueous solutions. These studies indicate that small solid particles may absorb ionizing radiation and transfer charge across the particle-liquid interface, initiating chemistry at the interface and in the surrounding solution. For SiO<sub>2</sub> particles, the fraction of energy (ionizing radiation) absorbed by the particles increases with loading. Meisel (see Schatz et al. 1998; Meisel and Camaioni 1998; Orlando et al. 1998a, 1998b) suggests that the absorption of radiation by the solid particles causes electrons to be ejected into the surrounding solution. If the radiation effects were localized within silica particles, the yield of solvated electrons should decrease. Instead, the yields follow the average sample densities that are calculated from particle concentrations and the density of silica. The results have many practical implications. For high-level wastes, they suggest that heterogeneous systems will generate the same radicals that are observed in homogeneous solution.

Relatively little information exists on the reaction mechanisms and kinetics of NO<sub>x</sub> radicals reacting with organic species such as those in tank wastes. While some rate data are available for O<sup>-</sup> reactions, information on reaction mechanisms and ultimate products is still limited.

### 2.1.2 Reactions of O<sup>-</sup> Radicals with Organic Species

Reactions of O<sup>-</sup> with many organic species have rate constants that are equal to or greater than the rate constant for reaction with nitrite ion. For example, formate, aminoacetate, and imino-diacetate have rate constants of 1.4×10<sup>9</sup> (Buxton 1969), 5.6×10<sup>8</sup> (Lati and Meyerstein 1972), and 9.1×10<sup>8</sup> M<sup>-1</sup> s<sup>-1</sup> (Bhattacharyya and Saha 1976). Thus, contributions to the degradation of organic complexants by O<sup>-</sup> depend on the concentrations of organic species, hydroxide, and nitrite in a given waste solution.

Mönig et al. (1985) studied the oxidation of amino acids by OH. Decarboxylation was a dominant reaction path in alkaline solutions with a pH above the pK<sub>a</sub> of an amino acid zwitterion (e.g., H<sub>3</sub><sup>+</sup>NCH<sub>2</sub>CO<sub>2</sub><sup>-</sup>). Radiolytic yields of CO<sub>2</sub> from glycine were high (G=4.6 molecules/100 eV), and from N,N-dimethylglycine, a tertiary amine, yields were nearly quantitative: G=5.4 molecules/100 eV. The mechanism of this reaction is uncertain. One possibility is that reactions with aminocarboxylates occur by electron transfer from N followed by decarboxylation of the radical zwitterion, R<sub>3</sub>N<sup>+</sup>CH<sub>2</sub>CO<sub>2</sub><sup>-</sup>. Precedent for such a path is found in the autoxidation of trialkylamines in alkaline aqueous solutions (Chen et al. 1990) and recently observed

decarboxylations of anilinoacetate radical cations (Su et al. 1997). It is unknown whether reactions at pH 13 or 14, where  $O^-$  becomes dominant, will be as efficient at producing  $CO_2$ . It may be that  $O^-$  reacts by H-abstraction such that oxalate production will increase. Alternatively, the same result may be obtained from the electron transfer intermediate since it might deprotonate when formed in solutions that are high in hydroxide (see Figure 2.1)

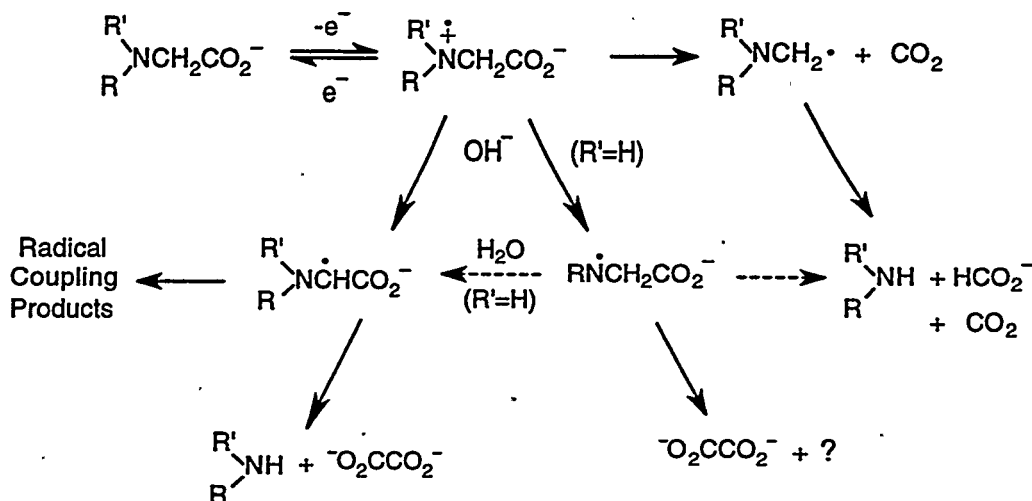
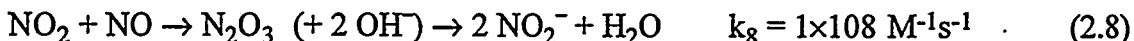
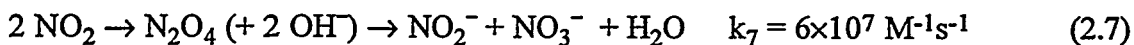


Figure 2.1. Pathways for Oxidation of Aminocarboxylates

### 2.1.3 Reactions of $NO_x$ Radicals

Quenching reactions exist for  $NO_2$  and  $NO$ , namely recombination and hydrolysis to nitrate and nitrite ion, as shown in Equations 2.7 and 2.8. Overall rate constants for Equations 2.7 and 2.8 are about  $10^8 \text{ mol}^{-1}\text{s}^{-1}$  (Lee and Schwartz 1981; Park and Lee 1988).



The oxidation potential of  $NO$  ( $E^\circ \sim 0.35 \text{ v}$ ) (Stanbury 1989) is not great enough for it to oxidize organic species.  $NO_2$  is a much better oxidizing agent ( $E=1.0 \text{ v}$ ) (Stanbury 1989). However, to be an effective oxidant of organic complexants, its reactions must be competitive with the hydrolysis reactions. For example, a radiation field of  $\sim 10^5 \text{ rad/h}$  generates  $\sim 10^{-7} \text{ M/s}$  of  $NO_2$ . In the absence of reducing agents, the steady-state concentration of  $NO_2$  will be  $\sim 10^{-8} \text{ M}$  such that the lifetime of  $NO_2$  defined by Equation 2.7 is  $\sim 0.1 \text{ s}$ .<sup>(a)</sup> From this, we conclude that rate constants for attack on organic species need only be on the order of 1 to  $10 \text{ M}^{-1}\text{s}^{-1}$  for 1% of

(a) Assume rate of generation equals rate of disappearance:

$$\text{rate} = 2k_7[\text{NO}_2]^2$$

$$\text{steady-state } [\text{NO}_2] = \sqrt{\frac{10^{-7}}{2k_7}}$$

NO<sub>2</sub> to oxidize organic species.<sup>(a)</sup> Furthermore, the fraction of attack is inversely dependent on the steady-state concentration of NO<sub>2</sub>, which has a square-root dependence on dose rate. With dose rates common to single-shell tank wastes (Parra 1994; Stauffer 1997), steady-state concentrations of NO<sub>2</sub> are much lower, so oxidation of organic species should be more efficient.

Work by Challis and Kyrtopoulos (1979) suggests that NO<sub>x</sub> dimers may nitrosate amines even under alkaline conditions, but these reactions generally require relatively high concentrations of NO<sub>x</sub> species to favor formation of nitrosating agents, N<sub>2</sub>O<sub>4</sub> and N<sub>2</sub>O<sub>3</sub>. With the low dose rates common to most tank wastes (Parra 1994; Stauffer 1997), steady-state concentrations of NO<sub>2</sub> should disfavor formation of N<sub>2</sub>O<sub>4</sub> and N<sub>2</sub>O<sub>3</sub>.

The reaction kinetics and products of NO<sub>2</sub> oxidations of organic complexants are being investigated by Environmental Management Science Program (EMSP) projects (Meisel and Camaioni 1998; Orlando et al. 1998a, 1998b). The experiments contact aqueous alkaline solutions of organic species with <100 ppm NO<sub>2</sub> in N<sub>2</sub> gas. Preliminary experiments have surveyed the reactions of nitrilotriacetate (NTA), iminodiacetate (IDA), glycine, and formate. Products were analyzed using <sup>1</sup>H and <sup>13</sup>C nuclear magnetic resonance spectroscopy and ion chromatography. The results show that NTA degrades via stepwise dealkylation giving mainly IDA, formate, carbonate, and oxalate. Formate degrades to carbonate when reacted with NO<sub>2</sub> but at a slower rate. Competition experiments that measured the initial rates of formate production from complexants and compared them with production of <sup>13</sup>CO<sub>3</sub><sup>2-</sup> from formate-<sup>13</sup>C gave relative reactivities of 19:11:5:1 for NTA:IDA:glycine:formate. The results suggest that the selectivity of NO<sub>2</sub> radical is significantly different from O<sup>-</sup>/OH. For example, formate is ~3 times more reactive than glycine towards O<sup>-</sup> and similar to glycine in its reactivity toward OH. Therefore, relative reactivity measurements are one way to show that NO<sub>2</sub> plays a role in the radiolytic degradation of complexants in wastes and waste simulants.

Meisel and coworkers have recently measured rate constants of reactions of NO<sub>2</sub> and NO<sub>2</sub><sup>-</sup> with organic radicals derived from formate and simple alcohols (methanol, ethanol, *i*-propanol, and *t*-butanol). For NO<sub>2</sub> radicals, two possible pathways were identified: 1) electron transfer to form nitrite, and 2) radical combination to form nitro compounds (see Figure 2.2). The latter pathway (2) occurs either at the O or the N atoms of NO<sub>2</sub> with near equal probabilities. The nitrite esters hydrolyze to produce NO<sub>2</sub><sup>-</sup>. For reactions of the same organic radicals with NO<sub>2</sub><sup>-</sup>, electron transfer is a leading pathway and becomes faster as the pH decreases. This reaction is important in tank chemistry because it generates a carbonyl compound (e.g., an aldehyde that may proceed to generate H<sub>2</sub> thermally) and NO from nitrite. As discussed above, the latter provides another route for production of N<sub>2</sub>O.

---

(a) Assume pseudo-first-order lifetime for attack on organic species is 10 s, i.e., 100 times slower than self-reaction lifetime. If concentration of species is 0.01 M, then  $1/10 = 2k[0.01]$  and  $k = 5$ .

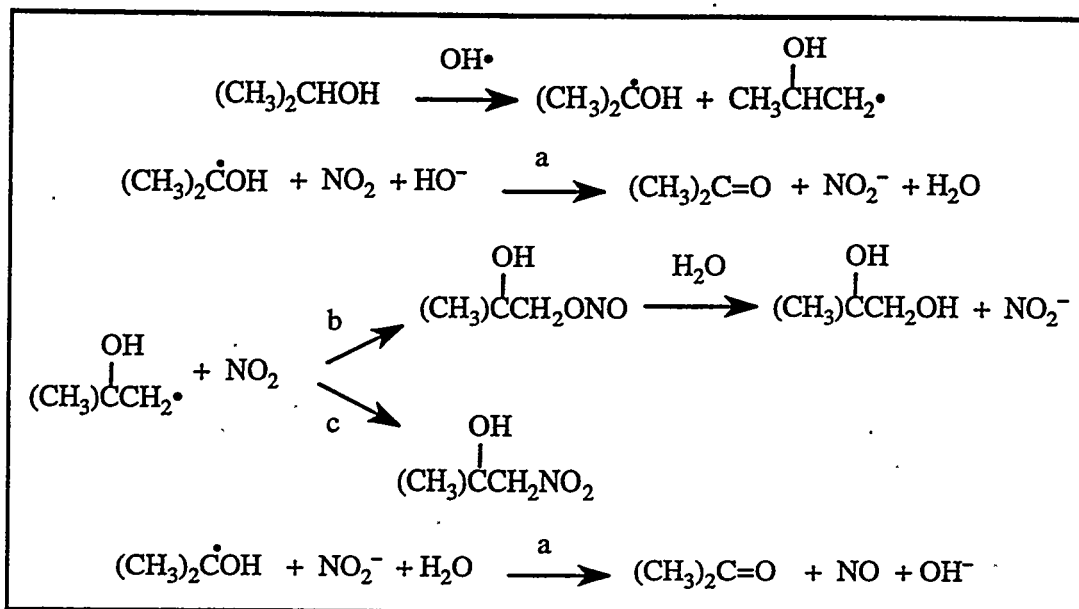


**Figure 2.2.** Electron Transfer (a) and Combination (b and c) Reactions of Organic Radicals with  $\text{NO}_2$  and  $\text{NO}_2^-$

## 2.2 Mechanisms and Kinetic Parameters for Thermal Aging

Our discussion of the literature on thermal aging focuses mainly on the work performed at Georgia Institute of Technology. First, we summarize the mechanistic conclusions, then we review and make estimates of activation barriers for thermal aging.

### 2.2.1 Mechanisms for Thermal Aging of Complexants

Workers at Georgia Institute of Technology (Ashby et al. 1994; Barefield et al. 1995, 1996) studied the thermal reactions of the major complexants in aqueous solutions. The studies show that citrate degrades to acetate and oxalate in the presence of hydroxide alone; glycolate and HEDTA degradations require nitrite and are catalyzed by aluminum and hydroxide ions; and EDTA is essentially inert. The reaction of citrate produced little gas and was not catalyzed by aluminate. Therefore, the reaction can be formulated “classically” as a “reverse Claisen” reaction, which is shown in Figure 2.3.

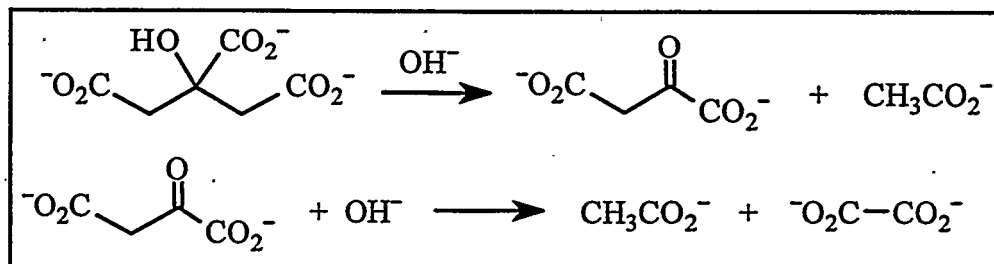


**Figure 2.3.** Mechanism for Base-Catalyzed Decomposition of Citrate Ion

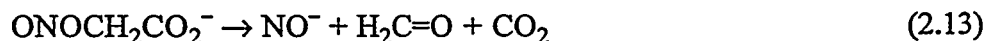
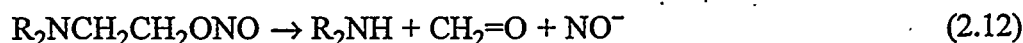
The overall reaction (Equation 2.9) shows that 2 C-C bonds are converted to 2 C-H bonds and a C=O bond. Consequently, the enthalpies of the organic species change little.



The observations of glycolate and HEDTA oxidations lead to conclusions that the mechanism involves heterolytic decomposition of the corresponding nitrite esters.

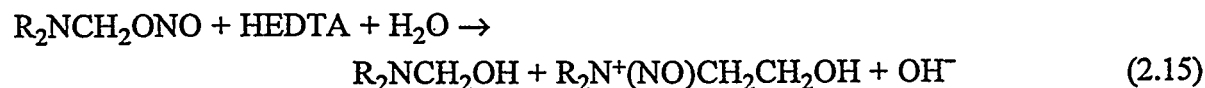


Aluminum hydroxides are proposed to complex with nitrite to generate a nitrosyl transfer agent, e.g.,  $[(\text{HO})_3\text{AlONO}]^-$ . The esters of HEDTA and glycolate then undergo concerted fragmentation to  $\text{NO}^-$ ,  $\text{CH}_2\text{O}$ , and imminium ion,  $\text{R}_2\text{N}^+=\text{CH}_2$  (from HEDTA) or  $\text{CO}_2$  (from glycolate).

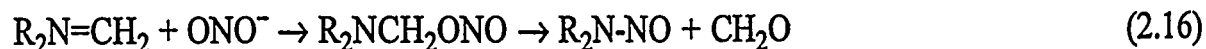


By this mechanism,  $\text{H}_2$  yields are strongly dependent on the dynamics of the caged species. Decomposition of formaldehyde in strong base produces  $\text{H}_2$  and formate. However, to explain less than stoichiometric yields of  $\text{H}_2$ , they suggest that  $\text{NO}^-$  adds to formaldehyde competitively with cage escape. The adduct then produces formate and hydroxylamine; the latter decomposes to nitrogenous gases. The imminium ion is competitively trapped by hydroxide and nitrite. These reactions produce  $\text{R}_2\text{NCH}_2\text{OH}$  and  $\text{R}_2\text{NCH}_2\text{ONO}$ , which may degrade to either formate and  $\text{H}_2$  or the nitrogenous gases  $\text{N}_2\text{O}$  and  $\text{NH}_3$ .

The oxidation kinetics are complex. Evidence for inhibition by  $\text{O}_2$  and autocatalysis has been observed. No satisfactory explanation of the effects of  $\text{O}_2$  have been advanced. The autocatalysis was attributed to generation of nitrite esters and N-nitroso compounds that form from HEDTA fragments. These compounds may transfer the nitrosyl group to HEDTA, as shown in Equations 2.14 and 2.15.



The investigators also pointed out that aminium ions (Keefer and Roller 1973) have been observed to react with nitrite to produce formaldehyde and N-nitrosamine, possibly via the nitrite ester (the second step in Equation 2.16 is not necessarily a unimolecular reaction).



Ashby et al. (1994) suggest that N-nitrosamines may act as nitrosyl transfer agents or decompose producing  $\text{NO}^-$ , aldehyde, and a primary amine (Equation 2.17).



## 2.2.2 Activation Barriers for Thermal Aging of HEDTA and Glycolate

Figure 2.4 shows a potential energy diagram for Equation 2.10. The equilibrium constant,  $K_{10}$ , for Equation 2.10 is  $\sim 10^{-11}$  such that  $\Delta G = 15$  kcal/mol for production of RONO from nitrite in alkaline conditions.<sup>(a)</sup> Rate constants for hydrolysis of primary alkyl nitrite esters (reverse of Equation 2.10) are on the order of  $5 \times 10^{-4}$  L/mol/s (Oae et al. 1978; Challis and Shuker 1979). Thus, the uncatalyzed rate constant for producing nitrite esters under alkaline conditions is  $\sim 10^{-14}$  L/mol/s at 35°C. The entropy change for ester production is negative, such that  $\Delta H \sim 10$  kcal/mol for ester production in alkaline solutions. Therefore,  $E_a$  for uncatalyzed Equation 2.10 is  $\sim 26$  kcal/mol. Clearly, this reaction is prohibitively slow and probably rate-controlling in the absence of catalysts. If Al catalyzes Equation 2.10, then  $E_a \geq 10$  kcal/mol.

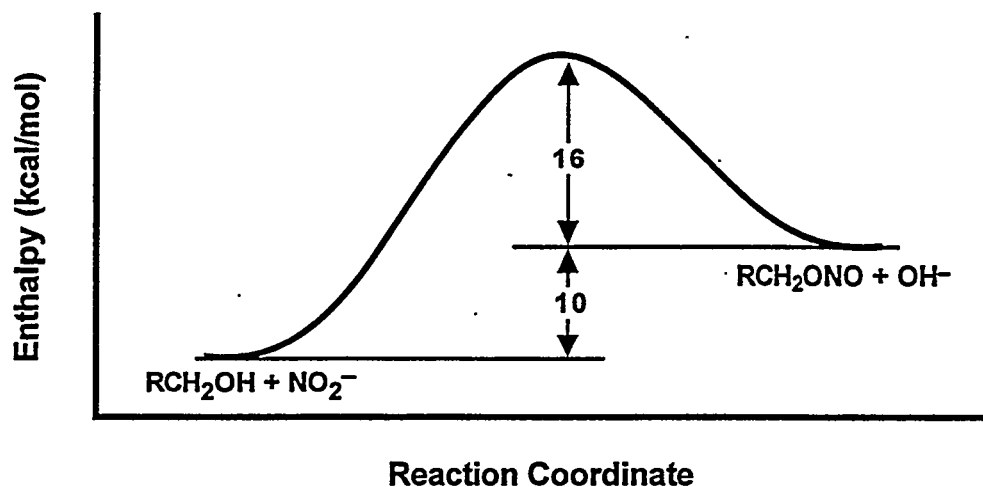


Figure 2.4. Potential Energy Surface for Nitrosation of Primary Alcohols by Nitrite Ion

Barefield et al. (1995) have estimated  $E_a$  for glycolate and HEDTA decomposition from kinetic analyses of  $\text{H}_2$  gas production rates. Their analysis suggested  $E_a$  for glycolate might be as low as 11 kcal/mol and  $E_a$  for HEDTA could be as low as 16 kcal/mol. The magnitude of these barriers is consistent with Equation 2.10 being rate-controlling, provided that catalysis by Al substantially reduces the 16 kcal/mol barrier for hydrolysis of nitrite esters and rates for Equation 2.12 are faster than rates for the reverse of Equation 2.10.

Assuming mechanisms proposed by Barefield et al. (1995), we estimate from thermochemical data that  $E_{a,s}$  for Equation 2.11 are on the order of 8 kcal/mol for glycolate and 22 kcal/mol for

(a) The equilibrium constant for reaction of primary alcohols with nitrous acid is  $\sim 1$  at 0 °C (Alred et al. 1982). Combining this with  $K_w$  and  $K_a$  for nitrous acid gives  $K$  for forming nitrite esters in alkaline conditions.

HEDTA. Given the magnitude of these barriers, if Equation 2.10 is rate limiting, then the Arrhenius A-factor for Equation 2.11 would need to be substantially larger than the A-factor for Equation 2.10. Because Equation 2.11 is a unimolecular reaction, we may expect larger A-factors compared with the reverse of Equation 2.10. However, information is insufficient to estimate the magnitudes of the A-factors. If barriers are as low as Barefield et al. (1995) estimate, then lifetimes of glycolate and HEDTA at 60°C would be on the order of a few years, so little of these compounds should now be present in tank wastes, provided that optimum levels of catalyst and hydroxide are present. Because samples from several tanks (e.g., U Farm tanks) have been found to contain significant glycolate and HEDTA, we must conclude that either higher barriers pertain or temperature and concentrations of catalysts and hydroxide are far from optimum for thermal degradation in these tanks. The latter case may well pertain and perhaps it could be established with relevant waste characterization data. On the other hand, if nitrite ester formation (Equation 2.10) is not rate-limiting, then  $k_{\text{observed}} = K_{10}k_{11}$  such that Arrhenius temperature dependencies are the sum of the free energy for nitrosation (Equation 2.10) and  $E_a$  for thermal degradation of nitrite ester (Equation 2.11), i.e., 15 kcal/mol +  $E_a$ . Therefore, we estimate  $E_{a,s}$  of 23 kcal/mol for glycolate and 37 kcal/mol for HEDTA would apply when Equation 2.11 is rate-controlling.<sup>(a)</sup> These estimates probably represent upper limits for the overall reactions. They are comparable to barriers measured for gas evolution from these compounds (Ashby et al. 1994) as well as from tank wastes (Person 1996; Pederson and Bryan 1996) and are qualitatively consistent with the relative reactivities observed by Barefield et al. (1995).

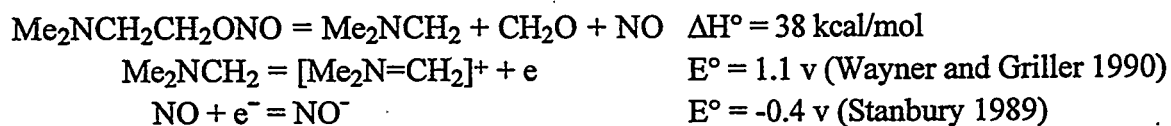
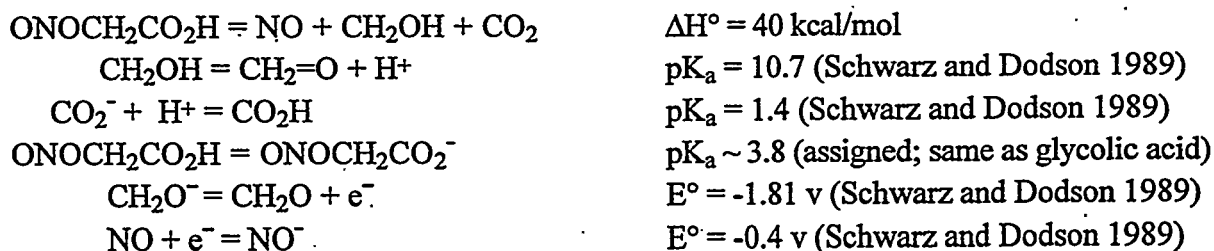
In conclusion, mechanisms for thermally initiated oxidations are not well understood and barriers are uncertain. These factors severely limit attempts to quantify the extent of aging due to thermal oxidations.

### 2.3 Synergistic Effects of Radiation on Thermal Reactions

Meisel et al. (1993) observed that preirradiation of waste simulants containing HEDTA yielded more gas from thermal treatment than unirradiated simulants. We have observed that

---

(a)  $E_{a,s}$  derived using thermochemical cycles;  $\Delta H^\circ$ s estimated from heats of formation data (Lias et al. 1988) and group additivity schemes:



radiolysis and reactions of  $\text{NO}_2$  cause deamination and decarboxylation of complexants, e.g.,  $\text{NTA} \rightarrow \text{IDA}$ , glycine, formate, and oxalate. It is probable that, in addition to reactions in Figure 2.1, nitrosation reactions may also occur (Equations 2.10, 2.11 and 2.13–2.16) because oxidation of carbon-centered radicals by  $\text{NO}_2$  can produce nitrite esters (see path b, Figure 2.2).<sup>(a)</sup> Nitrosamines could accumulate if produced at low temperatures and then degrade to gaseous products (Smith and Loeppky 1967) when heated.

---

(a) Personal communication with Dan Meisel, Argonne National Laboratory.

### 3.0 Relative Rate Constants for Radiolytic Aging of Organic Species

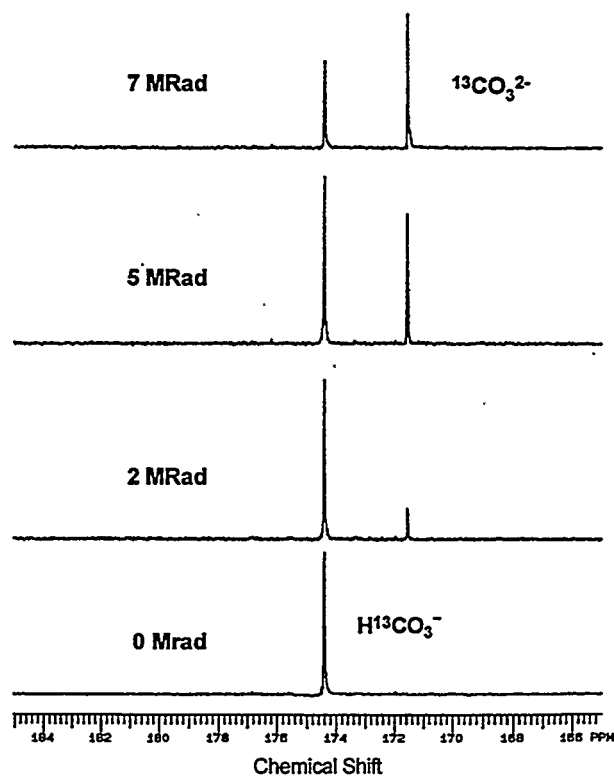
This section reports on studies of the radiolysis of organic complexants and related compounds in alkaline nitrate/nitrite solutions to elucidate reactivity and reaction paths. Our goals were to develop models for understanding and interpreting tank waste speciation results and to provide capabilities for predicting how TOC and energy content might evolve during interim storage. Reactivities of the complexants and several of their degradation products were measured relative to formate oxidation by irradiating binary mixtures of an organic compound and  $^{13}\text{C}$ -labeled formate in alkaline nitrate/nitrite solution. Conversions of organic species were measured by  $^{13}\text{C}$  and  $^1\text{H}$  nuclear magnetic resonance (NMR) spectrometry and corroborated by ion and liquid chromatography. Products were identified, as well, to provide reaction path information. In addition to binary competition experiments, oxidations of formate and glycine in the absence of other organic species were performed and modeled kinetically to obtain estimates of the absolute rate constant for reactions of  $\text{NO}_2$  with these species and the rate constant of another key reaction, oxidation of  $\text{NO}_3^{2-}$  by  $\text{NO}_2^-$ . This effort was substantially aided by close collaboration with EMSP projects on fundamental aspects of radiolytic effects in wastes, "The  $\text{NO}_x$  System in Nuclear Waste" and "Interfacial Radiolysis Effects in Waste Speciation."

#### 3.1 Reactivities of Organic Complexants Relative to Formate

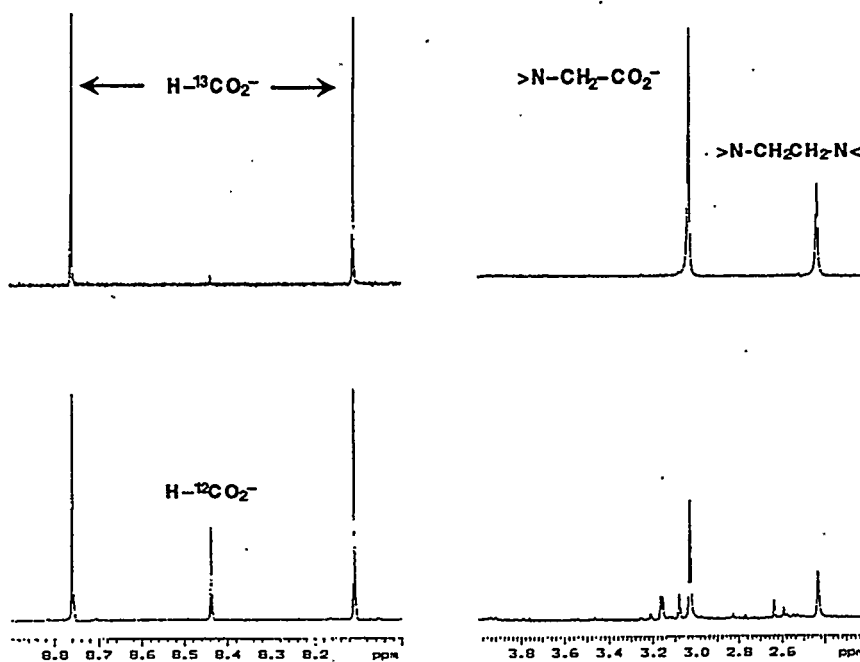
Formate degrades cleanly to carbonate during  $\gamma$  radiolysis. For this reason, we chose to measure reactivities of other organic species relative to formate ion.  $^{13}\text{C}$ -Formate was used to avoid interference from formate and carbonate produced by degradation of other organic species (e.g., see Figure 4.1). Figure 3.1 shows  $^{13}\text{C}$  NMR spectra of the formate/carbonate region before and after radiolysis. The ratio of the carbonate peak area to the formate peak area equals the conversion of formate to carbonate. Thus, for binary competition between an organic species and formate- $^{13}\text{C}$ , the relative reactivity of a species S is given by Equation 3.1:

$$\frac{k_S}{k_F} = \frac{\ln\left(\frac{[\text{S}]_t}{[\text{S}]_o}\right)}{\ln\left(1 - \frac{[\text{}^{13}\text{CO}_3^{2-}]_t}{[\text{H}^{13}\text{CO}_2^-]_o}\right)} \quad (3.1)$$

where S is the organic species that competes with  $^{13}\text{C}$ -formate for radiolytically generated oxidants, and subscripts o and t designate concentrations at the start of irradiation and after time t in the  $\gamma$  field. Scouting experiments were performed in which two ratios of EDTA/formate were irradiated for 5–11 days in a  $\gamma$ -field of  $8 \times 10^4$  rad/h. Figure 3.2 shows typical  $^1\text{H}$  NMR spectra obtained from unirradiated and irradiated samples. Products that appear in the irradiated sample are carbonate- $^{13}\text{C}$  from formate- $^{13}\text{C}$ , formate- $^{12}\text{C}$ , and a variety of other products from EDTA.



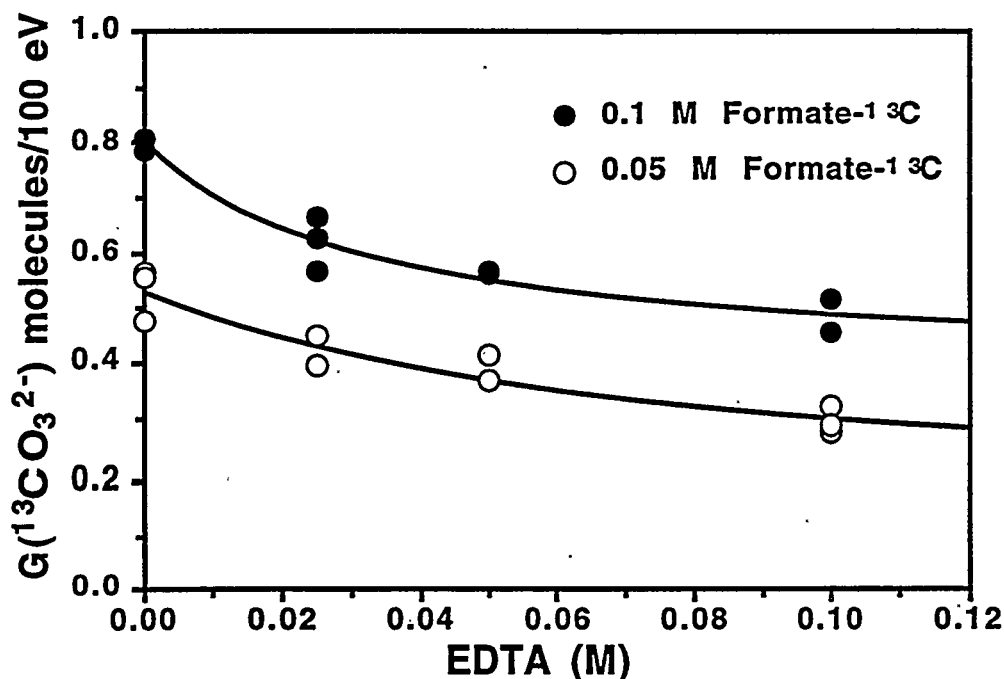
**Figure 3.1.**  $^{13}\text{C}$  NMR Spectra of 0.024 M Sodium Formate in 0.1 M  $\text{NaNO}_3$ , 0.03 M  $\text{NaNO}_2$ , 2 M  $\text{NaOH}$  before and after  $\gamma$  Radiolysis



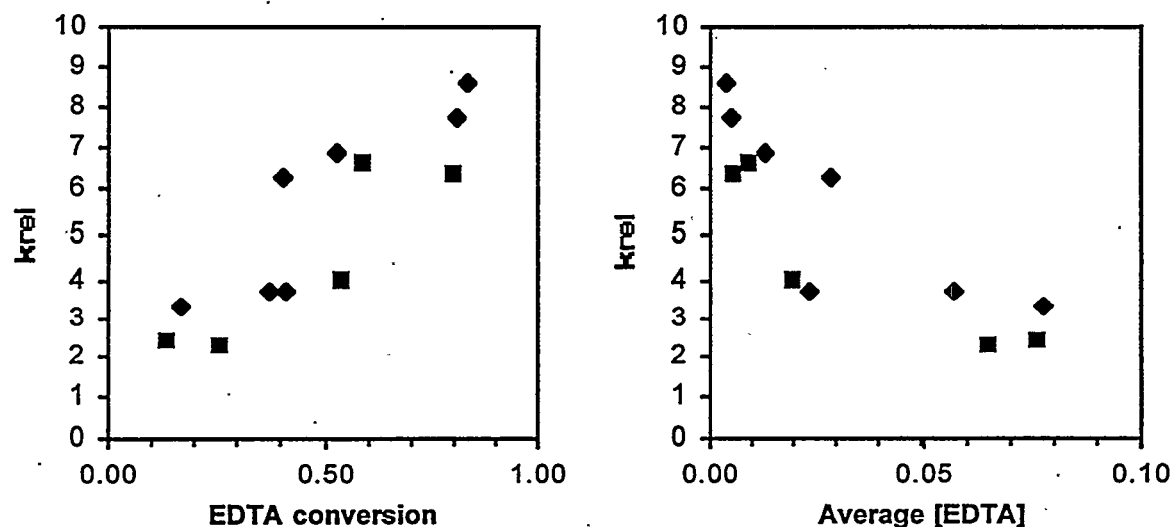
**Figure 3.2.**  $^1\text{H}$  NMR Spectra of Unirradiated (top) and Irradiated (bottom) EDTA/Formate- $^{13}\text{C}$  Solutions

Figure 3.3 shows the observed dependence of radiolytic yield,  $G(^{13}\text{CO}_3^{2-})$ , on initial formate and EDTA concentrations (see Table A.1, Appendix A for data). Note that in the absence of EDTA,  $G(^{13}\text{CO}_3^{2-})$  is greater at 0.1 M formate than at 0.05 M formate. This behavior is consistent with a mechanism in which oxidation of organic species by radiolytically generated radicals occurs in competition with  $\text{NO}_x$  disproportionation reactions shown in Equations 2.7 and 2.8 (Section 2.1.3). Also, at both initial concentrations of formate,  $G(^{13}\text{CO}_3^{2-})$  decreases as initial EDTA concentrations increase from 0 to 0.1 M. This behavior shows that formate and EDTA do *compete* for the radiolytically generated oxidants.

From measurements of the conversion of EDTA and formate, we obtain a relative rate constant,  $k_{\text{EDTA}}/k_{\text{formate}} = 5 \pm 2$ , using Equation 3.1. The uncertainty in  $k_{\text{EDTA}}/k_{\text{formate}}$  is larger than we expected, with values ranging from 2.1 to 9.3. We estimate uncertainties in measurements of EDTA, formate, and carbonate concentrations are  $\sim 5\%$ . Interestingly, we observed that the relative rate correlated linearly with the extent of EDTA conversion: the higher the conversion the greater the relative rate constant. Also, the relative rate and extent of conversion showed a general correlation with the initial concentration of EDTA: lower concentrations gave higher conversions and higher relative rates (see Figure 3.4). The origins of these effects are not fully understood; however, they may be a manifestation of two or more oxidizing radicals with different selectivities contributing to the oxidation of EDTA, e.g.,  $\text{O}^-$  and  $\text{NO}_2$ .



**Figure 3.3** Dependence of Radiolytic Yield of Carbonate from Formate versus Initial EDTA Concentration in a Solution of 3.75 M  $\text{NaNO}_3$ , 1.25 M  $\text{NaNO}_2$ , and 2 M  $\text{NaOH}$ ; dose rate =  $8 \times 10^4$  rad/h; irradiation times from 5 to 11 days



**Figure 3.4.** Reactivity (Equation 3.1) of EDTA Relative to Formate ( $k_{\text{EDTA}}/k_{\text{formate}}$ ) Correlates with Average EDTA and Conversion of EDTA; key: (■) 0.05 M formate; (◆) 0.1 M formate

Subsequent experiments were run to measure relative reactivities of other organic species under conditions that convert 30–70% of organic compound. The results are summarized in Table 3.1. The table lists starting concentrations, average fractions of formate- $^{13}\text{C}$  and organic species remaining after irradiation, and average  $k_{\text{rel}}$ . Standard deviations in the averages and number of measurements are also listed. The values  $C_o^{\text{S}}$  and  $C_o^{\text{F}}$  in Table 3.1 are the concentrations of species (superscript S) and  $^{13}\text{C}$ -formate (superscript F) before irradiation.

The reactivities in Table 3.1 show that glycolate and nitrogen-containing complexants HEDTA, EDTA, and their fragments are more reactive than formate by factors of 5 to 20. Compounds such as citrate and acetate are slightly less reactive than formate. Preliminary work on DBP, butyrate, and succinate suggest these compounds have reactivities similar to acetate and citrate. The reactivities of ethylenediaminetriacetate (ED3A) and ethylenediaminemonoacetate (EDMA) have not been measured, but by analogy to related compounds, similarly high reactivity is expected.

### 3.2 Kinetic Model for Radiolytic Oxidation

In this section we describe the development of chemical kinetic models for radiolytic oxidations of formate and glycine in solutions of nitrate, nitrite, and hydroxide. These models were developed to gain fundamental insight on and advance the understanding of radiolytic aging of organic complexants in waste solutions. Formate is the simplest system to model because only two one-electron transfer steps are required to convert it to carbonate. No oxalate or other intermediate organic products are produced. Formate is also a product of organic aging.

**Table 3.1.** Relative Rate Constants for Disappearance of Organic Species in Nitrate/Nitrite/Hydroxide<sup>(a)</sup> Solutions during  $\gamma$  Radiolysis

Specie	$C_o^S$	$C_o^F$	$k_{rel}$	n <sup>(b)</sup>
u-EDDA	0.0120	0.0900	13.0 ± 0.3	(3)
s-EDDA	0.0206	0.0991	13 ± 2	(3)
s-EDDA <sup>(c)</sup>	0.0797	0.100	10 ± 1	(4)
IDA	0.0486	0.133	12 ± 3	(3)
NTA	0.0164	0.127	9.8 ± 0.5	(3)
NTA <sup>(c)</sup>	0.0546	0.100	7 ± 2	(4)
HEDTA <sup>(c)</sup>	0.0406	0.102	19 ± 3	(3)
HEDTA	0.0395	0.103	14 ± 1	(3)
HEDTA	0.088	0.10	5.4 ± 0.4	(3)
Glycine	0.0549	0.111	7 ± 1	(3)
Glycolate	0.0401	0.101	6.1 ± 0.4	(2)
Glycolate	0.12	0.1	4 ± 2	(3)
EDTA <sup>(c)</sup>	0.0403	0.100	10 ± 2	(4)
EDTA	0.0200	0.103	5.7 ± 0.7	(3)
EDTA			5 ± 2 <sup>(d)</sup>	(13)
Formate			1 <sup>(e)</sup>	
Citrate <sup>(c)</sup>	0.0499	0.0526	0.4 ± 0.2 <sup>(f)</sup>	(4)
Citrate	0.0047	0.0670	0.6 ± 0.5	(3)
Citrate	0.0047	0.0670	0.7 ± 0.1	(3)
Acetate <sup>(c)</sup>	0.506	0.0530	0.24 ± 0.05 <sup>(f)</sup>	(3)
Acetate	0.0078	0.0995	0.7 ± 0.1	(3)

(a) In 3.75 M NaNO<sub>3</sub>, 1.25 M NaNO<sub>2</sub>, 2 M NaOH and at 20°C unless noted.

Concentrations of S and <sup>13</sup>C-formate measured by <sup>1</sup>H NMR and <sup>13</sup>C NMR, respectively.

(b) Number of measurements in parentheses.

(c) In 2 M NaNO<sub>3</sub>, 2 M NaNO<sub>2</sub>, 2 M NaOH, and at 25°C.

(d) From experiments in Figure 3.3 and Table A.1, EDTA concentrations are average of IPC and <sup>1</sup>H NMR measurements.

(e) Defined value.

(f) Based on amount of <sup>12</sup>C-formate produced.

Glycine is the simplest nitrogen-containing complexant. It is also a product of organic aging. Meisel et al. (1991a) described a chemical kinetic model for radiolysis of alkaline solutions of nitrate and nitrite. We adapted this model by adding reactions necessary to describe the oxidation of formate. Once this was accomplished, we added reactions for glycine oxidation.

### 3.2.1 Oxidation of Formate

Solutions containing  $^{13}\text{C}$ -formate, nitrate, nitrite, and hydroxide were irradiated to obtain data for developing the quantitative model for radiolytic aging. The  $^{13}\text{C}$ -formate was used so atmospheric carbon dioxide would not interfere with measurements of carbonate yields determined by  $^{13}\text{C}$  NMR spectroscopy. The concentration of formate was varied from 0.03 to 1.0 M (no other organic species were added). Figure 3.5 shows how the radiolytic yield of carbonate varied with formate concentration. Most experiments were run in 3.75 M  $\text{NaNO}_3$ , 1.25 M  $\text{NaNO}_2$ , 2 M  $\text{NaOH}$ , although the Ferrocyanide Project (Lilga et al. 1996) had reported results for experiments in which nitrate and nitrite were 0.1 M and 0.03 M, respectively. These data are represented by the "O" data point in Figure 3.5. The results depicted in the figure are tabulated in Table 3.3 (also in Appendix A, Tables A.3 and A.4).

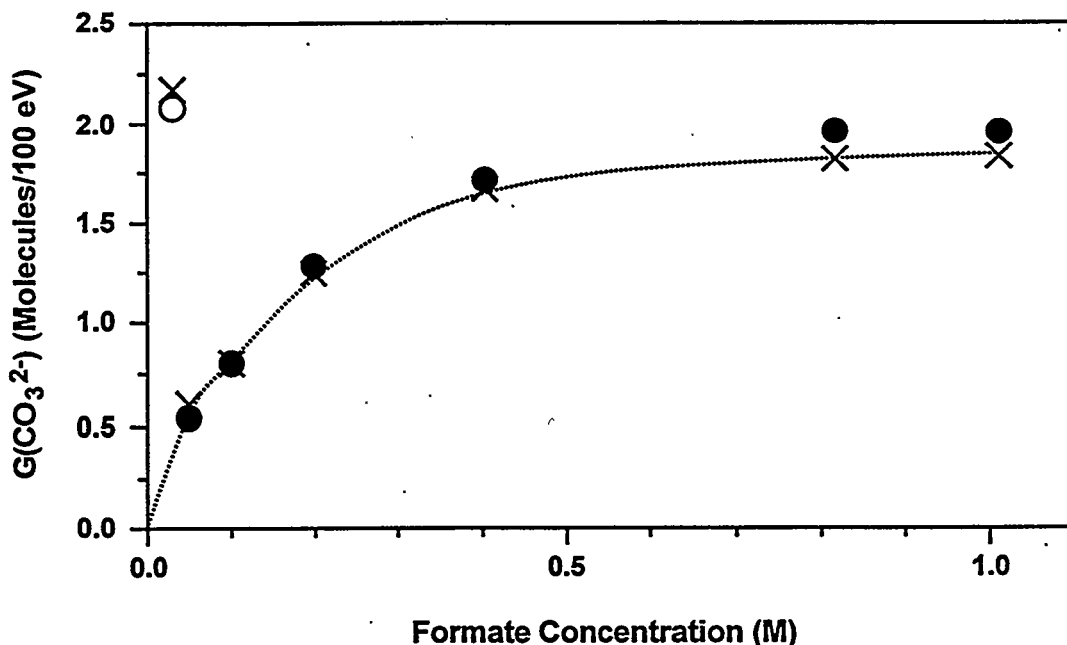


**Figure 3.5.** Measured and Modeled Radiolytic Yield of Carbonate (G, molecules/100 eV) Versus Formate Concentration: (●) experiment with 3.75 M nitrate, 1.25 M nitrite, and 2 M hydroxide; (○) experiment with 0.1 M nitrate, 0.03 M nitrite, 2 M hydroxide; (×) model

**Table 3.2.** Kinetic Model for Radiolytic Aging of Formate in Solutions Containing Nitrite, Nitrate and Hydroxide

Eq. No.	Reactant(a)			Products		k(s <sup>-1</sup> )	Note
1			→	NO <sub>3</sub> <sup>2-</sup>		4.9x10 <sup>-7</sup>	b
2			→	OH		5.2x10 <sup>-7</sup>	b
3			→	H		1.0x10 <sup>-7</sup>	b
4	NO <sub>3</sub> <sup>2-</sup>	+ H <sub>2</sub> O	→	NO <sub>2</sub>	+ 2OH <sup>-</sup>	5.5x10 <sup>4</sup>	c
5	NO <sub>3</sub> <sup>2-</sup>	+ NO <sub>2</sub> <sup>-</sup> (+H <sub>2</sub> O)	→	NO	+ NO <sub>3</sub> <sup>-</sup> (+2OH <sup>-</sup> )	2.0x10 <sup>4</sup>	d,e
6	OH	+ OH <sup>-</sup>	→	O <sup>-</sup>	+ H <sub>2</sub> O	1.3x10 <sup>10</sup>	f
7	OH	+ NO <sub>2</sub> <sup>-</sup>	→	NO <sub>2</sub>	+ OH <sup>-</sup>	1.0x10 <sup>10</sup>	c
8	OH	+ HCO <sub>2</sub> <sup>-</sup>	→	CO <sub>2</sub> <sup>-</sup>	+ H <sub>2</sub> O	4.1x10 <sup>9</sup>	c
9	H	+ NO <sub>2</sub> <sup>-</sup>	→	NO	+ OH <sup>-</sup>	1.6x10 <sup>9</sup>	c,g
10	H	+ HCO <sub>2</sub> <sup>-</sup>	→	CO <sub>2</sub> <sup>-</sup>	+ H <sub>2</sub>	2.4x10 <sup>8</sup>	c
11	O <sup>-</sup>	+ NO <sub>2</sub> <sup>-</sup>	→	NO <sub>2</sub>	+ OH <sup>-</sup>	3.1x10 <sup>8</sup>	c
12	O <sup>-</sup>	+ HCO <sub>2</sub> <sup>-</sup>	→	CO <sub>2</sub> <sup>-</sup>	+ OH <sup>-</sup>	1.4x10 <sup>9</sup>	c
13	NO <sub>2</sub>	+ HCO <sub>2</sub> <sup>-</sup>	→	CO <sub>2</sub> <sup>-</sup>	+ NO <sub>2</sub> <sup>-</sup>	10	e
14	CO <sub>2</sub> <sup>-</sup>	+ NO <sub>2</sub> <sup>-</sup>	→	CO <sub>2</sub>	+ NO	4.3x10 <sup>6</sup>	f
15	CO <sub>2</sub> <sup>-</sup>	+ NO <sub>2</sub>	→	NO <sub>2</sub> <sup>-</sup>	+ CO <sub>2</sub>	3.0x10 <sup>9</sup>	i
16	CO <sub>2</sub> <sup>-</sup>	+ NO	→	CO <sub>2</sub>	+ NO <sup>-</sup>	2.9x10 <sup>9</sup>	j
17	NO <sub>2</sub>	+ NO <sub>2</sub>	→	N <sub>2</sub> O <sub>4</sub>		4.5x10 <sup>8</sup>	k
18	N <sub>2</sub> O <sub>4</sub>		→	NO <sub>2</sub>	+ NO <sub>2</sub>	6.7x10 <sup>3</sup>	k
19	N <sub>2</sub> O <sub>4</sub>	(+2OH <sup>-</sup> )	→	NO <sub>2</sub> <sup>-</sup>	+ NO <sub>3</sub> <sup>-</sup>	1.0x10 <sup>3</sup>	k
20	NO <sub>2</sub>	+ NO	→	N <sub>2</sub> O <sub>3</sub>		1.1x10 <sup>9</sup>	k
21	N <sub>2</sub> O <sub>3</sub>		→	NO <sub>2</sub>	+ NO	8.0x10 <sup>4</sup>	k
22	N <sub>2</sub> O <sub>3</sub>	(+2OH <sup>-</sup> )	→	NO <sub>2</sub> <sup>-</sup>	+ NO <sub>2</sub> <sup>-</sup>	5.3x10 <sup>2</sup>	k
23	NO <sup>-</sup>	+ NO	→	N <sub>2</sub> O <sub>2</sub> <sup>-</sup>		1.7x10 <sup>9</sup>	k
24	N <sub>2</sub> O <sub>2</sub> <sup>-</sup>		→	NO <sup>-</sup>	+ NO	6.0x10 <sup>4</sup>	k
25	N <sub>2</sub> O <sub>2</sub> <sup>-</sup>	+ NO	→	N <sub>3</sub> O <sub>3</sub> <sup>-</sup>		4.9x10 <sup>6</sup>	k
26	N <sub>3</sub> O <sub>3</sub> <sup>-</sup>		→	N <sub>2</sub> O	+ NO <sub>2</sub> <sup>-</sup>	8.7x10 <sup>1</sup>	k
27	H	+ OH <sup>-</sup>	→	e <sup>-</sup> (aq)		2.0x10 <sup>7</sup>	d,h
28	e <sup>-</sup> (aq)	+ NO <sub>3</sub> <sup>-</sup>	→	NO <sub>3</sub> <sup>2-</sup>		9.7x10 <sup>9</sup>	c

(a) Reactants appearing in the rate law for each reaction step are listed; species in parentheses are shown for clarity but are not included in the rate law.

(b) Assigned based on G(NO<sub>3</sub><sup>2-</sup>) = 2.9, G(OH) = 2.9, G(H) = 0.4 (see Meisel et al. 1991a,b; Buxton et al. 1988).

(c) Buxton et al. 1988.

(d) D. Meisel, unpublished result, k < 5x10<sup>4</sup> M<sup>-1</sup>s<sup>-1</sup>.

(e) value adjusted to fit data in Table 3.3.

(f) Han and Bartels 1990.

(g) Mezyk and Bartels 1997.

(h) D. Meisel, unpublished result.

(i) assigned same rate constant as reaction 15.

(j) Czapski et al. 1994.

(k) Neta et al. 1988.

The yield of carbonate was strongly dependent on nitrite and formate concentrations. With 1.25 M nitrite, the yields of carbonate increased with increasing initial formate concentration, leveling off at G~1.8 molecules/100 eV (see Figure 3.5). When both nitrite and initial formate

concentrations were low (0.03 M), the yield was comparable to those obtained when formate concentrations were high. This behavior is well reproduced by the mechanistic kinetic model in Table 3.2. It includes the dominant reactions for  $e^-$ , H, HO,  $O^-$ , NO, and  $NO_2$ , a reaction of formate ion with  $NO_2$ , and a reaction of  $NO_3^{2-}$  with  $NO_2^-$ . Evidence for this last reaction has not been observed previously. However, recent experiments by Meisel et al.<sup>(a)</sup> show that it is thermodynamically favorable but occurs with a rate constant of  $<5 \times 10^4 \text{ M}^{-1}\text{s}^{-1}$ . The fit to the data shown in Figure 3.5 was obtained with rate constants of  $10 \text{ M}^{-1}\text{s}^{-1}$  for  $NO_2$  attack on formate and  $2 \times 10^4 \text{ M}^{-1}\text{s}^{-1}$  for reaction of  $NO_3^{2-}$  with  $NO_2^-$ . Figure 3.6 illustrates the time dependence of NO and  $NO_2$  as they approach steady state conditions in the radiolytic oxidation of formate ion in waste simulants.

Notice how different nitrite and formate concentrations affect the steady-state concentrations of NO and  $NO_2$ . With the high nitrite concentration, the steady-state concentration of NO is significantly higher, and that of  $NO_2$  is somewhat smaller. In either case, the concentration of NO under the reaction conditions is generally an order of magnitude greater than the concentration of  $NO_2$ , so cross-termination dominates over self-termination (Equations 18 and 21, respectively, in Table 3.2). Both reactions lead to a decrease in the oxidation efficiency and result in yields of products that are much less than stoichiometric.

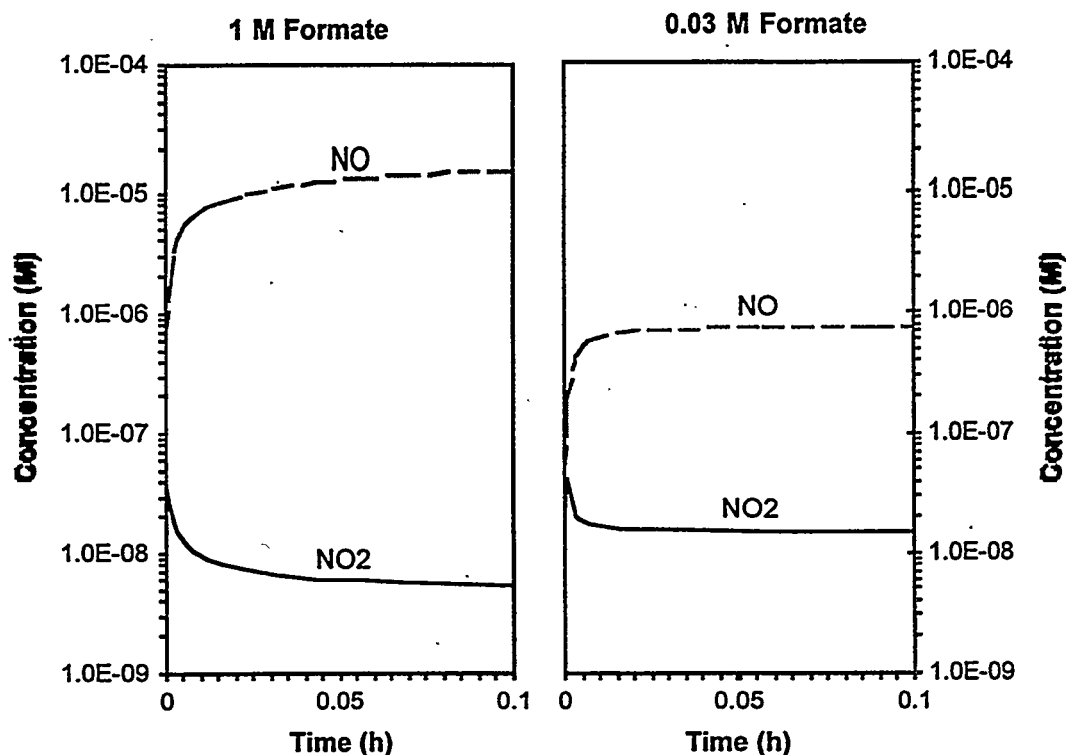


**Figure 3.6.** Time Dependence of NO and  $NO_2$  Radicals Predicted by Kinetic Model for Radiolytic Oxidation of 1 M Formate in 1.25 M  $NaNO_2$ , 3.75 M  $NaNO_3$ ,

(a) Unpublished result.

2 M NaOH (left) and 0.03 M Formate in 0.03 M NaNO<sub>2</sub>, 0.1 M NaNO<sub>3</sub>,  
2 M NaOH (right)

Consistent with finding no experimental evidence for conversion of formate to oxalate ion, the model predicts steady-state concentrations of CO<sub>2</sub><sup>-</sup> (<10<sup>-12</sup> M) that are too low to produce detectable amounts of oxalate ions by self-reaction. Even the cross reactions of CO<sub>2</sub><sup>-</sup> with NO or NO<sub>2</sub> do not appear to compete with its reaction with nitrite ion (Equation 14 in Table 3.2). Although reaction of NO with CO<sub>2</sub><sup>-</sup> is fast, k<sub>16</sub> = 3x10<sup>9</sup> M<sup>-1</sup> s<sup>-1</sup> (Czapski et al. 1994), NO cannot compete when NO<sub>2</sub><sup>-</sup> ion is present in mM concentrations. For example, when [NO<sub>2</sub><sup>-</sup>] = 0.03 M, the model calculates that the steady-state concentration of NO is ~ 6x10<sup>-7</sup> M such that reaction of CO<sub>2</sub><sup>-</sup> with NO<sub>2</sub><sup>-</sup> is still 70 times more favorable than reaction with NO (Equation 3.2 calculates the relative rate (r<sub>14</sub>/r<sub>16</sub>) for Equations 14 and 16 in Table 3.2).

$$\frac{r_{14}}{r_{16}} = \frac{k_{14}[\text{NO}_2^-]}{k_{16}[\text{NO}]} = \frac{4.3 \times 10^6 [0.03]}{3 \times 10^9 [6 \times 10^{-7}]} = 70 \quad (3.2)$$

Therefore, NO serves mainly as a trap for NO<sub>2</sub>. This result is consistent with observations that N<sub>2</sub>O was not radiolytically generated from waste simulants containing only formate ion (Meisel et al. 1993). If NO were to react with CO<sub>2</sub><sup>-</sup>, it would generate NO<sup>-</sup> (Czapski et al. 1994), which is a precursor to N<sub>2</sub>O (see Equations 23–26 in Table 3.2).

The relative amounts of CO<sub>3</sub><sup>2-</sup> produced by each oxidizing radical estimated from the model and experimental data are listed in Table 3.3: The highest fraction of attack (~51%) by NO<sub>2</sub> occurred when the nitrite concentration was high and the formate concentration was low. These conditions favor conversion of O<sup>-</sup>, OH, and H to NO<sub>2</sub>. High formate or low nitrite favor O<sup>-</sup> attack on formate. Direct attack of H on formate ion (and glycine) is minimal; only at very high organic concentrations, > 0.75 M, does direct attack contribute to more than 1% of the conversion yield. This result is consistent with observations by Meisel et al. (1993) that irradiation of waste simulants containing formate ion as the only organic species did not generate significant amounts of H<sub>2</sub> gas.

The observation that O<sup>-</sup> is a significant contributor to formate oxidation even at 1.25 M NO<sub>2</sub><sup>-</sup> suggests that it is important for understanding the relative reactivities listed in Table 3.1. Clearly, the observed relative reactivities are a composite of O<sup>-</sup> and NO<sub>2</sub> reactivities and therefore do not represent true reactivities of NO<sub>2</sub>. However, because formate is one of the more reactive compounds toward O<sup>-</sup>, the relative reactivities in Table 3.1 may qualitatively represent the reactivity of NO<sub>2</sub>. For example, EDTA probably is as reactive as formate toward O<sup>-</sup>. Because relative reactivities as high as 10 were observed in our competition experiments (Figure 3.4), NO<sub>2</sub> must be significantly more reactive toward EDTA than it is toward formate. Similarly, glycine is about three times less reactive than formate toward O<sup>-</sup> (Neta and Schuler 1975). Since we observed a relative reactivity of ~7 (Table 3.1), NO<sub>2</sub> reaction with glycine must be faster than reaction with formate.

**Table 3.3.** Total Yield and Fractions of Carbonate Produced from Radiolytically Generated Species<sup>(a)</sup>

Formate, M	G(CO <sub>3</sub> <sup>2-</sup> ) molecules/100 eV		% of Carbonate Yield by Oxidizing Species			
	Expt	Model	H	OH	O <sup>-</sup>	NO <sub>2</sub>
0.05	0.5	0.6	0	3	46	51
0.1	0.8	0.8	1	4	61	35
0.2	1.3	1.2	1	5	62	32
0.4	1.7	1.7	1	7	64	27
0.8	2.0	1.8	2	13	72	14
1	2.0	1.8	2	15	74	8
0.03 <sup>(b)</sup>	2.1	2.2	1	1	96	2

(a) Conditions: 1.25 M nitrite, 3.75 M nitrate, 2 M hydroxide; dose Rate ~0.5 Mrad/h.

(b) 0.03 M nitrite, 0.1 M nitrate, 2 M hydroxide, dose rate ~0.1 Mrad/hr (Lilga et al. 1996).

### 3.2.2 Oxidation of Glycine

Figure 3.7 shows results for radiolytic aging of <sup>13</sup>C-glycine in 2 M NaOH, 2 M NaNO<sub>3</sub>, and 2 M NaNO<sub>2</sub>. An equimolar mixture of 1- and 2-labeled glycines was used to avoid C-C couplings (doublets) in the glycine resonances. Furthermore, the appearance of any C-C couplings in oxalate would indicate that combination of radicals derived from two glycines. The spectrum is clean, showing conversion of glycine to three products: oxalate, formate, and carbonate.

The radiolytic yield for disappearance of glycine was G = -1.3 molecules/100 eV. This yield is more than double the yield for disappearance of formate under analogous conditions (see Table 3.3 where G<sub>carbonate</sub> = -G<sub>formate</sub>), suggesting glycine is more reactive than formate and consistent with relative reactivity measurements in Table 3.1. No doublets are observed in the resonances of oxalate; therefore, we rule out oxalate ion being formed from intermediates along the pathways that produce carbonate and formate ions and conclude that glycine degrades to the three products by competing pathways (Equations 3.3a and 3.3b):



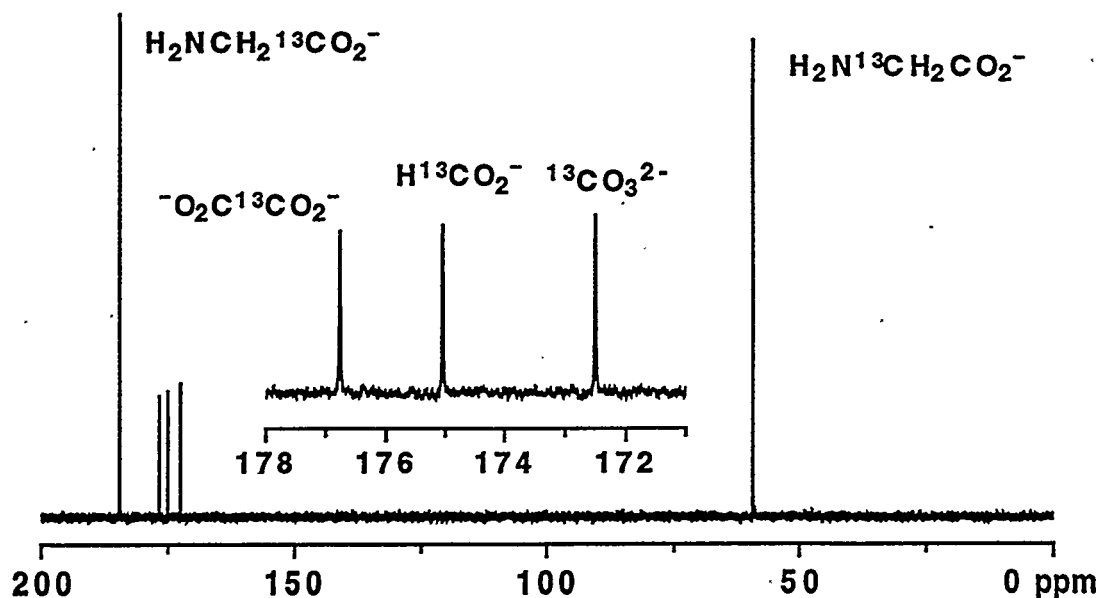


**Figure 3.7.**  $^{13}\text{C}$  NMR Spectrum of Equal Parts 1- $^{13}\text{C}$ -Glycine and 2- $^{13}\text{C}$ -Glycine in a Solution of 2 M  $\text{NaNO}_3$ , 2 M  $\text{NaNO}_2$ , and 2 M  $\text{NaOH}$  after a 16.8 Mrad  $\gamma$  Dose at  $22^\circ\text{C}$

The partitioning of products by these pathways may be caused by different oxidizing intermediates or the same one, i.e.,  $\text{O}^-$  and/or  $\text{NO}_2$ . We did not determine the fate of amino nitrogen in these experiments; it is reasonable that it goes to ammonia, although it could be oxidized to  $\text{N}_2$  or  $\text{N}_2\text{O}$ .

Figure 3.8 shows the  $^{13}\text{C}$  NMR spectrum of glycine simulant solution that was irradiated (29 Mrad) without  $\text{NaNO}_2$  present. This result is interesting in that different distributions of the three principal products are obtained along with other products. The other products appear to give doublet resonances indicating combination and addition reactions have occurred. Significantly higher conversions of glycine were observed; for example, a 7.8-Mrad dose gave 50% conversion of glycine for a  $G \sim -3.7$  molecules/100 eV, and nearly 70% of the glycine carbon went to other products. Oxalate, formate, and carbonate were obtained in a 28:31:19 distribution. Since only 2- $^{13}\text{C}$ -glycine was used in this experiment, the appearance of carbonate- $^{13}\text{C}$  requires that either formate or oxalate is further oxidized or that glycine is oxidized directly to carbonate:



When the nitrite ion concentration is low, as it was in this experiment (Figure 3.8), only the radiolytically generated electrons will produce  $\text{NO}_2$  radicals; conversion of  $\text{O}^-$  radicals to  $\text{NO}_2$  radicals (Equations 2.1 and 2.6) will be inefficient. Instead,  $\text{O}^-$  radicals will attack the organic

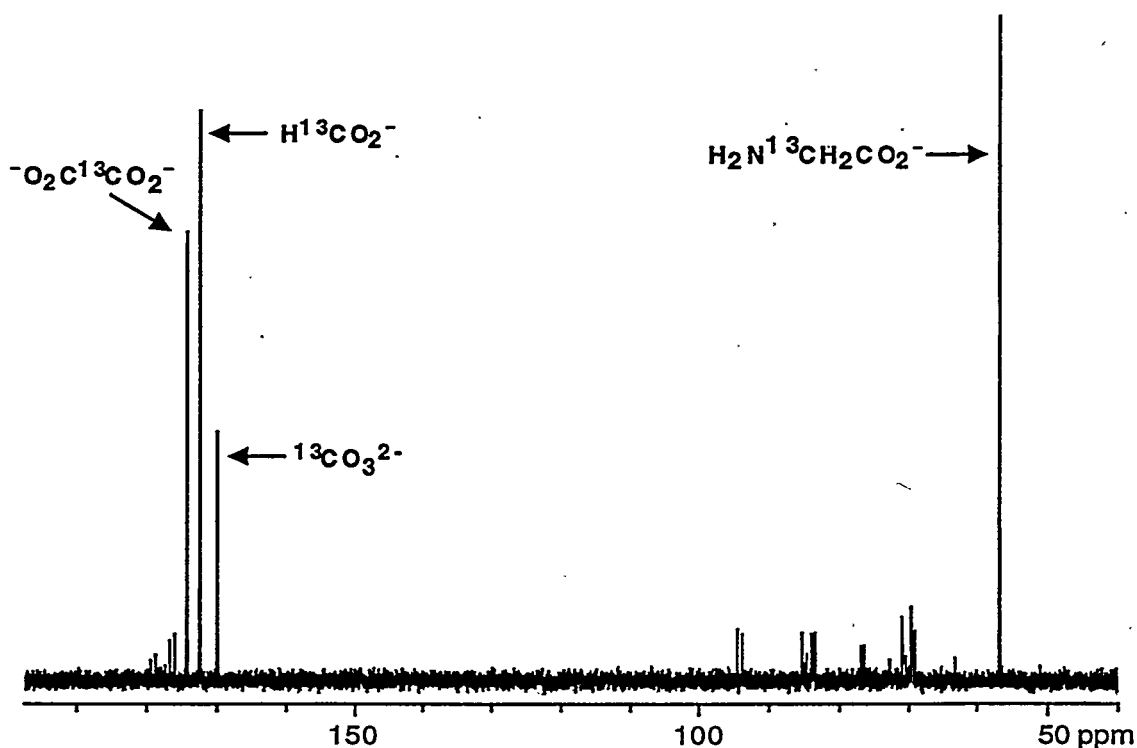


**Figure 3.8.**  $^{13}\text{C}$ -NMR Spectrum of a 2- $^{13}\text{C}$ -Glycine Simulant Solution after a 29 Mrad Dose at 25°C; solution initially contained 0.1 M 2- $^{13}\text{C}$ -glycine, 2 M  $\text{NaNO}_3$  and 2 M  $\text{NaOH}$

species that are present. Since  $\text{O}^-$  reactivity with formate is much greater than the reactivity of  $\text{NO}_2^-$  with formate, it is probable that the carbonate- $^{13}\text{C}$  in this experiment derives from  $\text{O}^-$  attack on formate.

The appearance of other products and the greater reactivity of formate in this experiment underscores the major role that  $\text{NO}_2^-$  plays in controlling the course of radiolytic reactions. Apparently,  $\text{NO}_2^-$  not only converts  $\text{OH}$  and  $\text{O}^-$  to  $\text{NO}_2$  (see Equations 2.1 and 2.6), it oxidizes organic radicals to products. Meisel and coworkers at Argonne National Laboratory recently measured rate constants for reactions of some organic radicals with  $\text{NO}_2^-$ . The rates are fast enough to allow reactions to compete favorably with organic radical combination/disproportionations reactions. While  $\text{NO}_2^-$  appears beneficial for clean oxidation of complexants, it suppresses the radiolytic yield by oxidizing  $\text{NO}_3^{2-}$ , a precursor for up to 50% of  $\text{NO}_2$ . Also, its reduction product,  $\text{NO}$ , combines with  $\text{NO}_2$  to give  $\text{N}_2\text{O}_3$ , which hydrolyses rapidly in alkaline conditions to  $\text{NO}_2^-$  (Park and Lee 1988). The  $\text{NO}$  radical combines with organic radicals giving rise to oxidized organic products and reduced forms of nitrogen, such as hydroxylamine, which give rise to  $\text{N}_2$ ,  $\text{N}_2\text{O}$  and  $\text{NH}_3$  (Meisel et al. 1993; Barefield et al. 1996).

To model the results for oxidation of glycine, we expanded the formate kinetic model (Table 3.2) by adding the reaction steps shown in Table 3.4. The model assumes the formation of a common intermediate, I, that partitions to formate and  $\text{CO}_3^{2-}$  via aminomethyl radical (A)

and to oxalate via glycine radicals (G).<sup>(a)</sup> When the model was run using literature rate constants for reactions of H, OH and O<sup>-</sup> with glycine (steps 29–31 in the table) and the rate constant for step 32 set to 0, it underestimated the conversion of glycine. Addition of k<sub>32</sub> provided both an improved fit to the experimentally observed glycine disappearance as well a reasonable fit to production of formate, oxalate and carbonate yields. Figure 3.9 shows model results for two experiments in which solutions containing 2-<sup>13</sup>C-glycine, NO<sub>2</sub><sup>-</sup>, NO<sub>3</sub><sup>-</sup>, and OH<sup>-</sup> were irradiated for 9–30 hours in a γ field of 0.5 Mrad/h. The second experiment (Figure 3.9) had formate-<sup>12</sup>C present in the solution initially. Numerical results are listed in Appendix A (Table A.5). Glycine conversion was less in this experiment because, as the model shows, formate reacted with a fraction of the O<sup>-</sup> and NO<sub>2</sub> radicals.

Table 3.5 summarizes results obtained at different nitrite concentrations and compares them with model results. As previously observed in the formate studies, O<sup>-</sup> dominates the oxidation pathways when the nitrite concentration is low.<sup>(b)</sup> However, when nitrite is high, NO<sub>2</sub> is the dominant oxidant of glycine. This result is consistent with the selectivity observed in competition experiments with glycine and formate-<sup>13</sup>C (see Section 3.1 and Table 3.1). The conversion

**Table 3.4.** Kinetic Reaction Steps Added to Formate Kinetic Model to Model Glycine Oxidation in Solutions of Nitrate, Nitrite, and Hydroxide

Eq.	Reactants			Products		k	Note
29	Gly	+ H	→	G	+ H <sub>2</sub>	4.5x10 <sup>7</sup>	a
30	Gly	+ O <sup>-</sup> (+ H <sub>2</sub> O)	→	I	+ 2OH <sup>-</sup>	5.6x10 <sup>8</sup>	b
31	Gly	+ OH	→	I	+ H <sub>2</sub> O	5.3x10 <sup>9</sup>	c
32	Gly	+ NO <sub>2</sub> (+ OH)	→	I	+ NO <sub>2</sub> <sup>-</sup> (+ H <sub>2</sub> O)	70	d
33	I		→	A	+ CO <sub>3</sub> <sup>2-</sup>	3x10 <sup>6</sup>	e
34	I	+ OH <sup>-</sup>	→	G	+ H <sub>2</sub> O	5x10 <sup>5</sup>	e
35	A	+ NO <sub>2</sub> <sup>-</sup>	→	NO	+ HCO <sub>2</sub> <sup>-</sup>	10 <sup>6</sup>	f
36	G	+ NO <sub>2</sub> <sup>-</sup>	→	C <sub>2</sub> O <sub>4</sub> <sup>2-</sup>	+ NO	10 <sup>6</sup>	f

(a) Assigned same rate constant as glycolate ion (Buxton et al. 1988).

(b) Neta and Schuler 1975.

(c) Lati and Meyerstein 1972.

(d) Varied to provide best fit to observed data.

(e) Set to reproduce observed ratio (3:1) of formate to oxalate.

(f) Assigned same magnitude as step 14 in Table 3.2.

(a) These steps are a simplified version of Figure 2.1, which shows the glycine zwitterion partitioning to three radicals: H<sub>2</sub>NCH<sub>2</sub>•, H<sub>2</sub>NCH(•)CO<sub>2</sub><sup>-</sup>, and •HNCH<sub>2</sub>CO<sub>2</sub><sup>-</sup>. The last radical may partition to formate and carbonate or to oxalate products. Therefore, including pathways in the model to A and G radicals is sufficient to model product yields.

(b) We did not model results obtained without initial nitrite because additional steps involving termination reactions of organic intermediate radicals are needed.

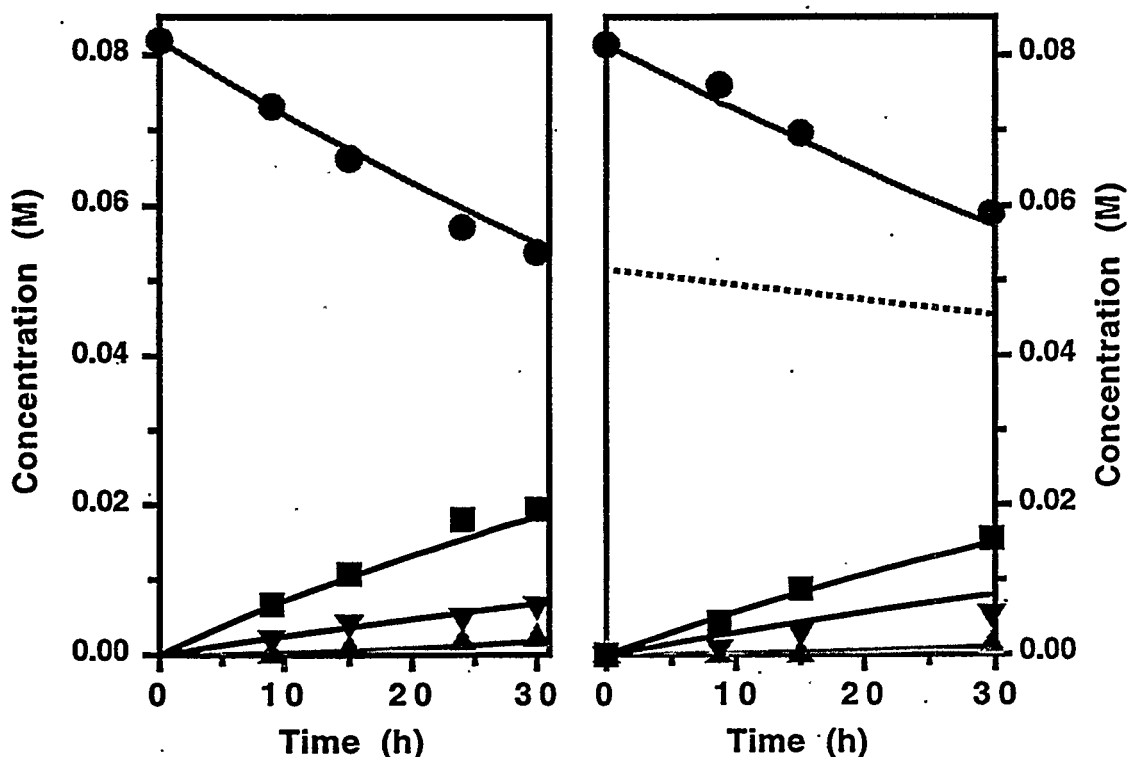


**Figure 3.9.** Results of Kinetic Model and Experiments for Radiolytic Degradation of Glycine: (left) 2-<sup>13</sup>C-glycine in 1.26 M NO<sub>2</sub><sup>-</sup>, 3.76 M NO<sub>3</sub><sup>-</sup>, and 2 M OH<sup>-</sup>; (right) mixture of 2-<sup>13</sup>C-glycine and <sup>12</sup>C-formate in 2.0 M NO<sub>2</sub><sup>-</sup>, 2.0 M NO<sub>3</sub><sup>-</sup>, and 2 M OH<sup>-</sup>. T = 22°C; flux = 0.5 Mrad/h; points are measured concentrations, solid and dotted lines are model predictions. Key: (●) 2-<sup>13</sup>C-glycine; (■) <sup>13</sup>C-formate; (▲) <sup>13</sup>C-carbonate; (▼) <sup>13</sup>C-oxalate; (---) <sup>12</sup>C-formate.

of glycine in the absence of nitrite is significantly higher than it is when nitrite is present (see Table 3.5). Such high yields are possible because organic radicals generated by attack of oxidizing radicals on glycine undergo self-termination reactions. When nitrite is present, these radicals react with nitrite to produce NO or other intermediate radicals that react with NO<sub>2</sub> radical (e.g., steps 18 and 19, Table 3.2), thereby limiting organic conversion.

A shortcoming of the glycine model is that it does not allow for producing N<sub>2</sub>O or N<sub>2</sub> in any significant quantities. In running the formate model, we observed that the NO radicals produced in reaction steps 5, 9, and 14 (Table 3.2) mainly reacted with NO<sub>2</sub>. Reaction of NO with CO<sub>2</sub><sup>-</sup> to make NO<sup>-</sup>, a precursor to N<sub>2</sub>O and N<sub>2</sub>, was negligible because nitrite ion reacted ~100 times faster with CO<sub>2</sub><sup>-</sup>. Although reactions of nitrite ion with radicals derived from glycine (A and G in Table 3.4) have not been measured, we expect the radicals will have comparable reactivities because hydroxyalkyl radicals do.<sup>(a)</sup> Thus the glycine model did not include reactions of NO

(a) For example, 1-hydroxy-1-ethyl and 2-hydroxy-2-propyl radicals have rate constants of 1×10<sup>6</sup> M<sup>-1</sup>s<sup>-1</sup> (unpublished result by Dan Meisel, Argonne National Laboratory).

with glycine-derived radicals. However, Meisel et al. (1991a) report that  $G(N_2O) = 0.15$  molecules/100 eV from 0.3 M glycine in a waste simulant. Meisel et al. also measured yields of  $N_2O$  from a number of other complexants: 0.085 M EDTA, 0.60 molecules/100 eV; 0.85 M HEDTA, 0.5 molecules/100 eV; 0.17 M NTA, 0.56 molecules/100 eV; 0.17 M IDA, 0.76 molecules/100 eV; 0.86 M glycolate, 0.42 molecules/100 eV; 0.17 M citrate, 0.045 molecules/100 eV.

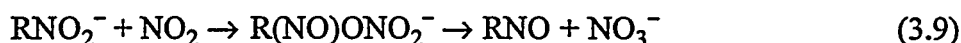
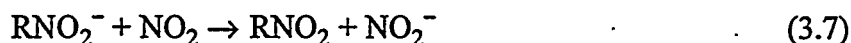
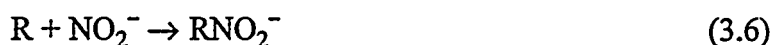
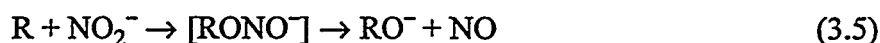
**Table 3.5.** Radiolytic Yields of Glycine in Solutions Containing Nitrite, Nitrate, and Hydroxide

[Glycine]	[Nitrite]	G(Glycine) <sup>(a)</sup>		% of Yield by Oxidizing Radicals			
		Expt	Model	H	HO	O <sup>-</sup>	NO <sub>2</sub> <sup>-</sup>
0.080	0	-3.7	--	3	1	77	19
0.082	1.25	-1.3	-1.2	0	2	14	83
0.080	2	-0.9	-0.8	0	3	11	86
0.081 <sup>(b)</sup>	2	-0.9	-1	0	3	10	87

(a) Molecules/100 eV.

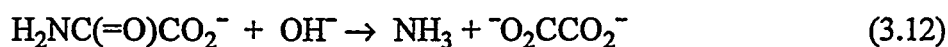
(b) With 0.05 M <sup>12</sup>C-formate.

Compatible mechanisms for forming nitrogen gases might involve intermediates formed by addition of organic radicals (R) to nitrite ion (Equations 3.5–3.9). Reaction at both O and N atoms of NO<sub>2</sub><sup>-</sup> are possible (Equations 3.5 and 3.6).



Equation 3.5 is analogous to the reaction of H with nitrite ion (Equation 2.2). The adduct, RONO<sup>-</sup>, may only be a transition state. However, intermediates such as the nitroanion radical formed in Equation 3.6, are sufficiently long-lived to be observed by electron spin resonance spectrometry (Zeldes and Livingston 1968; Madden et al. 1988; Gilbert et al. 1972, 1982). Electron transfer to an acceptor, e.g., NO<sub>2</sub> (Equation 3.7), produces a nitro compound. Numerous reactions leading to observed products are possible for nitro compounds in the alkaline wastes (Stock and Pederson 1997). The nitroanion radical may undergo combination/disproportionation reactions with NO and NO<sub>2</sub>. These reactions produce organic nitroso compounds that readily tautomerize to oximes and hydrolyze to observed products and hydroxylamine (Equations 3.10–3.12).





Few of the key rate constants are available to include Equations 3.5–3.9 in the glycine kinetic model. To the extent Equation 3.6 occurs, the stoichiometry for consumption of glycine may be different from that predicted by the model in Table 3.4. In that model, NO mainly disproportionates with NO<sub>2</sub> and limits the overall yield of organic oxidation. Equation 3.8 allows it to participate in oxidizing organic species so that the rate constant for NO<sub>2</sub> attack on glycine (Equation 32 in Table 3.4) probably would need to be smaller to fit the data. However, if Equations 3.5, 3.7, and 3.9 dominate, the model could be made to generate nitrogen gases without needing to change the rate constant for NO<sub>2</sub> attacking glycine.

### 3.3 Products of Degradation

When possible, products from competition experiments in Section 3.1 were identified from the chemical shifts of NMR peaks that appeared after  $\gamma$  irradiation. Irradiated, oxidized samples were spiked with authentic materials to corroborate assignments based on chemical shift information. The chemical shifts of compounds of interest were dependent on ionic strength such that they had to be specifically determined for the highly caustic and high-ionic-strength solutions used in these studies. Table A.6 in Appendix A shows the specific chemical shifts for reactants and products identified in these experiments. Table 3.6 lists the products identified by matching NMR chemical shifts. It also identifies products that cannot be present and some that are consistent with observed resonances but could not be unambiguously assigned.

Formate was almost always a significant product. More than two moles of formate are produced per mole of EDTA consumed, ~1 mole formate is formed per mole of glycolate consumed; and for citrate, acetate, and HEDTA, ~0.5 mole formate is formed per mole of species consumed. Oxalate is also produced, and presumably carbonate (e.g., see Figure 3.1).

The pathway for NTA degradation is better understood. Figure 3.10 shows spectra taken before and after irradiation of an NTA solution. Readily identifiable products are IDA, glycine, and formate. In one experiment, 45% of the starting NTA remained; 17% was IDA and 29% was glycine. These products accounted for 91% of the nitrogen originally present in NTA. We presume the missing N is due to inorganic N from oxidation of glycine. This progression of products is consistent with the reactivities measured for NTA, IDA, and glycine by competition with formate-<sup>13</sup>C (see Table 3.1). The yield of formate-<sup>12</sup>C was 83%, which suggests that cleavage of R<sub>2</sub>NCH<sub>2</sub>CO<sub>2</sub><sup>-</sup> by oxidative decarboxylation is a significant pathway for NTA and IDA.

The <sup>1</sup>H NMR spectra of EDTA in nitrate/nitrite/hydroxide solution before and after  $\gamma$  radiolysis are shown in Figure 3.11. The peaks identified (along with unidentified peaks) in the figure are also shown in tabular form in Appendix A. The major products of EDTA radiolysis besides formate are ED3A, s-EDDA and NTA. Peaks in the “after radiolysis” spectrum consistent with products such as IDA, glycine, u-EDDA, and glycolate are identified in Figure 3.11, which also shows a minor product peak that matches acetate outside the spectral region. Resonances for

**Table 3.6.** Products Identified by NMR from Radiolytic Oxidation of Complexants in Nitrate/Nitrite/Hydroxide Solutions

Substrate	Rel. Amt.	Products <sup>(a)</sup>		
		Positively Identified <sup>(b)</sup>	Possibly Present	Not Present <sup>(d)</sup>
EDTA	major	ED3A, s-EDDA, IDA, Formate		HEDTA
	minor	Acetate, Glycolate Glycine	u-EDDA, NTA <sup>(c)</sup>	
HEDTA	major	s-EDDA, IDA, Formate	NTA <sup>(c)</sup>	EDTA, ED3A
	minor	Glycine	u-EDDA	
u-EDDA	major	IDA, Formate	(c)	NTA
	minor	Glycine		
s-EDDA	major	IDA, Formate	EDMA	
	minor	Glycine	(c)	
NTA	major	IDA, Formate		
	minor	Glycine		
IDA	major	Glycine, Formate		

(a) In all cases, carbonate (and oxalate) is assumed to be a product based on the results with <sup>13</sup>C labeled glycine. In addition, almost all substrates yielded trace amounts of glycolate and acetate upon prolonged radiolysis.

(b) Assigned based on proton and <sup>13</sup>C NMR experiments.

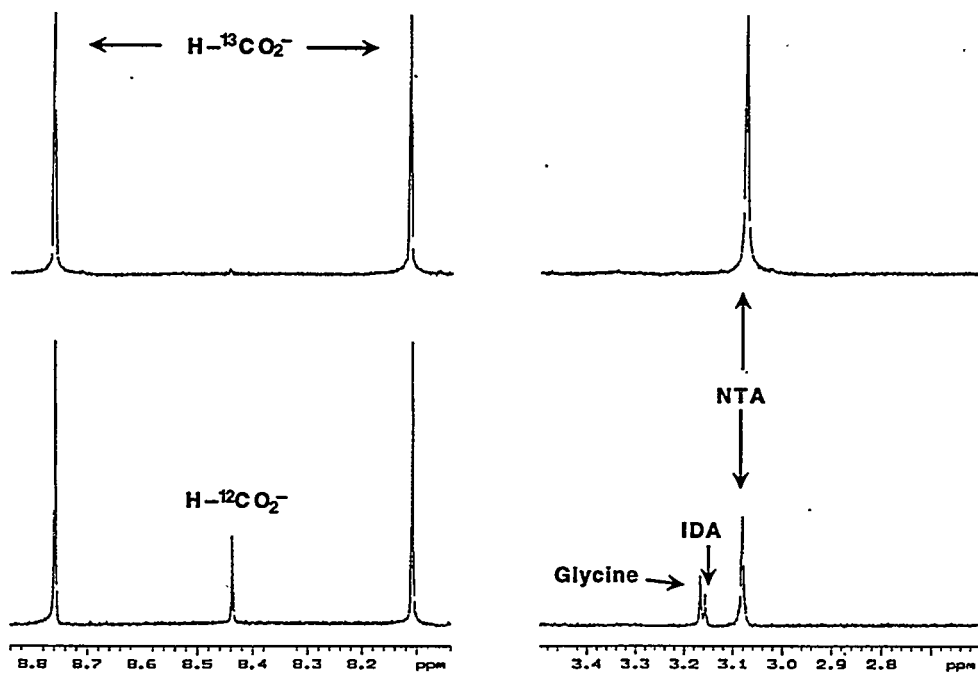
(c) Proton NMR resonances of unidentified products are present.

(d) NMR resonances of these compounds were not detected.

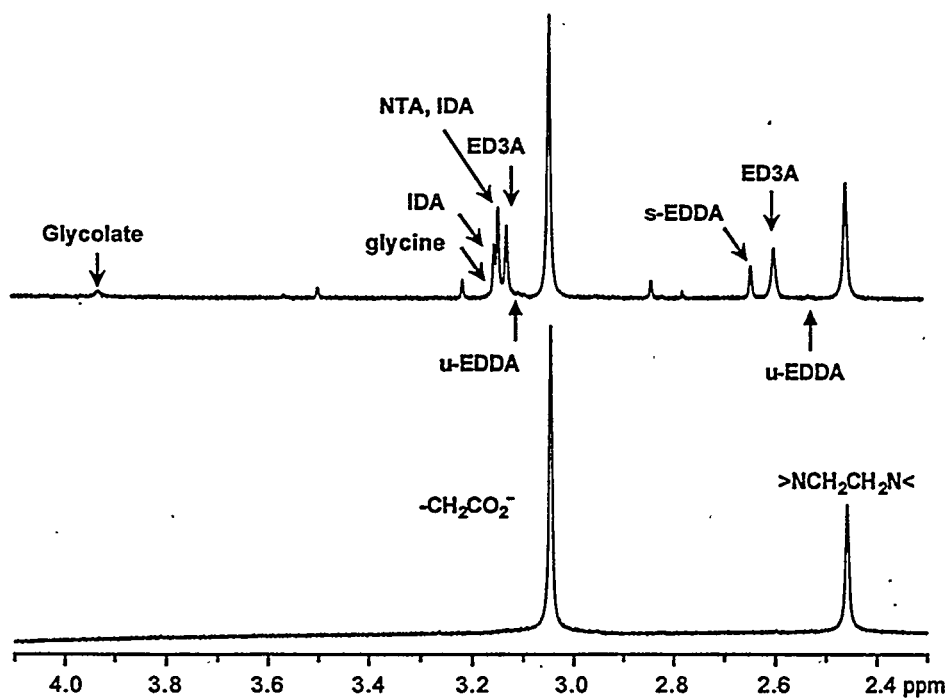
hydroxyethyl groups such as HEDTA (see Figure 3.12) are missing in Figure 3.11. The two small peaks near 3.5 ppm and 2.8 ppm are similar to peaks found after s-EDDA radiolysis. The peaks are currently unidentified but appear in positions that are similar to those of lactams.

Figure 3.12 shows the <sup>1</sup>H NMR spectra of a nitrate/nitrite/hydroxide solution of HEDTA before and after  $\gamma$  radiolysis. The major identified products of the HEDTA radiolysis are s-EDDA and IDA. Other major products have not been identified but are consistent with the N-hydroxyethyl group. The hydroxyethyl group of HEDTA shows up as two triplets in the <sup>1</sup>H NMR spectrum at 3.6 and 2.56 ppm, respectively. After radiolysis these triplets are much smaller, and new multiplets appear just downfield from the original HEDTA triplets. These multiplets may be overlapping triplets from isomers of hydroxyethylethylenediamine diacetate and hydroxyethylenediaminemonoacetate in Figure 3.13.

The EDDA product mixtures contained IDA and formate as the major products. A major product tentatively identified as EDMA was found in the s-EDDA but not u-EDDA mixture. Glycine was a minor product, and only trace quantities of acetate and glycolate were formed. No products other than formate could be identified from the <sup>1</sup>H NMR spectra of irradiated solutions of citrate, succinate, butyrate, butanol, and DBP.



**Figure 3.10.**  $^1\text{H}$  NMR Spectra Showing that NTA Degrades to IDA and Glycine During  $\gamma$  Radiolysis in Nitrate/Nitrite/Hydroxide Solution. Top spectrum, unirradiated sample; bottom spectrum, irradiated sample,  $\sim 8$  Mrad dose.



**Figure 3.11.**  $^1\text{H}$  NMR Spectra of EDTA before (bottom) and after (top)  $\gamma$ -Radiolysis in 2 M  $\text{NaNO}_2$ , 2 M  $\text{NaNO}_3$ , 2 M  $\text{NaOH}$  Solution; 18.4 Mrad Dose

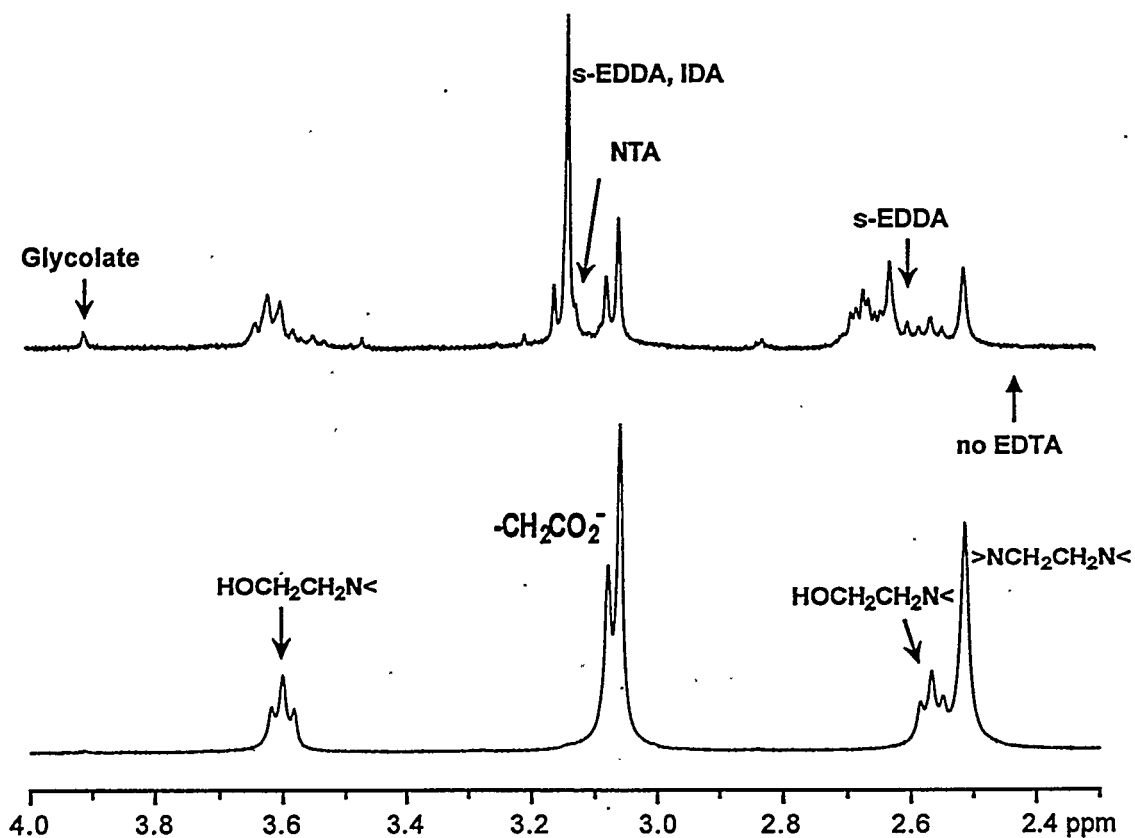


**Figure 3.12.** Proton NMR Spectra of HEDTA before (bottom) and after  $\gamma$  Radiolysis (top) in Nitrate/Nitrite/Hydroxide Solution (dose was 18.4 Mrad)

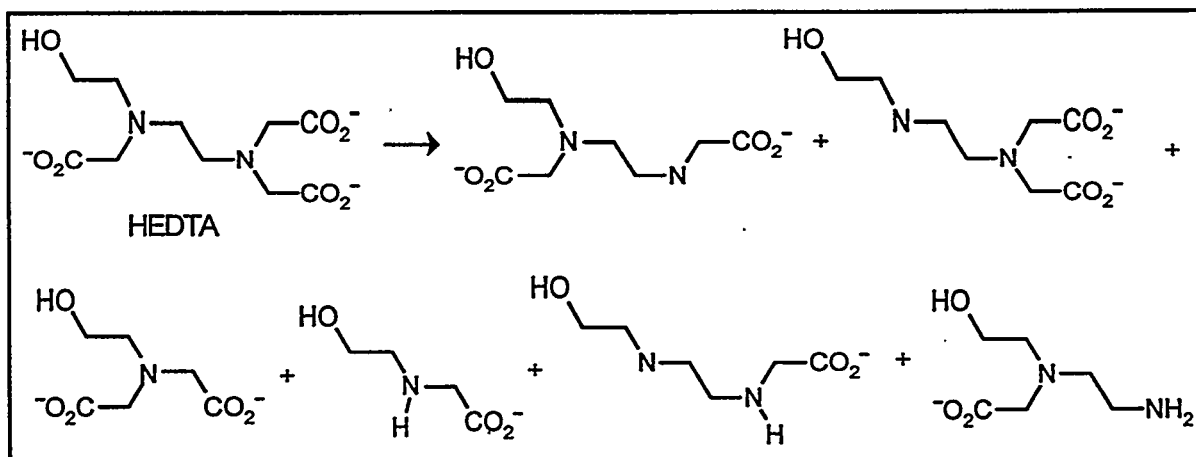


**Figure 3.13.** Structures Consistent with Hydroxyethylene Resonances in  $^1\text{H}$  NMR Spectra of  $\gamma$  Irradiated HEDTA Solutions (see Figure 3.12)

### 3.4 Experimental Section

Organic compounds were purchased from chemical suppliers with the exception of u-EDDA, which was provided by JA Campbell (PNNL). The purity of all compounds was established by  $^1\text{H}$  NMR. The water used in these experiments was purified using a Millipore deionization system; irradiations were performed in the PNNL High Dose  $^{60}\text{Co}$  Facility or the PNNL  $\gamma$  Facility.

The High Dose  $^{60}\text{Co}$  Facility is located in the 331 Building in the Hanford Site 300 Area. The irradiator, a Model Gammabeam 650 manufactured by Nordion International Inc., is located within a concrete vault that is 7.6 by 7.6 by 3.0 m high and has an adjacent control room. Cable raceways between the vault and control room are available for real-time monitoring of the test sample(s). Twelve vertical stainless steel source tubes are arranged in a circular array. The sources are operated pneumatically, and irradiations can be terminated using a preset timer. For irradiation of samples in the center of the array, the diameter can be adjusted from 12 to 80 cm. Each source tube contains from 115 to 7700 curies of  $^{60}\text{Co}$ . Dose rates from 3 rad/h up to 2.5 Mrad/h can be obtained. The facility can accommodate sample sizes of  $\sim 1\text{ m}^3$  (35  $\text{ft}^3$ ). For our experiments, all 12 sources were arrayed in a circle with a diameter of 24 cm, providing a nominal dose rate of  $6 \times 10^5$  rad/h. Three polyethylene cups (6.5 cm high by 10 cm diameter) were stacked in the center of the source array. Each cup was loaded with 3–4 samples (7-mL vials containing 2 mL test and/or dosimetry solutions). Fricke dosimetry demonstrated that the  $\gamma$  field was homogeneous, with dose rates within each cup varying by 1 to 3%.

The PNNL  $\gamma$  Irradiation Facility<sup>(a)</sup> is in the 3730 Building in the Hanford 300 Area. It contains 37 stainless steel irradiation tubes in a 2.13-m-diameter by 4.19-m-deep stainless steel in-ground tank. Two arrays of  $^{60}\text{Co}$   $\gamma$ -sources with a combined inventory of  $1.184 \times 10^{16}$  Bq are near the bottom of the tank. For radiation shielding purposes, the tank is completely filled with water, and a concrete wall, 1.1 m in height, surrounds the top of the tank. The irradiation tubes, which are sealed on the bottom, range in length from 4.9 to 5.5 m and in diameter from 4.6 to 5.1 cm. The irradiation fluxes of the tubes range from 2 to  $2 \times 10^6$  rad/h. The uniform flux region is 15.2 cm from the tubes closest to the sources and more than 30.5 cm from the tubes farthest from the sources. Samples are lowered into the tubes to a depth that yields the desired dose rate.

#### 3.4.1 Sample Preparation

In a typical procedure, stock solutions containing  $\text{NaNO}_3$ ,  $\text{NaNO}_2$ , and  $\text{NaOH}$  were prepared, sparged with  $\text{N}_2$ , and transferred to an inert atmosphere glovebox. Sample solutions were prepared by dissolving the solid organic and  $\text{NaHCO}_2$ , when desired, in stock solutions in 10 mL volumetric flasks. An autopipet was used to deliver 2 mL of the sample solutions to each of three or four 7-mL vials. Vials fitted with polyethylene-lined caps were sealed tight, removed from the glovebox, and arranged in polyethylene cups that served as sample holders. Samples were irradiated for times ranging from 9 to 30 hours in the High Dose Facility or up to 11 days in the PNNL  $\gamma$  Facility before being removed and analyzed. Tables A.1–A.3 (Appendix A) lists

---

(a) <http://www.pnl.gov/gamma/>

sample concentrations, irradiation schedules, and absorbed doses. Exceptions to the above procedures include EDTA scoping experiments (Figure 3.3, Table 3.1 entry 2; and Appendix A, Table A.1) that were performed in 5-mm-o.d. NMR tubes without N<sub>2</sub> purge and scouting experiments for HEDTA and glycolate (Table 3.1 entries 4 and 8, respectively) that were run in glass vials without N<sub>2</sub> purge. In the latter, vials were filled to capacity. Selected samples were also analyzed by ion-pair liquid chromatography (IPC) or ion chromatography (IC) to confirm the NMR results. The IC and HPLC methods are described in Section 4.3.2.

### 3.4.2 NMR Analysis

The relative rates of substrate disappearance compared with formate were determined by <sup>1</sup>H and/or <sup>13</sup>C NMR spectroscopies. In FY97 experiments (MH sample numbers in Table A.2, Appendix A), a 0.50-ml aliquot of the homogeneous sample solution was transferred to a 5-mm o.d. NMR tube along with 0.10 ml of a caustic (2.0 M NaOH) deuterated water solution containing 0.040 M 2,2-dimethylmalonic acid (an internal chemical shift and integration standard). In FY98 experiments (ML sample numbers in Table A.2, Appendix A), 0.20 mL of the irradiated sample solution was dried under a nitrogen stream at room temperature. The solid was then redissolved using 0.60 mL of a deuterium oxide solution containing 0.00184 M 2,2-dimethylmalonic acid. The three-fold dilution of the sample promoted dissolution of oxalate ion.

<sup>1</sup>H (300 MHz) and carbon (75 MHz) NMR spectra were recorded using a Varian VXR-300 NMR spectrometer. The following conditions for recording <sup>1</sup>H NMR spectra gave reproducible and quantitative results: 9° pulse, 7-second acquisition time, 1-second recycle time. The number of transients collected depended on the concentrations of the species; the minimum number was 200. The spectra were carefully integrated to eliminate any contribution from the <sup>1</sup>H signal between 5.5 and 4 ppm due to protonated water. The following conditions for recording <sup>1</sup>H decoupled <sup>13</sup>C NMR spectra gave reproducible and quantitative results: 70° pulse, acquisition time of 1.8 seconds, and recycle time of 60 seconds. A line broadening of 1 Hz was used to process each spectrum. The relative areas of the formate-<sup>13</sup>C and carbonate-<sup>13</sup>C peaks were used to calculate the conversion of formate-<sup>13</sup>C. The contribution to the NMR signal from natural abundance <sup>13</sup>C from formate or carbonate produced by radiolysis of other organic species was negligible in all cases. The reproducibility of triplicate spectral collections of the same sample was ±4%; triplicate reintegration of the same spectrum routinely gave reproducibility of ±1%. Product identifications were made by comparing the <sup>1</sup>H NMR spectra of authentic samples of potential products collected in the same reaction medium as the radiolytic experiments.

### 3.4.3 Fricke Dosimetry

Dose rates were determined by Fricke dosimetry (Draganic and Draganic 1971; Spinks and Woods 1964) using the same reaction vials and irradiation methods used in aging experiments. The dosimetry solution contained 0.01 M Fe(NH<sub>4</sub>)<sub>2</sub>(SO<sub>4</sub>)<sub>2</sub> and 0.001 M NaCl in 0.4 M H<sub>2</sub>SO<sub>4</sub>. The solution was purged with oxygen and placed in 7-mL glass capped vials. For the High Dose Rate Facility, vials containing the Fricke solution were arranged in polyethylene cups with identical vials containing sample solutions and irradiated for four minutes at the beginning of the irradiation run. For the PNNL  $\gamma$  Irradiation Facility, vials were arranged in an Inconel vessel,

lowered into the irradiator, and removed after 15, 30, or 60 minutes. A control solution was handled identically but was not irradiated. The concentration of Fe(III) formed was determined with use of a Cary 3E UV/Vis spectrophotometer. Doses absorbed by aging samples were calculated using appropriate corrections for solution density.

#### 3.4.4 Calculation of Radiolytic Yields

Radiolytic yields were calculated using Equation 3.13:

$$G(S) = \frac{\Delta M_s}{\text{dose} \times \rho} 965 \text{ molecules} / 100 \text{ eV} \quad (3.13)$$

where  $\Delta M_s$  is the measured change in molar concentration of a species,  $S$ , for an absorbed dose (Mrad) in a solution of density  $\rho$  (g/ml), and 965 converts units of moles/kg/Mrad to molecules/100 eV. Accordingly, the modeled radiolytic yields were determined from the predicted yield of carbonate as a function of time at a given dose rate. Table 3.3 compares the experimentally measured yield with the yield predicted by the formate model shown in Table 3.2.

#### 3.4.5 Mechanistic Kinetic Modeling

Two well-documented kinetic modeling approaches were used to run the models depicted in Tables 3.2 and 3.4: *Acuchem* (Braun 1988) and *GEAR* (Weigert and McKinney 1986).<sup>(a)</sup> *Acuchem* and *GEAR* are PC/DOS-based programs that output concentrations of species versus time for a user-specified isothermal chemical kinetic model (reaction steps and rate constants) from a set of initial concentrations. *Acuchem* provides an internal switch that permits the concentration of species to be output at 50 equally spaced times or at user-specified times. This latter feature was used to test the model against experimental data and to calculate predicted yields as in Tables 3.3 and 3.5 (also, Tables A.4 and A.5 in Appendix A). The former feature is useful for generating graphs with experimental data superimposed on model results, as in Figure 3.5. The output provided by *GEAR* is limited to monitoring no more than four species in a given analysis. However, the output varies the step size so that small steps are used early in the reaction, when concentrations are changing more rapidly. *GEAR* was used to examine the time-dependent reactivity of the transient intermediates. The output allows observation of the approach to steady-state concentrations of intermediates such as NO and NO<sub>2</sub> radicals, as in Figure 3.6.

Some rate constants in the models ( $k_{13}$  and  $k_{28}$  in Table 3.2 and  $k_{32}$  and  $k_{33}/k_{34}$  in Table 3.4) were adjusted to fit experimental data; the optimum fit was found by minimizing the sum of squared deviations,  $R(d)$ , between experimental,  $y_i$ , and calculated data points,  $f(t)$  (Equation 3.14).

---

(a) The *GEAR* program was adapted by TE Beukelman (EI du Pont de Nemours & Co.) from HAVCHEM (Stabler and Chesick 1978).

$$R(d)^2 = \sum_i [f(t_i) - y(t_i)]^2 \quad (3.14)$$

For the formate model,  $y(t_i)$  values are carbonate concentrations at times,  $t$ , under the seven different conditions listed in Table 3.3 (see also Appendix A, Table A.4). For the glycine model, deviations in concentrations of glycine, formate, carbonate, and oxalate (Appendix A, Table A.5) were included in the calculation of  $R(d)^2$  (Equation 3.15).

$$R(d)^2 = \sum_{ij} [f_j(t_i) - y_j(t_i)]^2 \quad (3.15)$$

The rates of formation of primary radiolytic radicals OH, H, and  $\text{NO}_3^{2-}$  were estimated for input to the models (Eq. 1–3 in Table 3.2). Equation 3.16 relates the rate of formation to dose rate of a sample.

$$\text{rate} = \text{radiolytic yield} \times \text{dose rate} \times \text{density} \times \text{conversion factor} \quad (3.16)$$

The conversion factor is  $1.04 \times 10^{-3} \frac{\text{moles/kg/Mrad}}{\text{molecules/100 eV}}$  when the units are M/s for rate, molecules/100 eV for radiolytic yield, Mrad/h for the dose rate, and kg/L for sample density.

#### 3.4.6 Calculation of Fractions of Formate and Glycine Oxidized by $\text{O}^-$ , OH, H, and $\text{NO}_2$

Tables 3.3 and 3.5 list the fractions of formate and glycine oxidized by radiolytically produced radicals. These fractions were estimated from the radiolytic yields of primary radicals (OH, H, and  $\text{NO}_3^{2-}$ ) and the reactions they undergo (Tables 3.2 and 3.4). According to the kinetic model, the radiolytic yield of carbonate,  $G(\text{CO}_3^{2-})_{\text{total}}$ , is the sum of contributions from H, OH,  $\text{O}^-$ , and  $\text{NO}_2$ :

$$G(\text{CO}_3^{2-})_{\text{total}} = G(\text{CO}_3^{2-})_{\text{H}} + G(\text{CO}_3^{2-})_{\text{OH}} + G(\text{CO}_3^{2-})_{\text{O}^-} + G(\text{CO}_3^{2-})_{\text{NO}_2} \quad (3.17)$$

where  $G(\text{CO}_3^{2-})_{\text{H}}$  is the yield of carbonate derived from H attack on formate,  $G(\text{CO}_3^{2-})_{\text{OH}}$  is the yield from OH attack,  $G(\text{CO}_3^{2-})_{\text{O}^-}$  is the yield from  $\text{O}^-$  attack, and  $G(\text{CO}_3^{2-})_{\text{NO}_2}$  is the yield of carbonate derived from  $\text{NO}_2$  attack. Each of the first three terms in Equation 3.17 may be evaluated analytically provided conversions are low so that initial concentrations may be used to estimate rates, and reactions of H, OH,  $\text{O}^-$ , and  $\text{NO}_2$  with products can be neglected. For example, the yield of carbonate,  $G(\text{CO}_3^{2-})_{\text{H}}$ , from formate ions that react with H is given by (Equation 3.18):

$$G(\text{CO}_3^{2-})_{\text{H}} = G(\text{H}) \frac{r_{10}}{r_9 + r_{10} + r_{27}} \quad (3.18)$$

where  $G(\text{H})$  is the radiolytic yield of H, and  $r_9$ ,  $r_{10}$ , and  $r_{27}$  are rates for the reactions listed in Table 3.2. The rate fraction is calculated from the respective reaction rate constants and initial concentrations of reactants, i.e., Equation 3.19.

$$\frac{r_{10}}{r_9 + r_{10} + r_{27}} = \frac{k_{10}[\text{HCO}_2^-]}{k_9[\text{NO}_2^-] + k_{10}[\text{HCO}_2^-] + k_{27}[\text{OH}^-]} \quad (3.19)$$

Substituting Equation 3.19 into Equation 3.18 gives Equation 3.20:

$$G(\text{CO}_3^{2-})_{\text{H}} = G(\text{H}) \frac{k_{10}[\text{HCO}_2^-]}{k_9[\text{NO}_2^-] + k_{10}[\text{HCO}_2^-] + k_{27}[\text{OH}^-]} \quad (3.20)$$

Analogous expressions give  $G(\text{CO}_3^{2-})_{\text{OH}}$  and  $G(\text{CO}_3^{2-})_{\text{O}^-}$  (Equation 3.21 and 3.22):

$$G(\text{CO}_3^{2-})_{\text{OH}} = G(\text{OH}) \frac{k_8[\text{HCO}_2^-]}{k_6[\text{OH}^-] + k_7[\text{NO}_2^-] + k_8[\text{HCO}_2^-]} \quad (3.21)$$

$$G(\text{CO}_3^{2-})_{\text{O}^-} = G(\text{O}^-) \frac{k_{12}[\text{HCO}_2^-]}{k_{11}[\text{NO}_2^-] + k_{12}[\text{HCO}_2^-]} \quad (3.22)$$

The  $G(\text{O}^-)$  is calculated from  $G(\text{OH})$  by Equation 3.23:

$$G(\text{O}^-) = G(\text{OH}) \frac{k_6[\text{OH}^-]}{k_6[\text{OH}^-] + k_7[\text{NO}_2^-] + k_8[\text{HCO}_2^-]} \quad (3.23)$$

The  $G(\text{CO}_3^{2-})_{\text{NO}_2}$  is estimated by combining Equations 3.17, 3.20, 3.21, and 3.22:

$$G(\text{CO}_3^{2-})_{\text{NO}_2} = G(\text{CO}_3^{2-})_{\text{total}} - G(\text{CO}_3^{2-})_{\text{H}} - G(\text{CO}_3^{2-})_{\text{OH}} - G(\text{CO}_3^{2-})_{\text{O}^-} \quad (3.24)$$

Analogous equations give the contributions radiolytic conversion of glycine:<sup>(a)</sup>

$$G(\text{glycine})_{\text{H}} = -G(\text{H}) \frac{k_{29}[\text{glycine}]}{k_9[\text{NO}_2^-] + k_{27}[\text{OH}^-] + k_{10}[\text{HCO}_2^-] + k_{29}[\text{glycine}]} \quad (3.25)$$

$$G(\text{glycine})_{\text{OH}} = -G(\text{OH}) \frac{k_{31}[\text{glycine}]}{k_6[\text{OH}^-] + k_7[\text{NO}_2^-] + k_8[\text{HCO}_2^-] + k_{31}[\text{glycine}]} \quad (3.26)$$

$$G(\text{glycine})_{\text{O}^-} = -G(\text{O}^-) \frac{k_{30}[\text{glycine}]}{k_{11}[\text{NO}_2^-] + k_{12}[\text{HCO}_2^-] + k_{30}[\text{glycine}]} \quad (3.27)$$

$$G(\text{O}^-) = G(\text{OH}) \frac{k_6[\text{OH}^-]}{k_6[\text{OH}^-] + k_7[\text{NO}_2^-] + k_{12}[\text{HCO}_2^-] + k_{30}[\text{glycine}]} \quad (3.28)$$

---

(a) Formate appears in the equations because a set of experiments with 2-<sup>13</sup>C-glycine also contained <sup>12</sup>C-formate (see Table 3.5).

$$G(\text{glycine})_{\text{NO}_2} = G(\text{glycine})_{\text{total}} - G(\text{glycine})_{\text{H}} - G(\text{glycine})_{\text{OH}} - G(\text{glycine})_{\text{O}} \quad (3.29)$$

## 4.0 Organic Aging Studies Using Waste Simulants

Aging tests were performed using a simulant that was developed for Fauske Associates, Incorporated (FAI) energetics and reactivity tests (Carlson and Babad 1996). The simulant, designated SIM-PAS-95-1c for FY 1996 studies and SIM-PAS-95-1d for FY 1997 studies, is a modified version of the SIM-PAS-94 simulant, which Scheele (1995) developed from B-plant chemical inventories and process flow sheets.

The simulant (Table 4.1) is a heterogeneous mix of metal oxide/hydroxide precipitates and aqueous solutions containing a variety of inorganic anions, mainly nitrate, nitrite, and hydroxide, and the organic complexants HEDTA, EDTA, citrate, and glycolate. The density is  $\sim 1.27$  g/mL and the carbon content is 21 g/L or 4.5 wt% (dry basis). The SIM-PAS-95-1d simulant has the same components as SIM-PAS-95-1c, although the concentration of EDTA was lower and that of glycolate was higher.

Aging tests were run over a variety of radiation doses, temperatures, and cover gas compositions of either pure Ar or 20/80 O<sub>2</sub>/Ar. The simulant was also heated at 90°C for up to eight months under cover gases that started out as either pure Ar or 20/80 O<sub>2</sub>/Ar. To foster reproducible results, the simulant was prepared before each irradiation by measuring exact quantities of three homogeneous stock solutions into the reactor vessel (see Section 4.3). The same vessel was used for each irradiation, and it was placed in the same location relative to the radiation source. The radiation flux was  $3 \times 10^5$  rad/h. After irradiation, the contents of the vessel were quantitatively transferred and analyzed for organic compounds carbonate, nitrate, and nitrite. In addition, another sample of the simulant was mixed and then analyzed without having been irradiated. Additional experimental information is provided in Section 4.3.

**Table 4.1.** Target Composition of SIM-PAS-95-1c and -1d Simulants

Species	mg/g	Species	mg/g	Species	mg/g
HEDTA <sup>3-</sup>	16.9	Al <sup>3+</sup>	1.493	Ca <sup>2+</sup>	0.080
EDTA <sup>4-</sup>	3.1	F <sup>-</sup>	1.281	Mn <sup>2+</sup>	0.068
Citrate <sup>3-</sup>	17.3	Pb <sup>2+</sup>	1.066	Cr <sup>3+</sup>	0.044
Glycolate	11.3	PO <sub>4</sub> <sup>3-</sup>	0.507	Cl <sup>-</sup>	0.004
NO <sub>3</sub> <sup>-</sup>	109	SO <sub>4</sub> <sup>2-</sup>	0.506	Pd <sup>2+</sup>	0.003
Na <sup>+</sup>	107	Bi <sup>2+</sup>	0.419	Rh <sup>3+</sup>	0.003
OH <sup>-</sup>	39.3	Ce <sup>3+</sup>	0.377	Ru <sup>4+</sup>	0.003
NO <sub>2</sub> <sup>-</sup>	37.9	Ni <sup>2+</sup>	0.099	H <sub>2</sub> O	640
Fe <sup>3+</sup>	2.61				

## 4.1 Results

Section 4.1 presents analytical results showing how organic aging is affected by temperature, time, radiolytic dose, and O<sub>2</sub> in the cover gas. Section 4.2 uses the data to show how nitrate reaction enthalpies ( $\Delta H_r$ ) and TOC of the simulant change with radiation dose and thermal exposure. This latter treatment of the data is of particular interest because energy content and TOC are used to screen wastes for the likelihood of propagating reactions in tanks. Section 4.3 describes experimental procedures. Tables in Appendix B list the results of analyses performed. Species analyzed include HEDTA, EDTA, glycolate, citrate, oxalate, formate, carbonate, nitrate, nitrite and ammonia. Gases analyzed in the headspace above the aged mixtures include Ar, O<sub>2</sub>, N<sub>2</sub>, N<sub>2</sub>O, H<sub>2</sub>, CO, CO<sub>2</sub>, and CH<sub>4</sub>.

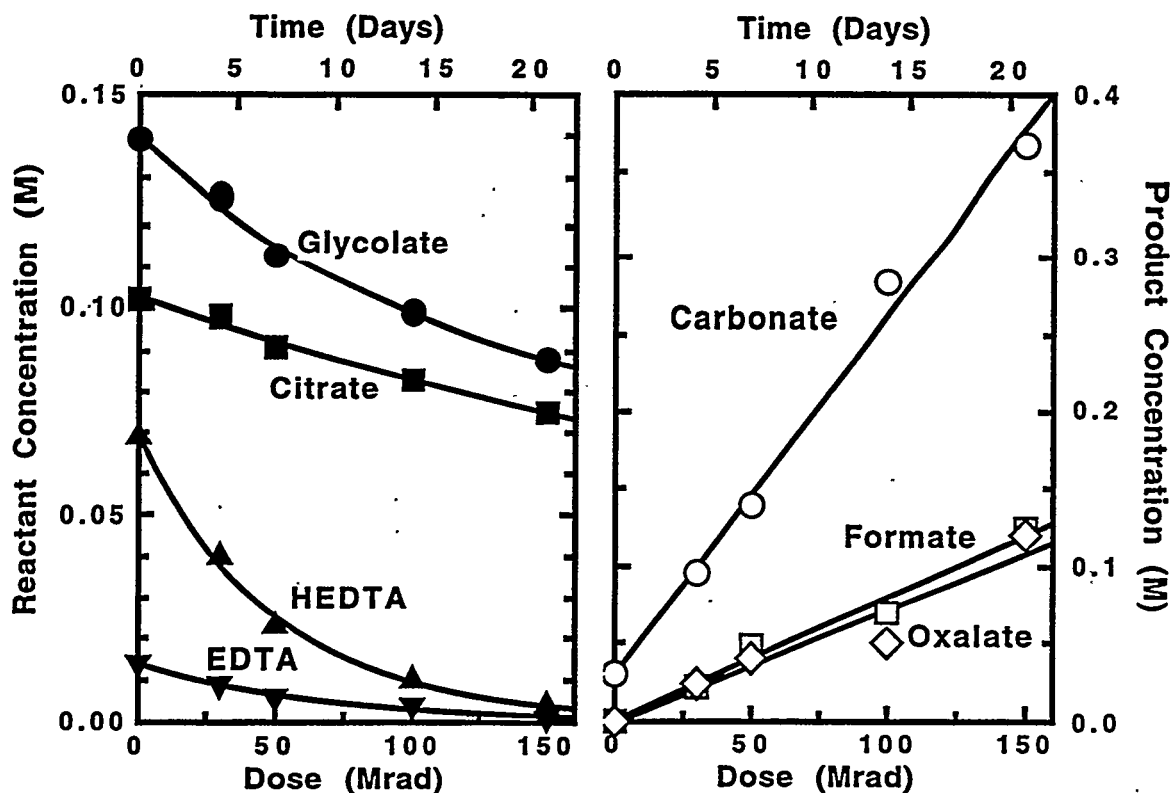
### 4.1.1 Effect of Radiation Dose on Aging

Figure 4.1 shows the disappearance of starting organic species and appearance of oxalate, formate, and carbonate as a function of radiation dose and time at 70°C. The results show that all the complexants and their remnants are susceptible to radiolytic degradation. The kinetic life-times obtained from fitting species concentrations to exponential decay functions ( $C=C_0e^{-t/\tau}$ ) suggest that reactivities of complexants decrease in the order HEDTA>EDTA>glycolate>citrate.<sup>(a)</sup> Similar results were obtained for runs at 40 and 90°C. The results also show that highly oxidized products grow in without delay. Nitrate decreases with increasing dose, while nitrite and ammonia increase (see Tables B.1, B.3, and B.4). And gaseous products H<sub>2</sub>, N<sub>2</sub>O, and N<sub>2</sub> accumulate in the headspace above the aged simulant (see Table B.10). These reaction products are all consistent with radiolysis-induced redox chemistry in which organic species are *reductants* and radiolytically generated species (O<sup>-</sup> and NO<sub>2</sub>) are *oxidants*.

The species listed in Figure 4.1 represent more than 75% of the organic carbon present in the aged simulants. Figure 4.2 shows how radiolytic aging affects the concentrations of organic carbon in the simulants at 70 and 90°C. The figure plots the concentrations of carbon in formate and oxalate, the starting species (glycolate, citrate, EDTA, and HEDTA), and unspciated or missing carbon, i.e., the difference of total carbon at start less total carbon at time, t. Tables B.1–B.4 contain the data used to generate these plots and provide similar data for other temperatures and conditions. This missing carbon is thought to largely be associated with chelator fragments such as ED3A, NTA, IDA, and EDDA. These particular species were identified by GC-MS analyses and by ion pair-liquid chromatography, but amounts were not quantified. Small amounts of acetic and succinic acids were detected by ion chromatography in irradiated simulants (see Tables B.1–B.4 in Appendix B).

---

(a) For example, half-lives in a 0.3 Mrad/h  $\gamma$  field at 70°C (Appendix B, Table B.2) were HEDTA: 7.7 days; EDTA: 9.3 days; glycolate: 43 days; citrate: 66 days. These rate data correspond to relative reactivities (HEDTA:EDTA:glycolate:citrate) of 8.6:7.1:1.5:1.



**Figure 4.1.** Disappearance of Complexants and Appearance of Products in a Radiation Field of  $\sim 3 \times 10^5$  rad hr<sup>-1</sup> at 70°C; headspace gas is initially 20/80 O<sub>2</sub>/Ar

As shown in Figure 4.2, the amounts of missing carbon goes through maximum values of  $\sim 25$  and  $\sim 15\%$  at  $\sim 100$  Mrad at 70 and 90°C, respectively. The lower amounts of missing carbon in 90°C experiments are probably due to the more rapid consumption of intermediate compounds and the fact that less EDTA was used in the simulant. Carbonate production at 90°C is nearly twice as fast as at 70°C (see Figure 4.1). The disappearance of carbon in starting species appears biexponential at 70° and exponential at 90°C. This behavior may be due to the higher fraction of glycolate in the 90°C, PAS-95-1d simulant.

#### 4.1.2 Effect of Temperature on Radiolytic Aging

Aging tests were run at 40, 70, and 90°C to evaluate the effect of temperature on radiolytic aging. Table 4.2 lists results for samples that received  $\gamma$  doses of 40 to 50 Mrad. The effects on disappearance of the chelators seem small and may be masked by experimental scatter. Amounts of glycolate, citrate, HEDTA, and EDTA found at 40 and 70°C are similar. At 90°C, less glycolate is present compared to 70°C, but the amounts of HEDTA and citrate present at 90°C are greater than at 70°C. The formate, oxalate, and carbonate products show a trend of increasing yield with increasing temperature. The results imply that rates of disappearance of chelators are controlled by the intensity of the radiation field (i.e., dose rate), whereas formation of products depends on thermally activated "ionic" processes (e.g., hydrolyses) that convert intermediates to

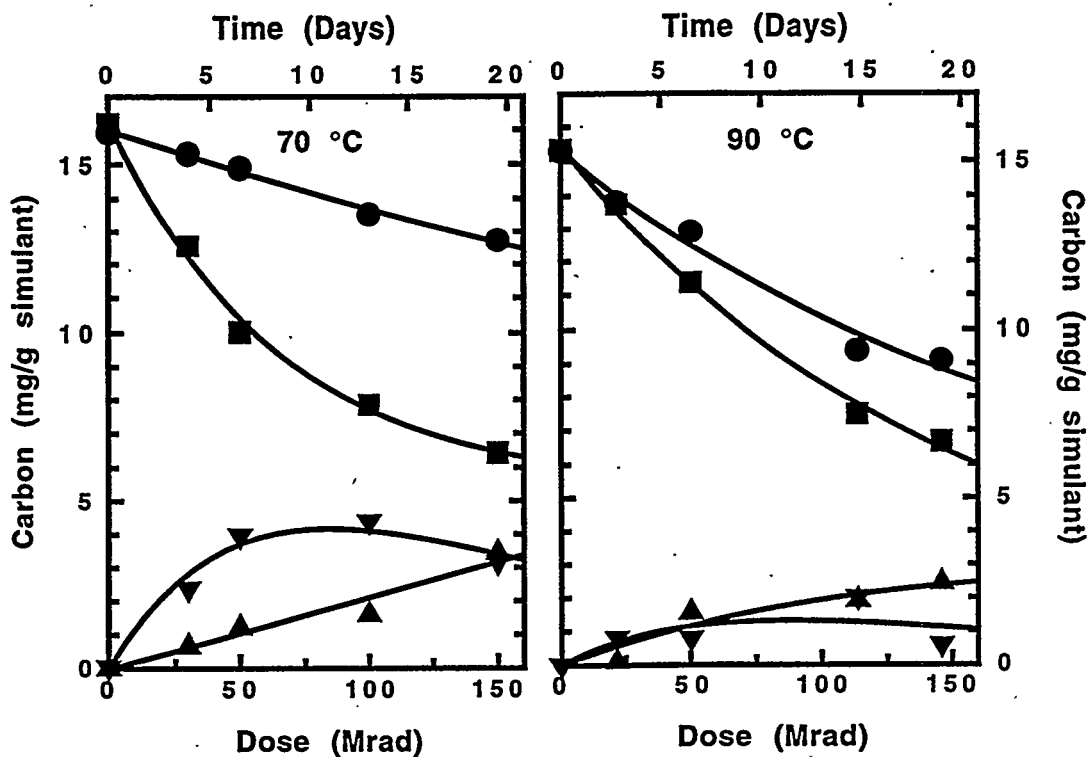


Figure 4.2. Plots of Carbon Content Versus Dose for 70 and 90°C Irradiations:  
 (●) Organic Carbon, (■) Carbon in Organic Starting Compounds,  
 (▲) Oxalate and Formate Carbon, (▼) Carbon in Other Organic  
 Compounds, e.g., ED3A, NTA, and IDA

end products. Consistent with this view, the fraction of unidentified carbon (subtract total carbon values in lines 2, 3, or 4 from line 1, Table 4.2) decreases with increasing temperature. Gas analyses show an increase in the yield of H<sub>2</sub> on going from 70 to 90°C. These analyses are summarized in Figure 4.3 (Tables B.7 and B.8).

Table 4.2. Effects of Temperature on Radiolytic Aging of SIM-PAS-95-1d

T, Dose (°C, Mrad)	Reactants/Products, mg C/g								
	Formate	Oxalate	Glycolate	Citrate	HEDTA	EDTA	CO <sub>3</sub> <sup>2-</sup>	Org C	Total
20°, 0	0.00	0.00	3.7	5.6	6.5	0.80	0.16	16.5	16.7
40°, 43	0.14	0.34	3.3	4.7	1.9	0.36	1.1	10.8	12.0
70°, 47(a)	0.21	0.41	3.3	5.0	1.8	0.38	1.4	11.1	12.5
90°, 50	0.52	1.0	2.7	5.7	2.6	0.37	1.7	12.9	14.7

(a) Average of two runs (see Tables C.1, C.7, and C.9).

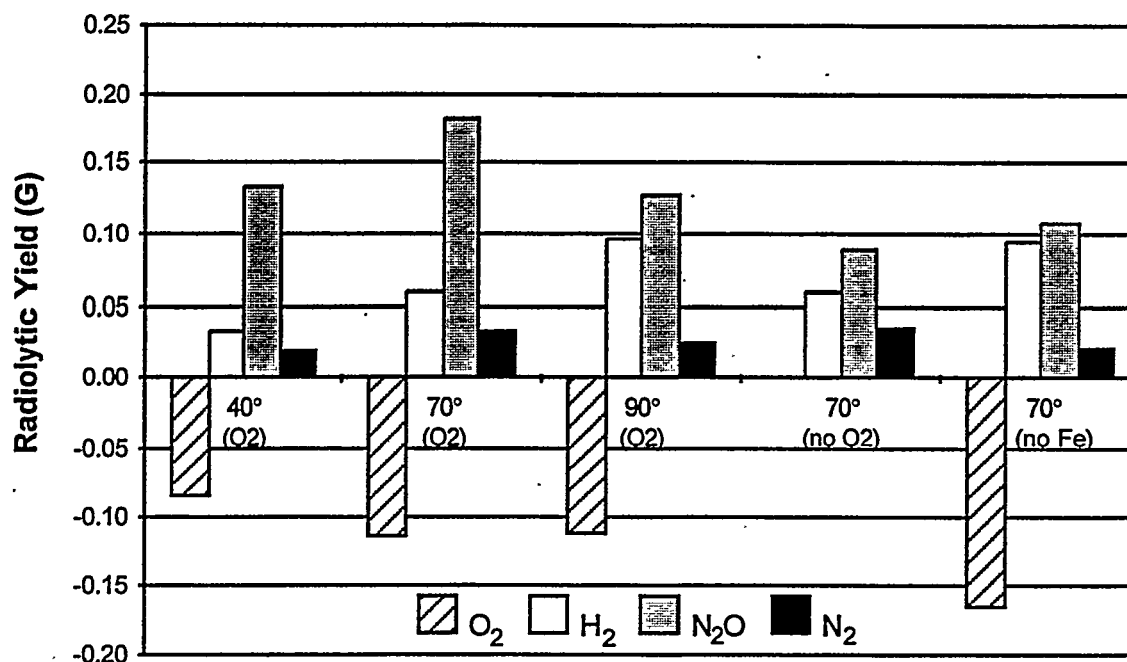
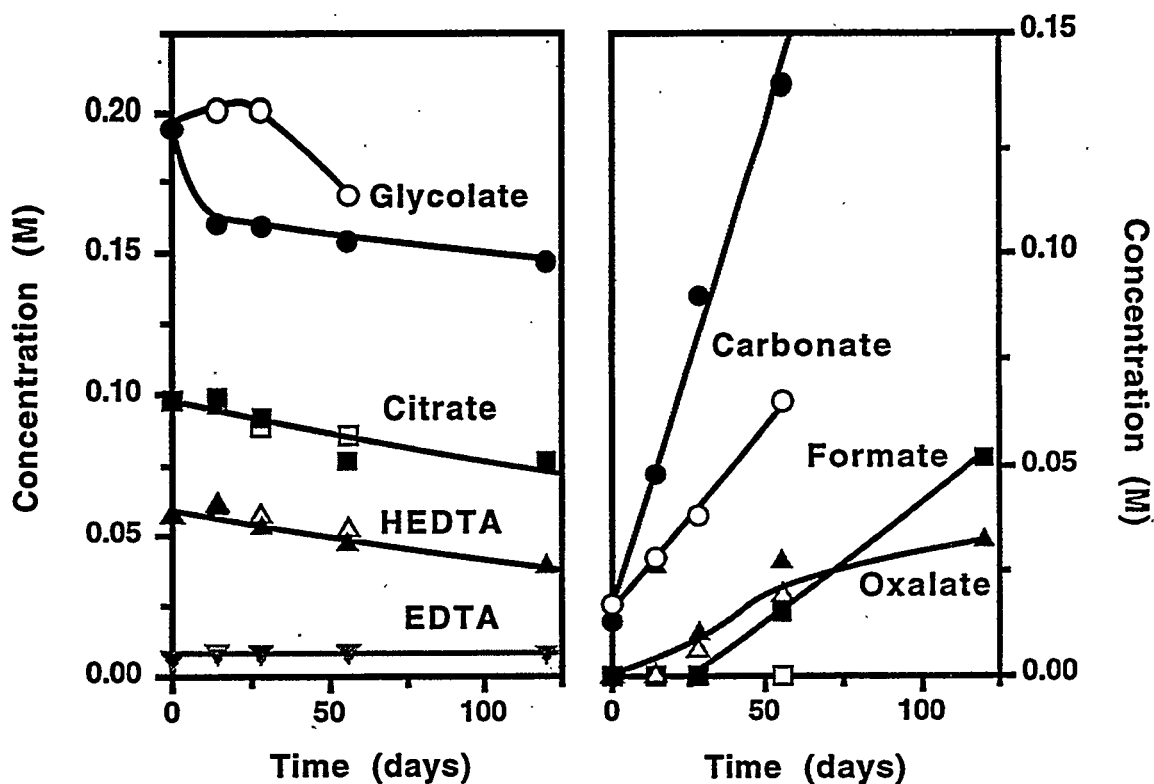


**Figure 4.3.** Effects of Temperature and Initial O<sub>2</sub> Concentration in Headspace Gas on Radiolytic Yields of Gases. (O<sub>2</sub>), starting with 20/80 O<sub>2</sub>/Ar; (no O<sub>2</sub>), starting with 100% Ar; (no Fe), starting with 20/80 O<sub>2</sub>/Ar and simulant prepared by substituting water for Fe(III) solution (see Section 4.3 and Table 4.6)

The bar chart in Figure 4.3 shows the radiolytic yields (G) in molecules/100 eV of O<sub>2</sub>, H<sub>2</sub>, N<sub>2</sub>O, and N<sub>2</sub> at 40, 70, and 90°C. The yield of H<sub>2</sub> increases from G~0.03 at 40°C to G~0.1 at 90°C. We noted a similar trend for H<sub>2</sub> production from radiolytic aging of simulant SY1-SIM-94C (Camaioni et al. 1996, 1995). This trend may indicate that reaction paths to H<sub>2</sub>-producing aldehyde intermediates are favored by higher temperatures. Formaldehyde and glyoxal degrade in alkaline solutions with irradiation producing H<sub>2</sub> (Ashby et al. 1993, 1994; Meisel et al. 1993; Karpoor et al. 1995). Finally, we mention that yields of H<sub>2</sub> are relatively unaffected by either the presence or absence of O<sub>2</sub> in the headspace gas or Fe in the simulant. These results will be discussed in Section 4.1.4.

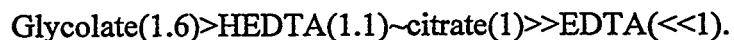
#### 4.1.3 Results for Thermal Aging of the Simulant

Figure 4.4 shows how the organic composition of the simulant changes with time at 90°C in the absence of  $\gamma$  radiation. Note that the time scale for thermal aging in Figure 4.4 is significantly longer than that for radiolytic aging in Figure 4.1 (120 days in the former, 20 days in the latter). Even after heating for three months at 90°C, negligible EDTA has reacted. *Thus, the degradation of organic species observed in Figure 4.1 is mainly caused by radiolysis.*

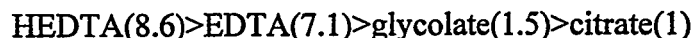


**Figure 4.4.** Disappearance of Starting Organic Compounds and Appearance of Products Versus Time at 90 °C in the Absence of  $\gamma$  Radiation; key: (filled symbols) headspace gas initially 20/80 O<sub>2</sub>/Ar, (open symbols) headspace gas initially 100% Ar

The relative reactivities of organic species toward thermal degradation are significantly different than those observed for radiolytic aging. Thermal rate constants for disappearance show the following trend (relative reactivities in parentheses):<sup>(a)</sup>



Whereas radiolytic reactivities (see Table 3.1 and Section 4.1.1) decrease in the order:



Thermal reactivities of citrate and EDTA are the inverse of their radiolytic reactivities. Under actual tank waste storage conditions, radiolytic dose rates are ~1000 times smaller than those used to obtain the results shown in Figure 4.1. Therefore, the time to achieve similar doses in tank wastes will be about 1000 times longer—several decades. Tank waste storage times are about 100 times (17 years = 6200 days) longer than times shown in Figure 4.4. Thus, thermally activated processes may contribute to organic aging of tank wastes and cause complexants to age

(a) Pseudo-first order lifetimes (t) in solutions with 20/80 O<sub>2</sub>/Ar cover gas: glycolate (~210 days), HEDTA (290 days), and citrate (330 days).

more uniformly than might be indicated by Figure 4.1. The results suggest that lifetimes and aging rates of organic complexants will strongly depend on the radiolytic and thermal history of individual tank wastes.

#### 4.1.4 Effects of O<sub>2</sub> and Fe on Aging

The effects of O<sub>2</sub> on thermal and radiolytic aging were explored by running tests with and without O<sub>2</sub> cover gas. Thermal aging tests were run at 90°C for times of up to two months. Radiolytic aging tests were run at 70°C with  $\gamma$  doses of ~50 Mrad. The initial compositions of the cover gas were either 20/80 O<sub>2</sub>/Ar or 100% Ar. At the end of the experiments, the headspace gas was sampled (see Section 3.2 and Table 3.8) and analyzed for O<sub>2</sub>, H<sub>2</sub>, N<sub>2</sub>O, N<sub>2</sub>, and Ar.

##### 4.1.4.1 Effects of O<sub>2</sub> and Fe on Radiolytic Aging

Table 4.3 shows organic and carbonate speciation results for radiolytically aged samples. The results suggest that there is little effect on the distribution of analytes whether O<sub>2</sub> is initially present or absent in the headspace. The differences do not significantly exceed experimental scatter. The experiments with 20/80 O<sub>2</sub>/Ar had 15.8 mmol of gas (3.2 mmol O<sub>2</sub>) in the headspace. Assuming a radiolytic yield of 6 molecules/100 eV of oxidizing radicals, a 47 Mrad dose yields 29 mmol of oxidizing radicals. Even if all of these attacked the complexants making organic radicals, there would only have been enough oxygen to scavenge 40% of radicals. Leaving Fe out of the simulant does not strongly affect the distributions either.

Headspace gas analyses (see Figure 4.3 and Tables B.7 and B.8) show O<sub>2</sub> was consumed when initially present. When O<sub>2</sub> was initially absent, small quantities were generated. Relatively more O<sub>2</sub> is consumed at 70° than at 40 or 90°C; however, the yield at 90° is based on data for a sample that was dosed with 146 Mrad. We observed in previous aging studies with SY1-SIM-94C that O<sub>2</sub> levels in the headspace reached steady state during irradiation that increased with

**Table 4.3** Effects of O<sub>2</sub> on Radiolytic Aging of SIM-PAS-95-1d at 70°C(a)

Conditions	Reactants/Products, M						
	Formate	Oxalate	Glycolate	Citrate	HEDTA	EDTA	CO <sub>3</sub> <sup>2-</sup>
Initial	0.000	0.000	0.20	0.098	0.057	0.0068	0.011
20/80 O <sub>2</sub> /Ar <sup>(b)</sup>	0.022	0.031	0.17	0.088	0.018	0.0040	0.11
100% Ar <sup>(b)</sup>	0.025	0.022	0.18	0.090	0.022	0.0040	0.10
No Fe <sup>(c)</sup>	0.042	0.020	0.18	0.089	0.025	0.0034	0.13

(a) From data in Appendix B, Table B.2; 47 Mrad dose, 0.3 Mrad/h dose rate.

(b) Average of two runs.

(c) Simulant prepared by substituting water for Fe(III) solution (solution 2 in Table 3.7); initial composition of headspace gas was 20/80 O<sub>2</sub>/Ar.

temperature (Camaioni et al. 1996). Steady state was achieved with a dose of 20 Mrad at 90°C. So, yields derived from such a large dose might be artificially low. Effects on H<sub>2</sub> and N<sub>2</sub> yields were negligible; however, less N<sub>2</sub>O was produced when O<sub>2</sub> was absent at start.

The effects of Fe on radiolytic aging are modest. Approximately 25% more HEDTA is consumed when Fe is present than when it is absent (O<sub>2</sub> and other simulant constituents present in both cases), more formate is produced, and relatively less oxalate is produced. Headspace gas analyses showed that leaving Fe out of the simulant caused increased consumption of O<sub>2</sub>, increased production of H<sub>2</sub>, and decreased production of N<sub>2</sub>O (see Figure 4.3 and Tables B.7 and B.8). Taken together, the results may suggest a synergistic effect of Fe and O<sub>2</sub> on the rate of HEDTA degradation and gas generation under radiolytic conditions.

#### 4.1.4.2 Effects of O<sub>2</sub> on Thermal Aging

Figure 4.4 shows results for aging in the presence and absence of O<sub>2</sub>. These results show a significant effect on glycolate. When O<sub>2</sub> is initially present, glycolate decreases, rapidly consuming about 20% of the initial amount. Then the decrease is gradual. The O<sub>2</sub> in the cover gas was maximally 0.2 mmol. There was 2.5 mmol of glycolate in condensed phase. Cover gas analyses showed that 71% of the O<sub>2</sub> was consumed after 1236 hours at 90°C. This is probably why consumption of glycolate (0.19 M at t=0) slowed down after 20% was consumed. In the absence of O<sub>2</sub>, glycolate degradation appears to be autocatalytic or initially inhibited. Effects of O<sub>2</sub> on citrate and HEDTA disappearance rates appear negligible. The effect on carbonate production is more pronounced—carbonate forms nearly *twice* as fast in the presence of O<sub>2</sub>. EDTA reactivity does not appear to be different, although heated samples in both cases were routinely found to contain ~30% higher concentrations of EDTA than were measured in unaged samples of the simulant. Reasons for this anomalous behavior are unknown; one possibility is that degradation products of HEDTA interfered with EDTA analyses.

Results for headspace gas analyses are shown in Figure 4.5. Yields for 1330- and 2330-hour runs are normalized to 1000 and 2000 hours and charted in a bar graph for visual comparison. Like radiolysis experiments, headspace gas analyses show that, when O<sub>2</sub> was initially present, it was consumed by aging reactions, and when it was initially absent, it was generated in small amounts. N<sub>2</sub>O and H<sub>2</sub> were generated at comparable rates when O<sub>2</sub> was initially present, but N<sub>2</sub>O was generated faster than H<sub>2</sub> when O<sub>2</sub> was initially absent.

Similar observations about the effects of O<sub>2</sub> on gas production have been reported for simulants (Barefield et al. 1995, 1996) and real wastes (Person 1996). However, our observations of the effects on organic aging contrasts with recent observations for HEDTA in a much simpler simulant (sodium nitrite, aluminum hydroxide, sodium hydroxide) were that consumption of HEDTA was inhibited by O<sub>2</sub>.

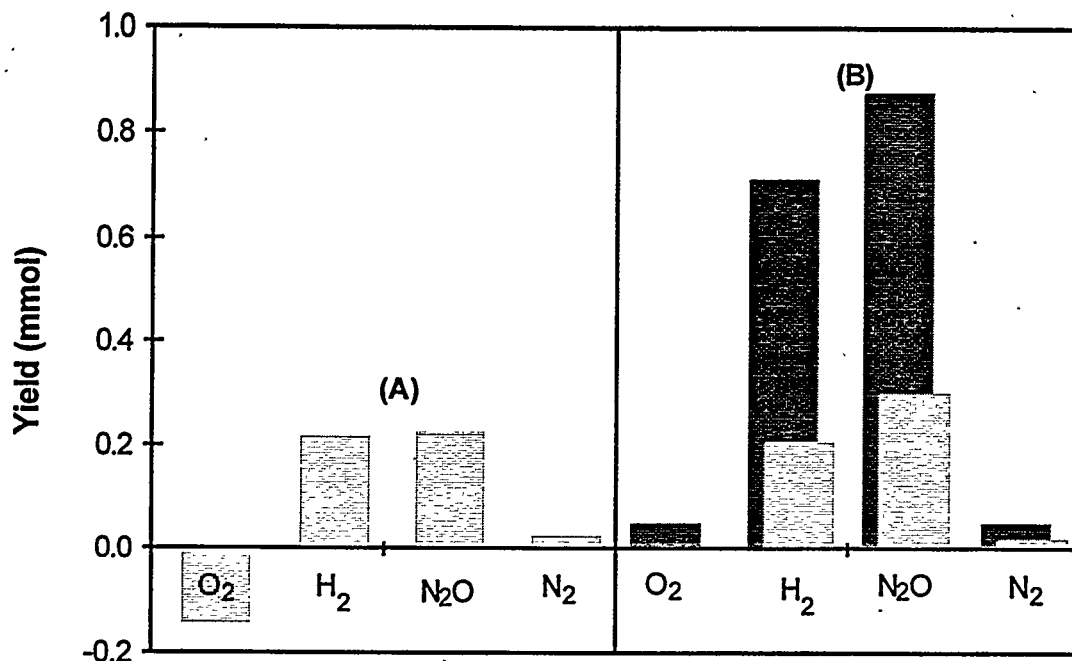


**Figure 4.5.** Effects of Initial Concentration of O<sub>2</sub> in Headspace Gas on Distribution of Gases Produced at 90°C: (A) starting with 20/80 O<sub>2</sub>/Ar; (B) starting with 100% Ar; ▨ 1000 hours; ■ 2000 hours

## 4.2 Radiolytic Effects on TOC and Nitrate Oxidation Enthalpies of Organic Species

The results in Section 4.1.1 show how organic carbon in SIM-PAS-95-1 redistributes as a function of aging conditions. We now examine how the TOC and enthalpy of the simulants change with aging. We define the enthalpy to be the heat that would be released from stoichiometric reaction of the organic species with nitrate on a dry weight basis, i.e., the mixtures have been concentrated to dryness. Since the starting and aged simulants all have excess nitrate and NaOH, we assume the products of reaction to be H<sub>2</sub>O, Na<sub>2</sub>CO<sub>3</sub>, and N<sub>2</sub> and then calculate the reaction enthalpy of each species from  $\Delta H_f$  data (Burger 1995). Table 4.4 lists the  $\Delta H_f$  and  $\Delta H_r$  data we used.

The concentrations of organic species and their nitrate reaction enthalpies in aged simulants are tabulated in Appendix B, Tables B.4–B.6. These data were used to calculate TOC and reaction enthalpies. The contribution that each organic species makes to  $\Delta H_r$  of the simulant is obtained by multiplying the concentration (mg C/g) of the species times the  $\Delta H_r$  (kJ/g C) of the species (Table 4.4). The  $\Delta H_r$  for missing organic species (calculated as the difference,  $\Sigma \text{organic } C_o - \text{inorganic } C_t - \Sigma \text{TOC}_t$ ) is assumed to be the average of values for Na<sub>3</sub>ED3A, Na<sub>2</sub>EDDA, Na<sub>3</sub>NTA, Na<sub>2</sub>IDA, and sodium glycinate (aminoacetate). Prior to aging, the reaction enthalpies of the simulants are 1340 J/g for SIM-PAS-95-1c and 1240 J/g for SIM-PAS-95-1d. Over the temperature range of 40–90°C, radiolytic aging decreases the magnitudes of nitrate reaction

**Table 4.4. Nitrate Reaction Enthalpies ( $\Delta H_r$ ) for Organic Species**

Compounds <sup>(a)</sup>	$\Delta H_f$ kJ/mol	$\Delta H_r$ <sup>(a)</sup>	
		kJ/mol	kJ/g C
Na <sub>3</sub> HEDTA	-2250	-42400	-35.4
Na <sub>4</sub> EDTA	-2720	-3850	-32.1
Na <sub>3</sub> ED3A	-2050 (b)	-3240	-33.8
Na <sub>2</sub> EDDA	-1390 (c)	-2630	-36.6
Sodium Glycinate	-765	-770	-32.1
Na <sub>3</sub> NTA	-2020 (d)	-2050	-28.5
Na <sub>2</sub> IDA	-1390 (e)	-495	-29.4
Sodium Glycolate	-901	-495	-25.5
Trisodium Citrate	-2260	-1450	-25.1
Disodium Oxalate	-1320	-269	-11.2
Sodium Formate	-667	-175	-17.9
Sodium Acetate	-709	-737	-30.7

(a)  $\Delta H_r$  and  $\Delta H_f$  from Burger (1995) except as noted.

(b)  $[\Delta H_f(\text{EDTA}) + \Delta H_f(\text{EDDA})]/2$ .

(c)  $[\Delta H_f(\text{EDTA}) + \Delta H_f(\text{ethylenediamine})]/2$ .

(d)  $\Delta H_f(\text{NTA}) - 716$  kJ/mol, the correction for converting the free acid to the trisodium salt (Burger 1995).

(e)  $[\Delta H_f(\text{NTA}) + \Delta H_f(\text{sodium glycinate})]/2$ .

energies. TOC parallels this trend. Figure 4.6 shows plots of  $-\Delta H_r$  and TOC versus dose for radiolytic aging at 40, 70, and 90°C. The slopes of the linear regression lines through the data points,  $\sim 1$  J/g/Mrad ( $\sim 2 \times 10^{-3}$  wt% C/Mrad) for 40 and 70°, and 1.3 J/g/Mrad ( $\sim 3 \times 10^{-3}$  wt% C/Mrad) for 90°C, correspond to the rates of decrease in the simulant reaction enthalpies (and TOC) as a result of radiolytic aging. The actual rate of energy decrease depends somewhat on the energy of the missing carbon. However, the missing carbon makes up small fractions of the TOC such that the rate is not strongly dependent on the value selected for the missing carbon. Furthermore, it is unlikely that any intermediates will be more energetic than the starting complexants or the remnants listed in Table 4.4 (see Appendix C). Radiolytic aging reduces not only the organic carbon and energy contents of the simulant, it also reduces average energy content per gram of carbon ( $-\Delta H_r$  in kJ/g C).<sup>(a)</sup>

(a) The average is calculated as the  $\Delta H_r$  (J/g) divided by the TOC (mg C/g).

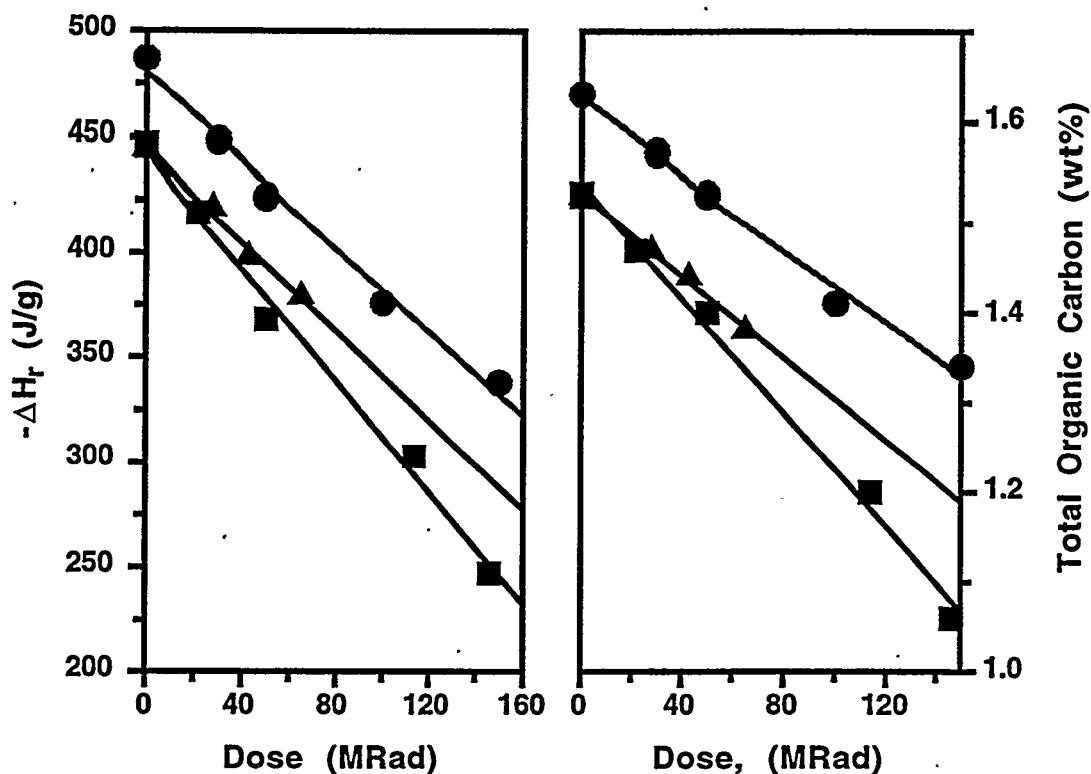


Figure 4.6. Nitrate Reaction Enthalpy and TOC of Simulants Versus Dose at 40, 70, and 90°C; SIM-PAS-95-1c: (●) 70°C; SIM-PAS-95-1d: 40° (▲) and (■) 90°C

The average energy content and organic carbon content of the simulants as a function of dose and temperature are shown in Table 4.5. The average energy content started out at ~30 kJ/g C. After

Table 4.5. Effect of Dose on Organic Carbon Content and Average  $-\Delta H_r$  (a) of SIM-PAS-95-1 Simulants

40°C(b)			70°C(c)			90°C(b)		
Dose (Mrad)	Org C (wt%)	$-\Delta H_r$ (kJ/g C)	Dose (Mrad)	Org C (wt%)	$-\Delta H_r$ (kJ/g C)	Dose (Mrad)	Org C (wt%)	$-\Delta H_r$ (kJ/g C)
0	4.3	29.1	0	4.5	29.9	0	4.3	29.1
28	4.1	28.6	30	4.4	28.6	22	4.1	28.4
43	4.0	27.7	50	4.3	27.8	50	3.9	26.2
65	3.8	26.7	100	3.9	26.8	114	3.3	25.3
			150	3.7	25.3	146	2.9	23.3

(a)  $\Delta H_r$  (J/g dry simulant) divided by TOC mg C/g dry simulant).

(b) SIM-PAS-95-1d; (c) SIM-PAS-95-1c.

a dose of 150 Mrad, the value had dropped to ~23-24 kJ/g C. An 150 Mrad dose at 70°C reduced the organic carbon content of SIM-PAS-95-1c from 4.5 wt% C to 3.5 wt% C and, at 90°C, reduced SIM-PAS-95-d from 4.3 wt% C to 2.9 wt% C. These results lend quantitative support to the idea that aging degrades the organic species in tank wastes to lower average energies and therefore results in safer storage conditions with respect to organic-nitrate reactions.

### 4.3 Experimental Section

All the chemicals used in this study were purchased from Aldrich Chemical Company, Eastman Kodak, or Baker Chemicals. Their purities were reagent grade or better, as defined by the American Chemical Society, and the chemicals were not further purified. Water used for preparing the simulant was deionized by a Milli-Q™ Deionization System (Millipore Corporation, San Francisco, CA).

Sample irradiation experiments were performed in the PNNL  $\gamma$  Facility described in Section 3.4. Vessels of the simulant are lowered manually into the irradiation tubes to the desired flux, where they are left for a specific length of time to attain the required exposure. A gas-manifold system was connected to the reaction vessels, providing headspace gas, pressure monitoring equipment, and a port for headspace gas removal. A datalogger recorded both the automated temperature and pressure measurements of the reaction vessels.

The cylindrical autoclave reactors used for this study were made from 316 stainless steel and were of two volumes, 500 mL and 30 mL. The larger one was used for radiolytic aging tests and the smaller for thermal aging tests. Reaction temperatures were measured by a K-thermocouple that inserted through a port in the reactor cover to within 5 mm of the bottom. Another port was connected to the gas manifold via small-diameter stainless steel tubing. The reactors were heated to operating temperatures by heating tape wrapped around the outside. Reaction temperatures were maintained at set temperatures by feedback control (Bryan and Pederson 1994). Pressure and temperature in the vessel were monitored with a datalogger. The gas volume of the reactors includes the reactor headspace, the tubing that connects the reactor to the manifold, and the portion of the manifold dedicated to the reactor. The tubing and manifold volume was measured to be 7.8 mL. The sample volumes were 130 mL for the large, 500-mL reactor and 13 mL for the small, 30-mL reactor. Thus, total headspace is 378 mL for the large reactor and 23 mL for the small reactor.

#### 4.3.1 Simulant Preparation and Irradiation

The SIM-PAS-95-1c and -1d simulants are based on recipes published in the test plan (Carlson and Babad 1996) for tube propagation experiments (Fauske 1996). We noted that addition of solid ferric nitrate to alkaline solutions containing nitrite ion produced copious amounts of NO<sub>2</sub> gas. On varying the order and timing of addition, we found that if sufficient time (~2 hours) were allowed for ferric nitrate to dissolve and hydrolyze to ferric hydroxide before addition of nitrite, then no gas was evolved. Therefore, *due caution should be taken in mixing the reagents in proportions or orders different from that recommended here* or in the test plan (Carlson and Babad 1996). To avoid errors associated with dispensing aliquots of a hetero-

geneous simulant, the simulant was prepared in the reaction vessel before each irradiation by mixing together three homogeneous stock solutions (Appendix B, Table B.11). These solutions were stored at approximately 4°C and were allowed to warm to room temperature before volumetric transfers were made. Simulant SIM-PAS-95-1d was prepared and dispensed as described above for SIM-PAS-95-1c, except that the quantities of all components were doubled to allow a greater number of tests. The three solutions were stored in 1-L plastic containers, sealed with tape, and refrigerated. Solution 1, which had a total volume of 2 L, was divided into two bottles. For each test run in the large reactor, 100 mL of solution 1, 20 mL of solution 2, and 10 mL of solution 3 were added sequentially to the reactor. Test runs in small reactors used 10, 2, and 1 mL of the respective stock solutions. No NO<sub>2</sub> gas was observed on mixing the solutions. Control runs were similarly mixed and analyzed without exposure to radiation. The measured density of the simulant was 1.27 g/mL. Water content is estimated to be 64%.

The charged reactors were sealed and transported to the  $\gamma$  irradiation facility, where the irradiation experiments were performed according to the procedures described in Table B.12. The gases generated during the irradiations were usually vented to the atmosphere, except for certain runs that were selected for gas analyses. In these cases, the gases were collected in an evacuated vessel and analyzed by mass spectrometry (Goheen 1994).

#### **4.3.2 Solution Phase Analyses**

The reactor was cooled to room temperature, removed from the gas manifold at the  $\gamma$  irradiation facility, sealed, and transported to analytical facilities. The contents were diluted 3.85-fold (130 mL in 500 mL for large reactor and 13 mL in 50 mL for small reactor) with deionized water. Aliquots of this were used for IC, IPC, ammonia, and carbonate analyses. EDTA and HEDTA were quantified using IPC. Organic acid anions, including formic, glycolic, citric, and oxalic acids, were quantified by IC; nitrate and nitrite were also analyzed by IC. TOC was determined with a carbon analyzer. Analysis of dissolved ammonia (NH<sub>3</sub>)<sub>aq</sub> was performed with an Orion 720A pH/ISE (ion selective electrode) meter equipped with an Orion 95-12 NH<sub>3</sub> ISE (Burt 1989).

##### **4.3.2.1 Ion Pair Chromatography Analyses of EDTA and HEDTA**

Using a volumetric pipet, 1 mL of the diluted aqueous solution was placed in a 10-mL volumetric flask to which 100  $\mu$ L of 0.5 M CuSO<sub>4</sub> was added and diluted to volume with water. The solution was analyzed using a Waters Associates high-performance liquid chromatography (HPLC) instrumentation with columns and conditions listed in Appendix B, Table B.13.

##### **4.3.2.2 Ion Chromatography Preparation/Analyses of Organic Acids**

Analyses were carried out using a Dionex model IC unit (Dionex Corp., Sunnyvale, CA) equipped with a Dionex, Model CD20 conductivity detector. Analyses of formate, oxalate, and citrate were carried out using a Dionex AS-11 column. A Dionex AS-6 column was used for glycolate, acetate, and succinate analyses, because glycolate co-eluted with acetate on the AS-11 column. The standard concentrations bracketed the estimated concentrations of the samples.

The AS-11 chromatographic conditions are listed in Appendix B, Tables B.14 and B.15. An aliquot of the simulant solution (Section 4.3.2) was diluted 250-fold for these analyses. The mobile phase contained a gradient of deionized water and a weak solution of sodium hydroxide for the AS-11 column. Two solutions, 5 mM and 100 mM NaOH, were prepared from 18.5 M NaOH stock solution. The water used to prepare the mobile phase and run the gradient was stirred under vacuum for over 12 hours, and then sparged with helium to avoid interference from dissolved carbon dioxide. Gradient conditions used for AS-11 column separation are shown in Appendix B, Table B.14. The column was allowed to equilibrate at initial conditions for at least seven minutes before each run.

The mobile phase for the AS-6 column (Appendix B, Table B.16) was made up of 0.4 mM heptafluorobutyric acid in deionized water. We used 5 mM tetrabutylammonium hydroxide as a suppression eluant. Concentrations were determined using a linear calibration curve. Quantification based on high dilution is not ideal but is possible, as the plots of standard concentration versus response exhibit linear behavior down to 100 ppb for the key analytes.

## 5.0 Organic Aging in Tank Wastes

This section compares results of waste aging studies with waste speciation results, discusses key factors such as dose rate, hydroxide concentration, and nitrite concentration that control rates and yields of radiolytic aging, and gives estimates of the contributions that radiolytic and thermal aging have made and are likely to make in the future toward reducing the organic carbon and energy content of organic tank wastes.

### 5.1 Organic Species Found in Tank Wastes

The preceding sections show that oxalate ion is a product of organic aging. Oxalate ion and TOC concentrations have been measured on samples from 52 single-shell waste storage tanks (SSTs). The data have been compiled in the *Organic Complexant Topical Report* (Meacham et al. 1998). The results for seven tanks are inconclusive; the TOC concentrations are below 0.1% in 13 tanks; the results for the other 32 are shown in Table 5.1. Seven SSTs had oxalate concentrations sufficient to account for more than 75% of the TOC (BY-109, BY-102, BY-105, BY-107, BY-110, BY-111, BY-112, and C-106); 18 tank wastes had oxalate concentrations sufficient to account for 25 to 75% of the measured TOC (A-101, AX-101, AX-103, BX-110, BY-101, BY-104, BY-108, BY-110, S-101, S-102, S-106, S-107, SX-101, SX-106, S-111, U-107, and U-108). Seven tanks had less than 25% of the TOC identified as oxalate (A-102, AX-102, C-104, C-105, U-102, U-105, and U-106).

Samples from a number of waste tanks have now been speciated for organic compounds. In general, the analyses clearly show the wastes have aged to the same compounds found in aging studies performed here and at Georgia Tech (Ashby et al. 1994). Some tanks have significant TOC that is not oxalate (AX-102, U-105 and U-106). Analyses of samples from these tanks show that the organic inventory is consistent with partial aging of these wastes. Table 5.2 lists organic results for several tanks (Meacham et al. 1998). The inventory of organic species includes the original complexants, a variety of intermediate degradation products, formate, and oxalate.

The quantitative analyses shown in Tables 5.1 and 5.2 are consistent with laboratory aging studies showing degradation of complexants to chelator fragments and carboxylate salts such as oxalate and formate. Oxalate ion appears to persist in the wastes, attaining higher concentrations than formate and many other aging intermediates. Oxalate ion probably has low reactivity compared with the chelators and other fragments. Also, the solubility of oxalate ion in tank waste supernates is very low (Barney 1995). Since oxidation of the organic species mainly occurs in the aqueous solution phase, these conditions favor the accumulation of oxalate ion in the solid components of the wastes.

**Table 5.1. Fractions of TOC that are Oxalate in Tank Wastes<sup>(a)</sup>**

Tank	TOC wt%, wet	%TOC as oxalate	Tank	TOC wt%, wet	%TOC as oxalate
A-101	0.31	44	BY-112	0.71	96
A-102	1.11	22	C-104	1.00	11
AX-101	0.62	38	C-106	1.34	>99
AX-102	1.87	12	S-101	0.22	52
AX-103	0.52	43	S-102	0.33	57
BX-110	0.15	62	S-106	0.23	58
BY-101	0.48	74	S-107	0.20	67
BY-102	0.33	>99	S-111	0.17	71
BY-104	0.67	52	SX-101	0.53	56
BY-105	0.73	95	SX-106	0.39	36
BY-106	0.51	75	U-102	0.74	18
BY-107	0.52	79	U-103	0.64	9
BY-108	0.39	46	U-105	1.23	22
BY-109	0.33	85	U-106	2.16	12
BY-110	0.64	43	U-107	0.18	38
BY-111	0.55	86	U-108	0.42	27

(a) TOC concentrations are mean values calculated from the best basis inventory and % carbon as oxalate ion evaluated from inventory or sampling data.

## 5.2 Radiolytic Aging in Wastes

To extrapolate effects observed in aging studies of waste simulants, we must understand the relationship between reaction conditions and radiolytic yields. We consider two kinds of effects: dose rate effects and matrix effects. Rates of radiolytic aging are governed by the dose rate. It determines the rate of production of oxidizing radicals. After that, the physical and chemical properties of the organic species and the medium determine organic reactivity.

### 5.2.1 Effects of Dose Rate, Nitrite, and Hydroxide on Radiolytic Yields

Radiation flux, nitrite, and hydroxide are all expected to affect the radiolytic yields of organic degradation. As we have shown for formate oxidation (Section 3.2.1), nitrite and hydroxide control the yield and distribution of products from  $\text{OH}(\text{O}^\cdot)$  and  $\text{NO}_2$  attack. For example,  $\text{O}^\cdot$  and  $\text{OH}^\cdot$  convert nitrite ion to  $\text{NO}_2$  and also convert  $\text{NO}_3^{2-}$  to  $\text{NO}$ . Since  $\text{NO}$  is not a strong, effective oxidant of organic complexants, this latter reaction causes the radiolytic yield of organic products to follow an inverse dependence on nitrite concentration. The dose rate is not expected to affect the yield of primary radicals and followup reactions that generate  $\text{NO}_2$  and  $\text{NO}$ . However, since reactions of  $\text{NO}_2$  with organic species compete with  $\text{NO}_x$  hydrolysis reactions that

Table 5.2. Analyses of Organic Species (wt%) in Tank Waste Samples

Tank Sample	Acetate	Citrate	Glycolate	Formate	Oxalate	EDTA <sup>4-</sup>	HEDTA <sup>3-</sup>	IDA <sup>2-</sup>	NTA <sup>3-</sup>	TOC
A-101 C154 S10 UH	0.214			0.269	3.764	0.0191				1.22
A-102 96-AUG-3	0.174	0.127		0.165	1.444					1.03
AW-101 C139 S21 UH	0.093	0.0165	0.0473	0.0988	1.045			0.0064		1.51
AX-102 95-AUG-007		0.509	0.7700	0.4780	1.795	0.302	0.147	1.188		3.49
B-106 C93 S1 UH	0.0032			0.0115						0.20
BY-102 C157 S4	0.0119			0.0040	6.825					1.94
BY-104 C116 SLG		3.020			5.350					1.75
BY-105 C108 S1 DL	0.108	0.208		0.0874						0.18
BY-107 C161 S1	0.140			0.0603	2.606					0.88
BY-110 C101 S7	0.0939			0.0350	9.468					2.09
BY-110 C103 S4 UH	0.0451				3.680					0.75
BY-110 C113 S8	0.0713			0.0119	0.044					0.21
C-104 C162 S2 UH	0.2530			0.190	0.227					0.91
C-105 C76 S1 DL	0.226	0.390		0.0459	0.0511			0.101	0.35	
C-201 TNK COMP	0.0951			0.0169	3.720			0.107		
U-105 C136 S7UH	0.0705	0.386	0.399	0.718	0.825	0.404	0.538			2.17
U-106 C148 S2UH	0.0356	0.591	0.451	0.267	0.475	0.633	0.667			2.37
U-107 C134 SLG	0.0385	0.0900		0.116	0.237					0.15
U-108 C141 S4 UH	0.0595		0.160	0.184	0.503	0.0993	0.026			0.63

are second order, lowering the rate of generation of radicals increases the yield of organic oxidation from  $\text{NO}_2$ . We demonstrate these effects with the model for formate oxidation (see Table 3.3) by reducing the rate of generation of  $\text{NO}_3^{2-}$  (from  $e^-$ ),  $\text{OH}$ , and  $\text{H}$  radicals to simulate the effects of changing the dose rate from 0.1 Mrad/hr to 10 rad/h (equivalent to changing the rate of radical and production from  $10^{-7}$  to  $10^{-11}$  M/s). Results are shown in Table 5.3 and Figure 5.1.

The yield of  $\text{CO}_3^{2-}$  increases significantly as the dose rate is decreased, approaching limiting values of  $\sim 1.9$  and  $2.9$  molecules/100 eV for high and low nitrite concentrations, respectively. Table 5.3 shows the percent (in parentheses) of formate that is oxidized by each oxidizing radical.

**Table 5.3. Summary of Radiolytic Aging Model Showing Effects of Dose Rate, Nitrite, and Hydroxide on Radiolytic Yield and Distribution of Oxidizing Species**

[Formate]	[ $\text{NO}_2^-$ ]	[ $\text{OH}^-$ ]	G( $\text{CO}_3^{2-}$ ) and Relative Contributions by Oxidants molecules/100 eV ( $\text{NO}_2^-:\text{O}^-:\text{OH}:\text{H}$ )	
			$10^5$ Rad/h	$10^1$ Rad/h
0.05	1.25	2	0.66 (55:42:2:0)	1.9 (84:15:1:0)
0.03	0.03	2	2.5 (5:93:1:1)	2.9 (19:79:0:1)
0.05	1.25	0.1	0.51 (84:8:8:0)	1.9 (96:2:2:0)

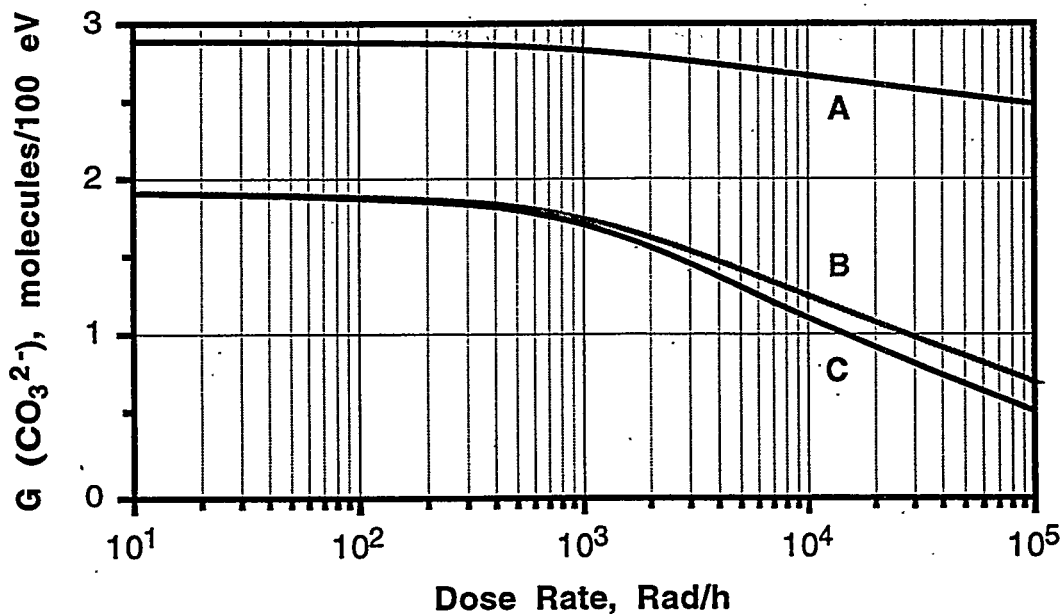


**Figure 5.1. Effects of Dose Rate, Nitrite, and Hydroxide on the Radiolytic Yield of  $\text{CO}_3^{2-}$  from Formate: (A) 0.03 M  $\text{HCO}_2^-$ , 0.03 M  $\text{NO}_2^-$ , 2 M  $\text{OH}^-$ ; (B) 0.05 M  $\text{HCO}_2^-$ , 1.25 M  $\text{NO}_2^-$ , 2 M  $\text{OH}^-$ ; (C) 0.05 M  $\text{HCO}_2^-$ , 0.05 M  $\text{NO}_2^-$ , 0.1 M  $\text{OH}^-$**

The increase is largely due to increased efficiency of formate oxidation by NO<sub>2</sub>. The steady-state concentrations of NO<sub>x</sub> radicals decrease with dose rate, and the rates of NO<sub>2</sub> termination (Equations 2.5 and 2.6) decrease too. The yields of primary radicals (OH, e<sup>-</sup>, and H) total 6.1 molecules/100 eV. The stoichiometry is two oxidants per CO<sub>3</sub><sup>2-</sup>, so a maximum yield of 3 CO<sub>3</sub><sup>2-</sup>/100 eV is theoretically possible. The oxidations at the lowest dose rate are still less than 100% efficient. With high nitrite ion, a significant fraction of NO<sub>3</sub><sup>2-</sup> and essentially all H atoms are converted to NO (Equation 5 in Table 3.3). With low nitrite ion, less of these oxidants convert to NO, and the yield of CO<sub>3</sub><sup>2-</sup> increases. The competing reactions of OH with NO<sub>2</sub><sup>-</sup> and OH<sup>-</sup> (Equations 2.1 and 2.5) cause the yield of CO<sub>3</sub><sup>2-</sup> to vary inversely with hydroxide ion (see Figure 5.1 and Table 5.3). The effect is smaller than the effect of nitrite ion and is more important at high dose rates because the steady-state concentration of NO<sub>2</sub> is proportional to dose rate. The fraction of NO<sub>2</sub> that disproportionates (Equations 2.7) or oxidizes NO (Equation 2.8) is thus greater at higher dose rates. In summary, the modeling results strongly support the idea that NO<sub>2</sub> is the dominant oxidizing species in tank wastes (Meisel et al. 1991b, 1993, 1997). They also paint important roles for O<sup>-</sup>, OH, and NO.

## 5.2.2 Radiolytic Contribution to Organic Aging in Tank Wastes

To estimate the amount of aging that has occurred or will occur in a given tank waste, we define a coefficient for radiolytic aging as the change in heat content or organic carbon content per Mrad of absorbed dose. Equating change per unit time with the product of the dose rate and the coefficient of aging gives an equation that expresses the rate of change in energy content or organic carbon content as a function of dose rate. For example,

$$d[C]/dt = -cF \quad (5.1)$$

$$d(-\Delta H_r)/dt = -hF \quad (5.2)$$

where [C] is organic carbon concentration, ΔH<sub>r</sub> is the heat content of the waste, c and h are coefficients of aging for changes in carbon and in heat content, respectively, and F is radiation flux (dose per unit time). Since the dose rate is determined mainly by radioactive decay of <sup>137</sup>Cs and <sup>90</sup>Sr with half-lives of 30 and 28 years respectively, knowledge of the dose rate, F<sub>0</sub>, at time, t<sub>0</sub>, allows the rate of change at time, t, to be written

$$d[C]/dt = -cF_0 e^{-0.0239(t-t_0)} \quad (5.3)$$

$$d(-\Delta H_r)/dt = -hF_0 e^{-0.0239(t-t_0)} \quad (5.4)$$

where the constant 0.0233 is the average of decay rate constants for <sup>90</sup>Sr and <sup>137</sup>Cs in y<sup>-1</sup>.

Integration of Equations 5.3 and 5.4 leads to expressions for the change that occurs during the time interval t-t<sub>0</sub>:

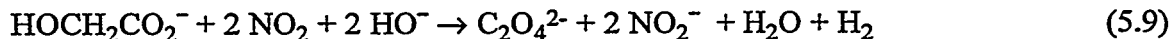
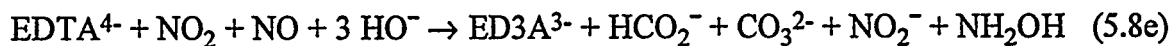
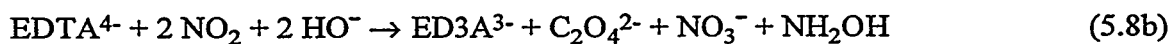
$$\Delta[C] = 41.8[1-e^{-0.0239(t-t_0)}]cF_0 \quad (5.5)$$

$$\Delta\Delta H_r = 41.8[1-e^{-0.0239(t-t_0)}]hF_0 \quad (5.6)$$

where  $t$  is in years, 41.8 years is the reciprocal of the exponential decay constant ( $0.0239 \text{ y}^{-1}$ ),  $c$  is the aging coefficient in wt% C/Mrad,  $h$  is the aging coefficient in J/g/Mrad, and  $F_0$  is the radiation flux at  $t_0$  in Mrad/y.

In Section 4.2, we calculated aging coefficients from speciation data for radiolytic aging of the PAS-95-1 simulant. The coefficients for this simulant are 1.0 J/g/Mrad at 40 and 70°C and 1.3 J/g/Mrad at 90°C. In terms of TOC, the coefficients are  $2.3 \times 10^{-3}$ ,  $2.0 \times 10^{-3}$ , and  $3.2 \times 10^{-3}$  wt% C/Mrad at 40, 70, and 90°C, respectively.

Coefficients for aging can be derived from other basic information. The radiolytic yield of oxidants is expected to be  $\sim 6$  molecules/100 eV absorbed dose (Meisel et al. 1997). This translates to  $6 \times 10^{-3}$  moles/kg waste/Mrad.<sup>(a)</sup> Because the oxidants are one-electron oxidants, and whereas products have even numbers of electrons, the stoichiometry for conversion is generally 2 moles of oxidants per mole of reactant converted (Equations 5.7–5.9).



Mechanistic studies show that the nitrogen-containing complexants cleave carboxymethyl groups, giving formate, carbonate and oxalate ions. If reactions such as Equation 5.8a are dominant, a maximum value of  $3.7 \times 10^{-3}$  wt% C/Mrad would be obtained for the TOC aging coefficient.<sup>(b)</sup> This is about 1.1–1.8 times the TOC coefficients measured for the PAS-95 simulants. However, for reasons discussed in Section 5.2.1, we should not expect theoretical yields to be obtained at the high doses used in simulant aging studies. Also, to the extent that pathways to oxalate ion such as Equation 5.9 occur, yields of carbonate ion will be smaller.

The aging coefficient in energy units is derived by calculating the enthalpy change for known or plausible oxidation pathways of the complexants and their fragments. Multiplying these enthalpy changes by the radiolytic yield gives the aging coefficient for the reaction path. Typical values for oxidation reactions of complexants are summarized in Table 5.4. In general, we find

(a) The conversion from molecules/100 eV to  $10^{-3}$  mol/kg/Mrad is as follows:

$$\frac{1 \text{ molecule}}{100 \text{ eV}} \times \frac{1 \text{ mol}}{6.02 \times 10^{23} \text{ molecule}} \times \frac{1 \text{ eV}}{1.6 \times 10^{-19} \text{ J}} \times \frac{1 \text{ J/kg}}{100 \text{ rad}} = 1.04 \times 10^{-3} \frac{\text{mol/kg}}{\text{Mrad}}$$

(b) If  $G = 3$  molecules/100 eV for carbonate production, then  $3.1 \times 10^{-3}$  moles  $\text{CO}_3^{2-}$ /kg/Mrad are produced such that

$$c = 3.1 \times 10^{-3} \frac{\text{mol/kg}}{\text{Mrad}} \times 12 \frac{\text{g C}}{\text{mol}} = 3.7 \times 10^{-2} \frac{\text{g C/kg}}{\text{Mrad}} \text{ or } 3.7 \times 10^{-3} \text{ wt\% C/Mrad}$$

**Table 5.4. Changes in Nitrate Reaction Enthalpies Due to Aging Reactions**

Reaction Type	$\Delta\Delta H_r$ kJ/mol	Aging Coef. (J/g/Mrad)	
		G=2	G=3
$R_2NCH_2-CH_2NR_2 \rightarrow 2 HCO_2^- + R_2NH$	-540±60	1.1	1.6
$R_2NCH_2-CH_2NR_2 \rightarrow R_2NCH_2CO_2^- + R_2NH$	-410±30	0.8	1.2
$R_2NCH_2CO_2^- \rightarrow R_2NH + HCO_2^- + CO_3^{2-}$	-330±20(a)	0.7	1.0
$R_2NCH_2CO_2^- \rightarrow R_2NH + C_2O_4^{2-}$	-350±20(a)	0.7	1.1
$HOCH_2CO_2^- \rightarrow C_2O_4^{2-}$ or $HCO_2^- + CO_3^{2-}$	-330	0.7	1.0
$HCO_2^-$ or $C_2O_4^{2-} \rightarrow 1$ or $2 CO_3^{2-}$	-170±10	0.3	0.5

(a) Value for sodium salt of glycine is ~50% greater than average.

values for oxidation reactions of complexants are summarized in Table 5.4. In general, we find that the aging coefficients for reactions cluster between 0.3 and 1.6 J/g/Mrad with values of ~1 predominating for reactions in Equations 5.7 through 5.9.

Contributions to radiolytic aging up to the present and into the future can be estimated with knowledge of the waste dose rates. Stauffer (1997) reports current  $\gamma$  dose rates, historical  $\gamma$  doses, and past and current temperatures for SST wastes. Best-basis tank inventories of  $^{90}Sr$  and  $^{137}Cs$  are listed in the Tank Waste Inventory Network System (TWINS).<sup>(a)</sup> We estimated dose rates that included contributions from  $^{90}Sr$  (a  $\beta$  emitter) using Equation 5.10:

$$\text{Dose Rate} = \frac{(Ci_{Cs} \times 0.8 \text{ MeV} + Ci_{Sr} \times 1.13 \text{ MeV})}{\text{kg Waste}} \times 2.13 \times 10^3 \frac{\text{rad} \cdot \text{kg}}{\text{h} \cdot \text{Ci} \cdot \text{MeV}} \quad (5.10)$$

where the units for dose rate are rad/h and 0.8 MeV and 1.13 MeV are average decay energies for  $^{137}Cs$  and  $^{90}Sr$ , respectively (Meisel et al. 1991a; Spinks and Woods 1964).<sup>(b)</sup> For many tanks, the contribution from  $^{90}Sr$  is negligible. However, for some tanks of interest such as AX-102 (TOC ~5.7 wt% C, wet), the dose rate computed in Equation 5.10 is 2300 rad/h, seven-fold greater than the  $\gamma$  dose rate estimated by Stauffer (1997). Using average aging coefficients (~1 J/g/Mrad and  $2.4 \times 10^{-3}$  wt% C/Mrad) and a starting dose rate of 3700 rad/h (ca. 1978), we calculate from Equations 5.5 and 5.6 that the energy decrease over a 50-year period would be ~950 J/g (2.3 wt% C). Tanks U-105 and U-106, with ~1.2 wet wt% carbon, have dose rates of ~450 and 490 rad/h, respectively, according to Equation 5.10, compared with 200 and 215 rad/h

(a) TWINS 2 database is on the World-Wide Web (<http://twins.pnnl.gov:8001/>).

(b) The factor in Equation 5.10 is derived as follows:

$$\text{factor} = \frac{1.33 \times 10^{14} \text{ disintegrations/h}}{\text{Ci/disintegration}} \times \frac{1.6 \times 10^{-13} \text{ J}}{\text{MeV}} \times \frac{100 \text{ rad}}{\text{J/kg}} = 2.13 \times 10^3 \frac{\text{rad} \cdot \text{kg}}{\text{h} \cdot \text{Ci} \cdot \text{MeV}}$$

$\gamma$  dose rates estimated by Stauffer (1997). Using a starting dose rate of  $\sim 760$  rad/h (ca. 1978), we calculate that the energy decrease over a 50-year period will be *only* 200 J/g (0.5 wt% C).

### 5.3 Thermally Activated Organic Aging

Non-radiolytic (thermal) decomposition reactions contribute to aging. When tank temperatures are high, thermally activated processes can rapidly age the organic constituents. The results for thermal aging of the PAS-95 simulant (see Section 4) shows that TOC and energy content decrease with increasing time of exposure at 90°C. Analytical results show that HEDTA, glycolate, and citrate were degraded and that carbonate grew in approximately linearly with time. The initial rates of carbonate production were 0.6 wet wt% C/y in the presence of O<sub>2</sub> and 0.3 wet wt% C/y in the absence of O<sub>2</sub>. Extrapolated over several years, this rate of production could yield significant reductions in TOC.

Tank wastes at higher temperatures show more aging than those at lower temperatures. For example, of Tanks A-101, AX-102, U-105, and U-106, only A-101 has a significant fraction (44%) of its TOC as oxalate. The dose rate for U-105, U-106, and A-101 are relatively low. Stauffer (1997) estimates the  $\gamma$  dose rate for A-101 is 301 rad/h. The amount of <sup>90</sup>Sr in A-101 is  $\sim 8$  times smaller than the amount of <sup>137</sup>Cs, so the  $\beta$  dose rate is inconsequential. Stauffer (1997) lists the historical temperatures of A-101, AX-102, U-105, and U-106 as 79, 46, 35, and 36°C, respectively; current temperatures are 66, 27, 34, and 35°C (Stauffer 1997). Review of temperature measurements for U-106<sup>(a)</sup> shows that in or about 1976, U-106 was filled with waste that was only  $\sim 50^\circ\text{C}$ ; it then cooled rapidly to  $\sim 30^\circ\text{C}$ . Under such conditions, little thermal aging would have occurred. The fraction of TOC that is oxalate in U-106 is only 12% (see Table 5.2). The aging that has occurred (see Table 5.2) can be attributed to radiolytic effects. Tank A-101 waste was  $\sim 80^\circ\text{C}$  when it was filled; current temperature is  $\sim 66^\circ\text{C}$ . Accordingly, a significant fraction (44%) of the TOC in this waste is oxalate. We conclude that the degree of aging depends on the temperature history of the waste.

### 5.4 Rates of Aging in High Heat-Load Waste Tanks

Certain tanks such as AZ-101 and AZ-102 have significant enough radionuclide inventories that dose rates and temperatures are elevated more than other tanks. These tanks must be actively ventilated to maintain supernatant temperatures below bulk waste or supernate boiling points. If active ventilation were interrupted, the wastes could dry out within several years and perhaps heat these wastes enough to cause bulk runaway reactions. However, if the complexants in these wastes are substantially aged already, or age rapidly during the time that water is boiled off, the propagation hazard will be mitigated.

The results and discussion in previous sections provide information that may be used to estimate rates of thermal and radiolytic aging for these tanks. The PAS-95 aging experiments performed with and without irradiation provide baseline data for estimating complexant aging to acetate, succinate, formate, oxalate, and carbonate. Table 5.5 lists the thermal rate of formation

---

(a) TWINS2 database, <http://twins.pnl.gov:8001/>.

**Table 5.5. Radiolytic Yield and Thermal Rates of Formation of Aging Products from PAS-95 Simulants at 90°C**

Aging Product	Radiolytic Yield (gC/kg/Mrad)	Thermal <sup>(a)</sup> (gC/kg/y)
Formate	0.007	
Acetate	0.0003	1
Succinate	0.008	5
Oxalate	0.001	3
Carbonate	0.036	2.3

(a) In the absence of O<sub>2</sub>.

and the radiolytic yields measured at 90°C. Multiplying the radiolytic yield by the dose rate (Mrad/y) gives a rate of formation that can be combined with the thermal rate of aging to obtain an overall rate.

The AZ-101 and AZ-102 wastes may be similar to the PAS-95 simulants, but they certainly are not identical. Therefore, the rates in Table 5.5 must be scaled to correct for differences. For thermal aging, studies (Ashby 1994; Delegard 1987) suggest that rates of aging depend on TOC, aluminate, hydroxide and nitrite concentrations. Also, gas production rates show large temperature dependencies with  $E_a \sim 90$  kJ/mol (Ashby 1994; Person 1996; Pederson and Bryan 1996). Therefore, the PAS-95 thermal aging rates ( $r_{s,thermal}$ ) may be scaled as in Equation 5.11:

$$r_{w,thermal} = r_{s,thermal} \times \frac{TOC}{TOC_s} \times \frac{[Al]}{[Al]_s} \times \frac{[OH^-]}{[OH^-]_s} \times \frac{[NO_2^-]}{[NO_2^-]_s} \times e^{\frac{E_a}{R} \left( \frac{1}{363} - \frac{1}{T} \right)} \quad (5.11)$$

where  $r_{w,thermal}$  is the thermal rate of waste aging and the factors corrected for concentration and temperature differences from simulant results (denoted with s subscript). Assuming a boiling temperature for tank supernates of  $\sim 120^\circ\text{C}$ , the exponential factor in Equation 5.11 is 9.7 for  $E_a = 90$  kJ/mol.

As discussed in Section 5.2.2, the radiolytic rate depends mainly on dose rate and radiolytic yield of oxidants. If concentrations of organic complexants are sufficiently high, then the yield of products may approach or even exceed one-half the yield of oxidants. If TOC concentrations are not sufficiently large to scavenge oxidants competitively with disproportionation reactions (Equations 2.7 and 2.8), then smaller yields may occur. Since TOC in the AZ tanks is significantly less than in PAS-95 simulants, the expression for computing radiolytic aging rates ( $r_{w,radiolytic}$ ) from PAS-95 simulant radiolytic aging rates ( $r_{s,radiolytic}$ ) includes a scaling factor for TOC (Equation 5.12):

$$r_{w,radiolytic} = r_{s,radiolytic} \times \text{Dose Rate} \times \frac{TOC}{TOC_s} \quad (5.12)$$

Table 5.6 lists characterization data taken from a double-shell tank composition status quarterly report.<sup>(a)</sup> Data are provided for liquid and sludge fractions of the wastes, and a third entry for each tank shows data taken from the best Basis Inventory/Best Basis/TCR Tank Inventory database. These data are used to obtain average total dose rates and TOC concentrations for entire tank wastes.

**Table 5.6. AZ-101 and AZ-102 Characterization Data**

Tank Waste	Vol (kL)	H <sub>2</sub> O (%)	SpG	TOC (g/L)	TOC (wt%)	[NO <sub>2</sub> ]	[Al] <sup>(a)</sup>	[OH]	<sup>90</sup> Sr Ci/kg	<sup>137</sup> Cs Ci/kg
AZ-101 liquid	3230	70.7	1.21	1.13	0.093	1.35	0.03	0.75	0.0011	1.4
AZ-101 sludge	132	43.1	1.48	13.50	0.91	1.39	0.03	0.75	33	1.5
AZ-101 <sup>(b)</sup>	3280		1.22	1.85	1.5				1.6	1.9
AZ-102 liquid	3000	82.9	1.11	1.62	0.15	0.65	0.06	0.12	0.0017	1.0
AZ-102 sludge	357	53.8	1.41	6.35	0.45	0.59	0.06	0.13	7.0	0.81
AZ-102 <sup>(b)</sup>	3360		1.14	1.7	1.5				0.97	1.1

(a) From sample analysis data in the Tank Waste Inventory database.

(b) Values derived from Best Basis Inventory database, except that specific gravity (SpG) is weighted average of values for liquid and sludge fractions.<sup>(a)</sup>

Table 5.7 lists the resulting aging rates calculated using Equations 5.11 and 5.12. Rates are estimated for liquid (supernate) fractions and for the entire waste. The entire waste estimate assumes that the total dose rate from solid and liquid fractions contributes to radiolytic aging.

**Table 5.7. Estimated Rates of Organic Aging to Carbonate, Formate, and Oxalate Ions at 120°C in AZ Tank Wastes**

Tank Waste	TOC (gC/kg)	Dose Rate (MRad/y)	Thermal Rate (g C/kg/y)		Radiolytic Rate (g C/kg/y)		Total Rate <sup>(b)</sup> (g C/kg/y)	
			CO <sub>3</sub> <sup>2-</sup>	C <sub>2</sub> O <sub>4</sub> <sup>2-</sup>	CO <sub>3</sub> <sup>2-</sup>	C <sub>2</sub> O <sub>4</sub> <sup>2-</sup>	CO <sub>3</sub> <sup>2-</sup>	C <sub>2</sub> O <sub>4</sub> <sup>2-</sup>
AZ-101 (L) <sup>(a)</sup>	0.93	30	0.3	0.2	0.07	0.02	0.3	0.2
AZ-101	1.4	57			0.13	0.03	0.4	0.2
AZ-102 (L) <sup>(a)</sup>	1.5	21	0.1	0.04	0.07	0.02	0.1	0.06
AZ-102	1.5	36			0.13	0.03	0.2	0.1

(a) Liquid (supernate) fraction.

(b) Sum of radiolytic and thermal rates; entries for entire waste are sums of liquid thermal rates and entire waste radiolytic rates.

(a) Stauffer LA. September 2, 1997. "Double-Shell Tank Composition Status—Quarterly Report." Memo 74650-97-013, Lockheed Martin Hanford Corporation, Richland, Washington.

Thermal aging is assumed to occur only in the liquid fraction because the complexants, except oxalate (Barney 1995), are very soluble. So the liquid thermal rates are combined with the entire waste radiolytic rates to obtain the total entire waste aging rate. Because  $^{90}\text{Sr}$  is largely in the sludge fraction and  $^{137}\text{Cs}$  mainly in the liquid fraction, the entire waste rate estimates effectively combine the radiolytic effects of both  $^{137}\text{Cs}$  and  $^{90}\text{Sr}$  decay. For this reason, the rates are higher than the liquid aging rates. Since the supernates will concentrate over time, these aging rates may increase as the radionuclides and reactants concentrate.

In conclusion, the results suggest that if the wastes were allowed to heat to boiling, much of the existing inventory of TOC would convert to carbonate and oxalate within two to five years. The results for AZ-101 sum to  $\sim 0.6$  g C/kg/y (average of the sum for liquid and entire waste aging rates to carbonate and oxalate ions) so that the TOC would oxidize in two to three years. The estimated drying time for AZ-101 is four years (Meacham 1998). The AZ-102 rates sum to  $\sim 0.3$  g C/kg/y, so the TOC in this tank would convert to oxalate and carbonate ions in about five years. The estimated time for AZ-102 to dry out (Meacham 1998) is 10 years. The rates of conversion to carbonate ion are about two times the rates to oxalate ion. However, the PAS simulant measurements model the disappearance of the more reactive, more energetic carbon remaining in the waste, i.e., the higher energy carbon of the original complexants and their immediate remnants such as NTA and IDA. The AZ-101 and AZ-102 wastes are already aged.<sup>(a)</sup> Therefore, if one-third of the TOC is now oxalate, then the TOC in these tanks may age to equal amounts of carbonate and oxalate ions during the times it would take the wastes to dry out in the event that active cooling is interrupted. Significant production of formate, acetate, and succinate is also predicted by the PAS-95 model (see Table 5.4). These compounds are less reactive thermally (Ashby et al. 1994) and radiolytically (see Table 3.1) than the nitrogen containing complexants and their remnants. However, as they build up and more reactive species disappear, radiolytically generated oxidants may be expected to degrade these remnants to oxalate and carbonate ions as well.

---

(a) During sludge characterization and washing tests on AZ-102, TOC was noted to be five times higher in the sludge than in the supernate (Herting DL. 1995. *Caustic Washing of Sludge Samples from Tank AZ-102*. Memo 75764-PCS95-086, Westinghouse Hanford Company). Indeed, characterization data (Stauffer LA. 1997. "Double Shell Tank Composition Status—Quarterly Report." Interoffice Memo 74650-97-013, Lockheed Martin Hanford Corporation) compiled in Table 5.6 show that a disproportionate amount of TOC appears in the sludge fractions: AZ-101 sludge is 5% of the waste mass but contains 33% of the TOC; AZ-102 sludge is 13% of the waste mass but 32% of the TOC. Considering the low solubility of sodium oxalate (Barney 1995) in supernates, it is probable that the TOC in the sludge is mainly oxalate, which would indicate that significant aging of the complexants in these wastes has already occurred.

## 6.0 Conclusions

The Waste Aging Studies task has shown that radiation and heat promote redox reactions between organic compounds (reducing agents) and nitrates/nitrites (precursors to oxidizing agents) in the wastes. Radiolysis and heating of waste simulants causes conversion of  $\text{NO}_3^-$  to  $\text{NO}_2^-$ ,  $\text{N}_2$ , and  $\text{N}_2\text{O}$  and probably  $\text{NH}_3$  concurrent with the disappearance of organic species and appearance of highly oxidized fragments of the original species. The observations are consistent with progressive degradation to species with more C-O bonds and fewer C-H and C-C bonds, resulting in an overall lower energy content of the organic inventory.

### 6.1 Effects of Aging on Organic Nitrate Reaction Enthalpies

The simulated waste aging studies using the PAS-95 simulants show quantitatively that energy content of the wastes should decrease due to aging (see Table 3.6). The theoretical energy content of the simulants declined steadily with increasing radiolytic dose; a radiation dose of 100 Mrad at 70°C decreased the energy content of the waste simulant by ~25% from a starting value of ~1300 J/g dry simulant. Much of the remaining enthalpy is due to undegraded glycolate, citrate, and chelator fragments. We also established that the decline in energy content is temperature dependent, declining more rapidly at 90°C than at 40 or 70°C. Aging occurs at a much slower rate in the absence of radiation, but for long storage times at elevated temperatures, certain species, namely HEDTA, citrate, and glycolate, are susceptible to thermal degradation (see also Delegard 1987; Ashby et al. 1993; Barefield et al. 1995, 1996). The results suggest that lifetimes and aging rates of organic complexants are strongly dependent on radiolytic and thermal histories. This partly explains the tank-to-tank variations in organic aging (based on organic analyses) observed in actual waste samples (see Tables 5.1 and 5.2).

TOC measurements have been obtained from a significant number of tank wastes. These results have been used to screen for tanks that could have sufficient fuel to undergo propagating reactions (Webb et al. 1995; Meacham et al. 1998). The assessment essentially converts TOC to enthalpy by assuming a proportionality factor:

$$\Delta H_r (\text{kJ/g waste}) = \text{TOC (mg/g waste)} \times \Delta H (\text{kJ/g C}) \quad (6.1)$$

Presently, the conversion factor is taken to be the reaction enthalpy of sodium acetate. Our PAS-95 simulants aging tests suggest that the actual conversion factor decreases as a consequence of aging. Recent analytical data (see Table 5.2) for actual waste samples enables the reaction enthalpy of the samples to be calculated. We estimated the enthalpies per gram of carbon in the samples and found that the energy was only ~70% of the energy for pure acetate. Thus, as currently used, TOC is a conservative, and therefore a useful initial screen for problem tanks.

## 6.2 Mechanistic Understanding of Organic Aging

Mechanistic and kinetic results of Waste Aging Studies corroborate the hypothesis (Meisel et al. 1991b, 1993, 1997) that  $\text{NO}_2$  is the dominant radical responsible for radiolytic oxidation of complexants. We note that the reactivities of citrate, glycolate, EDTA, and HEDTA measured in simple homogeneous simulants of Section 3 are comparable to those observed in the more complex heterogeneous simulants studied in Section 4. This suggests that the same oxidizing species are acting in homogeneous and heterogeneous systems. The modeling results for formate and glycine suggest that the oxidizing species in alkaline systems are primarily  $\text{NO}_2$  and  $\text{O}^-$ . However, under conditions likely to be encountered in actual wastes such as low dose rates, the dominant oxidizing species is  $\text{NO}_2$  (see Table 5.3).

The modeling effort provides the first measurements of rate constants for reactions of  $\text{NO}_2$  with carboxylates and complexants. The absolute rate constant for formate is  $\sim 10 \text{ M}^{-1}\text{s}^{-1}$  and, for glycine,  $70 \text{ M}^{-1}\text{s}^{-1}$ . The ratio of these rate constants agree well with the relative reactivities listed in Table 3.1. Thus rate constants for the other complexants may be estimated from newly determined relative rate constants.

Finally, the multiple roles that nitrite plays are noteworthy. First, it reduces  $\text{OH}/\text{O}^-$  and forms  $\text{NO}_2$ . Second, it oxidizes  $\text{NO}_3^{2-}$  radicals (formed by reaction of electrons with  $\text{NO}_3^-$ , Equations 2.3 and 2.4 and 3 of Table 3.3). This reaction acts to reduce the efficiency of radiolytic aging. It has a small rate constant and requires high nitrite concentrations. Thirdly, nitrite ion combines with organic radicals, thereby facilitating the conversion of complexants to simple innocuous products such as oxalate, formate, and carbonate. Without this step, the products from complexants would be complicated (see Figure 3.7) and perhaps more troublesome issues for storage, retrieval, and pretreatment activities. Finally, nitrite also is required for thermal degradation of complexants.

## 6.3 Recommendations

Although the safety issue surrounding safe storage of organic wastes nears closure, we suggest directions that continued studies could follow. We note that the product identifications and subsequent modeling of the reactions of higher complexants are incomplete. We suggest that continued work to expand the model is worthwhile, especially if the effort also leads to the addition of thermal and thermal-plus-radiolytic reaction mechanisms, so the combined processes can be modeled and understood. Steps for reactions that lead to gaseous products may also be added so that the model yields information about generation rates and distributions of gaseous products. The acquisition of such capabilities could facilitate resolution of flammable gas safety issues as well as answer questions regarding reactions that may be induced by retrieval and pretreatment activities.

## 7.0 References

- Agnew SF. 1996a. *Hanford Defined Wastes: Chemical and Radionuclide Compositions*. LA-UR-94-2657 Rev. 2, Los Alamos National Laboratory, Los Alamos, New Mexico.
- Agnew SF. 1996b. *Hanford Tank Chemical and Radionuclide Inventories*. LA-UR-96-858, Los Alamos National Laboratory, Los Alamos, New Mexico.
- Agnew SF. 1996c. *History of Organic Carbon in Hanford HLW Tanks: HDW Model Rev. 3*. LA-UR-96-989, Los Alamos National Laboratory, Los Alamos, New Mexico.
- Allen GK. 1976. *Estimated Inventory of Chemicals Added to Underground Waste Tanks, 1944 Through 1975*. ARH-CD-610B, Atlantic Richfield Hanford Company, Richland, Washington.
- Alred SE, DLH Williams, and M Garley. 1982. *J Chem Soc J Perkin Trans II:777-782*.
- Ashby EC, F Doctorovich, CL Liotta, HM Neumann, EK Barefield, A Konda, K Zhang, and J Hurley. 1993. "Concerning the Formation of Hydrogen in Nuclear Waste. Quantitative Generation of Hydrogen via a Cannizzaro Intermediate." *J Am Chem Soc* 115:1171.
- Ashby EC, A Annis, EK Barefield, D Boatright, F Doctorovich, CL Liotta, HM Neumann, A Konda, C-F Yao, K Zhang, and NG Duffie. 1994. *Synthetic Waste Chemical Mechanism Studies*. WHC-EP-0823, Westinghouse Hanford Company, Richland, Washington.
- Barefield EK, D Boatright, A Deshpande, F Doctorovich, CL Liotta, HM Neumann, and S Seymore. 1995. *Mechanisms of Gas Generation from Simulated SY Tank Farm Wastes: FY 1994 Progress Report*. PNL-10822, Pacific Northwest Laboratory, Richland, Washington.
- Barefield EK, D Boatright, A Deshpande, F Doctorovich, CL Liotta, HM Neumann, and S Seymore. 1996. *Mechanisms of Gas Generation from Simulated SY Tank Farm Wastes: FY1995 Progress Report*. PNNL-11247, Pacific Northwest Laboratory, Richland, Washington.
- Barney GS. 1995. *The Solubilities of Significant Organic Compounds in HLW Tank Supernate Solutions*. WHC-SA-2565-FP, Westinghouse Hanford Company, Richland, Washington.
- Bhattacharyya SN and NC Saha. 1976. *Radiat Res* 68: 234-43
- Braun W, JT Herron, and DK Kahaner. 1988. "Acuchem: A Computer Program for Modeling Complex Chemical Reaction Systems." *J Chem Kinet* 20:51-62.
- Bryan SA and LR Pederson. 1994. *Composition, Preparation, and Gas Generation from Simulated Wastes of Tank 241-101-SY*. PNNL-10075, Pacific Northwest Laboratory, Richland, Washington.
- Burger LL. 1995. *Calculation of Reaction Energies and Adiabatic Temperatures for Waste Tank Reactions*. PNL-8557 Rev 1, Pacific Northwest National Laboratories.
- Burt RW. 1989. *Ammonia (nitrogen) in Aqueous Samples*. PNNL-ALO-226 RO, -226.1, -226.2, -226.3, Pacific Northwest Laboratory, Richland, Washington.

Buxton GV. 1969. *Trans. Faraday Soc.* 65:2150-8.

Buxton GV, WP Greenstock, WP Helman, and AB Ross. 1988. "Critical Review of Rate Constants for Reactions of Hydrated Electrons, Hydrogen Atoms, and Hydroxyl Radicals (OH/O<sup>-</sup>) in Aqueous Solution." *J. Phys. Chem. Ref. Data*, 17:513.

Camaioni DM, WD Samuels, SA Clauss, BD Lenihan, KL Wahl, JA Campbell, and WJ Shaw. 1995. *Organic Tanks Safety Program FY95 Waste Aging Studies*. PNNL-10794, Pacific Northwest National Laboratory, Richland, Washington.

Camaioni DM, WD Samuels, JC Linehan, SA Clauss, AK Sharma, KL Wahl, JA Campbell. 1996. *Organic Tanks Safety Program FY96 Waste Aging Studies*. PNNL-11312, Pacific Northwest National Laboratory, Richland, Washington.

Camaioni DM, WD Samuels, JC Linehan, AK Sharma, MO Hogan, MA Lilga, SA Clauss, KL Wahl, and JA Campbell. 1998. *Organic Tanks Safety Program FY97 Waste Aging Studies*. PNNL-11670 Rev. 1, Pacific Northwest National Laboratory, Richland, Washington.

Carlson CD and H Babad. 1996. *Test Plan for Fauske and Associates to Perform Tube Propagation Experiments with Simulated Hanford Tank Wastes*. PNNL-10970 Rev 1, Pacific Northwest National Laboratory, Richland, Washington.

Challis BC and SA Kyrtopoulos. 1979. "The Chemistry of Nitroso-Compounds. Part 11. Nitrosation of Amines by the Two-Phase Interaction of Amines in Solution with Gaseous Oxides of Nitrogen." *J. Chem. Soc., Perkin Trans. 1*, 299-304.

Challis BC and DEG Shuker. 1979. "Rapid Nitrosation of Amines in Aqueous Alkaline Solutions by  $\beta$ -Substituted Alkyl Nitrites." *J Chem Soc, Chem. Commun.*, 315-16.

Chen MJ, JC Linehan, and JW Rathke. 1990. "Autoxidation of Trimethylamine in Aqueous Solutions." *J. Org. Chem.*, 55:3233.

Cleveland JM. 1967. "Plutonium Recovery and Waste Disposal." *Plutonium Handbook*, Vol. II, OJ Wick, ed. Gordon and Breach, Science Publishers, New York.

Creed MJ and HK Fauske. 1990. "An Easy, Inexpensive Approach to the DIERS Procedure." *Chem. Eng. Prog.*, 45-49.

Czapski G, J Holcman, and BHJ Bielski. 1994. "Reactivity of Nitric Oxide with Simple Short-Lived Radicals in Aqueous Solutions." *J Am Chem Soc* 116:11465-11469.

Delegard CH. 1987. *Identities of HEDTA and Glycolate Degradation Products in Simulated Hanford High-Level Waste*, RHO-RE-ST-55P, Rockwell Hanford Operations, Richland, Washington.

Draganic IG and ZD Draganic. 1971. *The Radiation Chemistry of Water*. Academic Press, New York.

- Fauske HK. 1995. *Summary of Laboratory Scoping Tests Related to Organic Solvents Combustion by Nitrate Oxidation and Organic Solvent Ignitability*. Fauske & Associates, Burr Ridge, Illinois.
- Fauske HK. 1996. *An Update of Requirements for Organic-Nitrate Propagating Reactions Including RSSST and Tube Propagation Test Results with Simulants*. FAI/96-48, Fauske & Associates, Burr Ridge, Illinois.
- Fauske HK and M Epstein. 1995. *The Contact-Temperature (CTI) Criteria for Propagating Chemical Reactions Including the Effect of Moisture and Application to Hanford Waste*. WHC-SD-WM-ER-496 Rev 0, Westinghouse Hanford Company, Richland, Washington.
- Gerber MA, LL Burger, DA Nelson, JL Rayan, and RL Zollars. 1992. *Assessment of Concentration Mechanisms for Organic Wastes in Underground Storage Tanks at Hanford*. PNL-8339, Pacific Northwest Laboratory, Richland, Washington.
- Gilbert BC, JP Larkin, and ROC Norman. 1972. "Electron Spin Resonance Studies. Part XXXIV. The Use of The *aci*-Anion from Nitromethane as a Spin Trap for Organic Radicals in Aqueous Solutions." *J Chem Soc, Perkin Trans II* 1272-1279.
- Gilbert BC and ROC Norman. 1982. "Radical Reactions in aqueous Solutions: Use of the *aci*-Anion of Nitromethane as a Spin Trap." *Can J Chem* 60:1379.
- Goheen MW. 1994. *Quantitative Gas Mass Spectrometry*. PNNL-ALO-284 Rev. 1, Pacific Northwest Laboratory, Richland, Washington.
- Han P and DM Bartels. 1990. "Reevaluation of Arrhenius Parameters for  $H\cdot + OH^- \rightarrow (e^-) + H_2O$  and the Enthalpy and Entropy of Hydrated Electrons." *J. Phys. Chem.* 94:7294-7299.
- Karpoor S, FA Barnabas, MC Sauer, Jr., D Meisel, and CD Jonah. 1995. "Kinetics of Hydrogen Formation from Formaldehyde in Aqueous Solutions." *J. Phys. Chem.* 99:6857-6863.
- Keefer LK and PP Roller. 1973. *Science* 181.
- Kingsley RS. 1965. *Solvent Extraction Recovery of Americium with Dibutyl Butyl Phosphonate*. RL-SEP-518, Hanford Atomic Products Operation, Richland, Washington.
- Klem MJ. 1990. *Inventory of Chemical Used at Hanford Site Production Plants and Support Operations (1944-1980)*. WHC-EP-0172 Rev. 1, Westinghouse Hanford Company, Richland, Washington.
- Knutsen K and TM Orlando. 1997. "Low Energy (5-100 eV) Electron- and Ultraviolet (6.4 eV) Photon-Stimulated Desorption of Neutral Fragments from  $NaNO_3$  Single Crystal." *Appl. Surf. Sci.*, in press.
- Lati J and D Meyerstein. 1972. *Inorg. Chem.* 11:2397-401.
- Lee Y-N, and SE Schwartz. 1981. "Reaction Kinetics of Nitrogen Dioxide with Liquid Water at Low Partial Pressure." *J Phys Chem*, 85:840-848.

Lilga MA, RT Hallen, EV Alderson, MO Hogan, TL Hubler, GL Jones, DJ Kowalski, MR Lumetta, WF Reimath, RA Romine, GF Schiefelbein, and MR Telander. 1996. *Ferrocyanide Safety Project Ferrocyanide Aging Studies Final Report*. PNNL-11211, Pacific Northwest National Laboratory, Richland, Washington.

Lias, SG, JE Bartmess, JF Liebman, JL Holmes, RD Levin and WG Mallard. 1988. "Gas Phase Ion and Neutral Thermochemistry." *J Phys Chem Ref Data* 17, Sup. 1.

Madden KP, H Taniguchi, and RW Fessenden. 1988. "A Time-Resolved ESR Study of the Kinetics of Spin Trapping by Nitromethane *aci*-Anion." *J Am Chem Soc* 110:2753-2758.

Meacham JE, AB Webb, NW Kirch, JA Lechelt, DA Reynolds, GS Barney, DM Camaioni, F Gao, RT Hallen, and PG Heasler. 1998. *Organic Complexant Topical Report*. HNF-SD-WM-CN-058 Rev. 2, DE&S Hanford, Richland, Washington.

Meisel D, H Diamond, EP Horwitz, MS Matheson, MC Sauer Jr, JC Sullivan, F Barnabas, E Cerny, and YD Cheng. 1991a. *Radiolytic Generation of Gases from Synthetic Waste*. ANL-91/41, Argonne National Laboratory, Argonne, Illinois.

Meisel D, H Diamond, EP Horwitz, MS Matheson, MC Sauer Jr, and JC Sullivan. 1991b. *Radiation Chemistry of Synthetic Waste*. ANL-91/40, Argonne National Laboratory, Argonne, Illinois.

Meisel D, CD Jonah, S Kapoor, MS Matheson, and MC Sauer Jr. 1993. *Radiolytic and Radiolytically Induced Generation of Gases from Synthetic Wastes*. ANL-93/43, Argonne National Laboratory, Argonne, Illinois.

Meisel D, A Cook, D Camaioni, and T Orlando. 1997. "Chemistry, Radiation, and Interfaces in Suspensions of Nuclear Waste Simulants." *Photoelectrochemistry*, K Rajeshwar, LM Peter, A Fujishima, D Meissner, M Tomkiewicz, eds. The Electrochemical Society Pub., 97-20:350-7.

Meisel D and DM Camaioni. July 1998. "The NO<sub>x</sub> System in Nuclear Waste." *EMSP Project Summaries, Environmental Management Science Program Workshop*. CONF-980736, U.S. Department of Energy, Washington, D. C., pp. 125-127.

Mezyk SP and DM Bartels. 1997. "Temperature Dependence of Hydrogen Atom Reaction with Nitrate and Nitrite Species in Aqueous Solution." *J Phys Chem A* 101:6233-6237.

Mönig J, R Chapman, and KD Asmus. 1985. "Effect of the Protonation State of the Amino Group on the •OH Radical Induced Decarboxylation of Amino Acids in Aqueous Solutions." *J Phys Chem* 89:3139-3144.

Neta P, RE Huie, and AB Ross. 1988. "Rate Constants for Reactions of Inorganic Radicals in Aqueous Solution." *J Phys Chem Ref Data* 17:1027-1284.

Neta P and RH Schuler. 1975. "Rate Constants for the Reaction of O<sup>-</sup> Radicals with Organic Substrates in Aqueous Solution." *J Phys Chem* 79:1-6.

Oae S, N Asai, and K Fujimori. 1978. "Alkaline Hydrolysis of Alkyl Nitrites and Related Carboxylic Esters." *J Chem Soc, Perkin Trans II* 571-577.

- Orlando TM, DM Camaioni, and D Meisel. 1998a. "Interfacial Radiolysis Effects in Tank Waste Speciation." *EMSP Project Summaries, Environmental Management Science Program Workshop*. CONF-980736, U.S. Department of Energy, Washington, D. C., pp. 127-130.
- Orlando TM, DM Camaioni, and D Meisel. 1998b. "Interfacial Radiolysis Effects in Tank Waste Speciation." *Science to Support DOE Site Cleanup: The Pacific Northwest National Laboratory Environmental Management Science Program Awards*, pp. 1.1-1.13. PNNL-11899, Pacific Northwest National Laboratory, Richland, Washington.
- Park J-Y and Y-N Lee. 1988. "Solubility and Decomposition of Kinetics of Nitrous Acid in Aqueous Solution." *J Phys Chem* 92:6294-6302.
- Parra SA. 1994. "Integrated Beta and Gamma Radiation Dose Calculations for the Ferrocyanide Waste Tanks." WHC-SD-WM-TI-634 Rev. 1, Westinghouse Hanford Company, Richland, Washington.
- Pederson LR and SA Bryan. 1996. *Status and Integration Studies of Gas Generation in Hanford Wastes*. PNNL-11297, Pacific Northwest National Laboratory, Richland, Washington.
- Person JC. 1996. *Effects of Oxygen Cover Gas on NaOH Dilution on Gas Generation in Tank 241-Sy-101 Waste*. WHC-SD-WM-DTR-043, Westinghouse Hanford Company, Richland, Washington.
- Schatz T, AR Cook, and D Meisel. 1998. "Charge Carrier Transfer Across the Silica Nanoparticle/ Water Interface" (*in press*).
- Scheele RD, JL Sobolik, RL Sell, and LL Burger. 1995. *Organic Tank Safety Project: Preliminary Results of Energetics and Thermal Behavior Studies of Model Organic Nitrate and/or Nitrite Mixtures and a Simulated Organic Waste*. PNNL-10206, Pacific Northwest Laboratory, Richland, Washington.
- Schwarz HA and RW Dodson. 1989. "Reduction Potentials of  $\text{CO}_2^-$  and the Alcohol Radicals." *J Phys Chem* 93:409-414.
- Sederburg JP, and JA Reddick 1994. *TBP and Diluent Mass Balances in the PUREX Plant at Hanford 1955-1991*. WHC-SD-WM-ER-396 Rev. 0, Westinghouse Hanford Company, Richland, Washington.
- Smith PAS and RN Loeppky. 1967. *J Am Chem Soc* 89:1147-1157.
- Spinks JWT and RJ Woods. 1964. *An Introduction to Radiation Chemistry*. John Wiley and Sons, New York.
- Stabler RN and JP Chesick. 1978. "HAVCHM: A Program System for Computer Integration of Multi-Step Reaction Rate Equations Using the Gear Iteration Method." *Int J Chem Kinet* 10:461-469.
- Stanbury DM. 1989. "Reduction Potentials Involving Inorganic Free Radicals in Aqueous Solution." *Adv Inorg Chem* 33:69-138.

- Stauffer LA. 1997. *Temperature and Radiation Dose History of Single-Shell Tanks*: HNF-SD-WM-TI-815, Lockheed Martin Hanford Corporation, Richland Washington.
- Stock LM and LR Pederson. 1997. *Chemical Pathways for the Formation of Ammonia in Hanford Wastes*. PNNL-11702 Rev. 1, Pacific Northwest National Laboratory, Richland, Washington.
- Su Z, DE Falvey, UC Yoon, and PS Mariano. 1997. "The Dynamics of  $\alpha$ -Anilino Carboxylate and Related Cation Radical  $\alpha$ -Heterolytic Fragmentations." *J Am Chem Soc* 119:5261.
- Warneck P and C Wurzinger. 1988. "Product Quantum Yields for the 305-nm Photodecomposition of  $\text{NO}_3^-$  in Aqueous Solution." *J Phys Chem* 92:6278.
- Wayner DDM and D Griller. 1990. "Free Radical Thermochemistry." *Advances in Free Radical Chemistry*, D. Tanner, ed. JAI Press Inc., Vol. 1, pp. 159-192.
- Webb AB, JL Stewart, DA Turner, MG Plys, G Malinovic, JM Grigsby, DM Camaioni, PG Heasler, WD Samuels, and JJ Toth. 1995. *Preliminary Safety Criteria for Organic Watch List Tanks at the Hanford Site*. WHC-SD-WM-SARR-033 Rev. 0, Westinghouse Hanford Company, Richland, Washington.
- Wiegert FJ and RJ McKinney. 1986. *GEAR Iterator: Fitting Experimental Data with GEAR Algorithm Iteration of Chemical Kinetics Equations*, Ver. #QCMP022 for PC. Quantum Chemistry Program Exchange, Indiana University, Bloomington, Indiana.
- Zeldes H and R Livingston. 1968. "Paramagnetic Resonance Study of Liquids during Photolysis. VI. Aliphatic Nitroanions." *J Am Chem Soc* 90:4540-4544/

## **Appendix A**

### **Data for Relative Rate Determinations**

Table A.1. Scoping Experiments Run with 0.049 M  $\text{H}^{13}\text{CO}_2^-$  and 0 to 0.1 M EDTA

No.	Time h	Dose <sup>(a)</sup> Mrad	[EDTA] <sub>0</sub> mM <sup>(b)</sup>	Final Concentration, mM			Radiolytic Yield, G (molecules/100 ev)				
				EDTA <sup>(b)</sup>	$^{13}\text{CO}_3^{2-}$	$\text{H}^{12}\text{CO}_2^-$	$k_{\text{rel}}$	$^{13}\text{CO}_3^{2-}$	EDTA	$\text{H}^{12}\text{CO}_2^-$	
1	120	9.6	0		6.52			0.48			
2	192	15.3	0		12.3			0.57			
3	216	17.3	0		13.7						
4	0	0.0	22.5								
5	120	9.6	22.5	9.3	6.13	17.0	6.6	0.45	-0.97		1.25
6	216	17.3	22.5	5.6	9.67	26.7	6.4	0.40	-0.69		1.09
7	0	0.0	44.5	44.5							
8	192	15.3	44.5		9.02			0.41			
9	216	17.3	44.5	19.7	9.04	30.4	4.0	0.37	-1.01		1.24
10	0	0.0	93.1								
11	120	9.6	93.1	76.6	3.82	16.2	2.4	0.28	-1.21		1.19
12	192	15.3	93.1		7.06			0.32			
13	216	17.3	93.1	65.1	7.12	31.5	2.3	0.29	-1.14		1.28

(a)  $\gamma$  dose-rate ~ 0.08 Mrad/h; (b) Average of determinations by NMR and ion pair chromatography.

Table A.1. (contd)

No.	Time h	Dose <sup>(a)</sup> Mrad	[EDTA] <sub>0</sub> mM <sup>(b)</sup>	Final Concentration, mM			Radiolytic Yield, G (molecules/100 ev)				
				EDTA <sup>(b)</sup>	<sup>13</sup> CO <sub>3</sub> <sup>2-</sup>	H <sup>12</sup> CO <sub>2</sub> <sup>-</sup>	k <sub>rel</sub>	<sup>13</sup> CO <sub>3</sub> <sup>2-</sup>	EDTA	H <sup>12</sup> CO <sub>2</sub> <sup>-</sup>	
14	120	9.6	0		10.7			0.79			
15	264	21.1	0		24.2			0.81			
16	0	0.0	23.3								
17	120	9.6	23.3	13.3	7.72	14.3	6.9	0.57	-0.73		1.05
18	240	19.2	23.3	4.9	18.1	32.0	7.8	0.67	-0.68		1.18
19	264	21.1	23.3	3.8	18.8	33.9	8.6	0.63	-0.65		1.13
20	0	0.0	47.9								
21	120	9.6	47.9	28.8	7.72	17.7	6.3	0.57	-1.40		1.30
22	264	21.1	47.9	23.9	16.8	36.5	3.7	0.56	-0.80		1.22
23	0	0.0	99.0								
24	120	9.6	99.0	77.7	7.03	15.9	3.3	0.52	-1.56		1.17
25	264	21.1	99.0	56.9	13.7	37.4	3.7	0.46	-1.41		1.24

(a)  $\gamma$  dose-rate  $\sim 0.08$  Mrad/h; (b) Average of determinations by NMR and ion pair chromatography.

Table A.2. Concentrations, Irradiation Times, and Total Doses in Aging Experiments

Competitor	Initial Concentration					Dose Rate		Irradiation Time (h)	Total Dose Mrad
	[Organic]	[H <sup>13</sup> CO <sub>2</sub> ]	[HCO <sub>2</sub> ]	[NO <sub>2</sub> ]	[NO <sub>3</sub> ]	[OH]	Mrad/h		
Glycolate	0.100	0.0992	0	1.25	3.75	2.00	0.0761	144.00	11.0
							0.0696	144.00	10.0
							0.0701	144.00	10.1
	0.0439	0.0992	0	1.25	3.75	2.00	0.0784	119.85	17.1
Glycolate							0.0770	100.00	
							0.0775	119.78	16.9
							0.0761	100.00	
							0.0687	119.65	15.0
Glycolate							0.0677	100.00	
	0.0786	0.0530	0	1.99	2.01	2.00	0.519	9.07	4.7
							0.519	15.00	7.8
							0.602	24.07	14.5
Glycine							0.559	30.07	16.8
	0.0434	0.0992	0	1.25	3.75	2.00	0.0784	119.85	9.4
							0.0775	119.78	9.3
							0.0687	119.65	8.2
Glycine (2- <sup>13</sup> C)	0.0814	0	0.0515	2.00	2.00	2.04	0.620	8.67	5.4
							0.620	15.00	9.3
							0.612	23.67	14.5
							0.620	29.73	18.4
Glycine (2- <sup>13</sup> C)							0.519	9.07	4.7
	0.0805	0	0	1.99	2.01	2.00	0.519	15.00	7.8
							0.602	24.07	14.5
							0.559	30.07	16.8
Glycine (2- <sup>13</sup> C)	0.0819	0	0	1.26	3.76	2.05	0.519	9.07	4.7
							0.519	15.00	7.8
							0.602	24.07	14.5
							0.559	30.07	16.8
Glycine (2- <sup>13</sup> C)	0.0802	0	0	0.00	2.01	2.04	0.519	9.07	4.7
							0.519	15.00	7.8
							0.602	24.07	14.5
							0.559	30.07	16.8

Table A.2. Continued.

Competitor	Initial Concentration					Dose Rate			Irradiation Time (h)	Total Dose Mrad
	[Organic]	[ $^{13}\text{C}$ ]	[ $\text{HCO}_2^-$ ]	[ $\text{NO}_2^-$ ]	[ $\text{NO}_3^-$ ]	[OH $^-$ ]	Mrad/h	Sample No.		
Glycine (1- & 2- $^{13}\text{C}$ )	0	0	0	1.99	2.01	2.00	0.519	2-ML-5-1	9.07	4.7
	0.0798 <sup>(a)</sup>						0.519	2-ML-5-2	15.00	7.8
							0.602	2-ML-5-3	24.07	14.5
							0.559	2-ML-5-4	30.07	16.8
IDA	0.0435	0.0992	0	1.25	3.75	2.00	0.0784	MH-84-5-1	119.85	9.4
							0.0775	MH-84-5-2	119.78	9.3
							0.0687	MH-84-5-3	119.65	8.2
IDA	0.0794	0.100	0	2.02	2.00	2.02	0.620	1-ML-18-1a	8.67	5.4
							0.620	1-ML-18-2	15.00	9.3
							0.612	1-ML-18-3	23.67	14.5
							0.620	1-ML-18-1b	29.73	18.4
NTA	0.0145	0.0992	0	1.25	3.75	2.00	0.0784	MH-84-4-1	119.85	9.4
							0.0775	MH-84-4-2	119.78	9.3
							0.0687	MH-84-4-3	119.65	8.2
NTA	0.0546	0.100	0	2.02	2.00	2.02	0.620	1-ML-16-1a	8.67	5.4
							0.620	1-ML-16-2	15.00	9.3
							0.612	1-ML-16-3	23.67	14.5
							0.620	1-ML-16-1b	29.73	18.4
EDTA	0.0218	0.0992	0	1.25	3.75	2.00	0.0784	MH-84-1-1	119.85	9.4
							0.0775	MH-84-1-2	119.78	9.3
							0.0687	MH-84-1-3	119.65	8.2
EDTA	0.0403	0.100	0	2.02	2.00	2.02	0.620	1-ML-15-1a	8.67	5.4
							0.620	1-ML-15-2	15.00	9.3
							0.612	1-ML-15-3	23.67	14.5
							0.620	1-ML-15-1b	29.73	18.4
HEDTA	0.100	0.0992	0	1.25	3.75	2.00	0.0761	MH-79-2-1	144.00	11.0
							0.0696	MH-79-2-2	144.00	10.0
							0.0701	MH-79-2-3	144.00	10.1
HEDTA	0.0218	0.0992	0	1.25	3.75	2.00	0.0784	MH-84-7-1	119.85	9.4
							0.0775	MH-84-7-2	119.78	9.3
							0.0687	MH-84-7-3	119.65	8.2

Table A.2. Continued.

Competitor	Initial Concentration						Dose Rate Irradiation			Total Dose Mrad
	[Organic]	[H <sup>13</sup> CO <sub>2</sub> ]	[HCO <sub>2</sub> ]	[NO <sub>2</sub> ]	[NO <sub>3</sub> ]	[OH]	Mrad/h	Time (h)	Mrad	
HEDTA	0.0406	0.102	0	1.99	2.01	2.00	0.519	9.07	4.7	
							0.519	15.00	7.8	
							0.602	24.07	14.5	
							0.559	30.07	16.8	
ED3A	0.0426	0.103	0	1.99	2.01	2.00	0.519	9.07	4.7	
							0.519	15.00	7.8	
							0.602	24.07	14.5	
							0.559	30.07	16.8	
s-EDDA	0.0217	0.0992	0	1.25	3.75	2.00	0.0784	119.85	9.4	
							0.0775	119.78	9.3	
							0.0687	119.65	8.2	
							0.620	8.67	5.4	
s-EDDA	0.0797	0.100	0	2.02	2.00	2.02	0.620	15.00	9.3	
							0.612	23.67	14.5	
							0.620	29.73	18.4	
							0.0770	99.92	7.7	
u-EDDA	0.0781	0.0990	0	1.25	3.75	2.00	0.0761	99.92	7.6	
							0.0677	99.92	6.8	
							0.519	9.07	4.7	
							0.519	15.00	7.8	
EDMA	0.0859	0.0546	0	1.99	2.01	2.00	0.602	24.07	14.5	
							0.559	30.07	16.8	
							0.0784	119.85	9.4	
							0.0775	119.78	9.3	
Acetate	0.0041	0.0500	0	1.25	3.75	2.00	0.0687	119.65	8.2	
							0.620	8.67	5.4	
							0.620	15.00	9.3	
							0.612	23.67	14.5	
Acetate	0.0506	0.0530	0	2.00	2.00	2.04	0.620	29.73	18.4	

Table A.2. Continued.

Competitor	Initial Concentration						Dose Rate		Irradiation		Total Dose Mrad
	[Organic]	[H <sup>13</sup> CO <sub>2</sub> ]	[HCO <sub>2</sub> ]	[NO <sub>2</sub> ]	[NO <sub>3</sub> ]	[OH]	Mrad/h	Time (h)	Mrad		
Acetate (1- & 2- <sup>13</sup> C)	0.101 <sup>(b)</sup>	0	0	1.99	2.01	2.00	0.519	9.07	4.7		
Butyrate	0.0125	0.0500	0	1.25	3.75	2.00	0.0784	119.85	9.4		
							0.0775	119.78	9.3		
							0.0687	119.65	8.2		
Citrate	0.100	0.0020	0	1.25	3.75	2.00	0.0761	144.00	20.9		
							0.0690	144.00			
							0.0696	144.00	20.8		
							0.0749	144.00			
							0.0701	144.00	20.0		
							0.0685	144.00			
Citrate	0.0063	0.0500	0	1.25	3.75	2.00	0.0784	119.85	9.4		
							0.0775	119.78	9.3		
							0.0687	119.65	8.2		
Citrate	0.0499	0.0526	0	2.00	2.00	2.04	0.620	8.67	5.4		
							0.620	15.00	9.3		
							0.612	23.67	14.5		
							0.620	29.73	18.4		
Succinate	0.0125	0.0500	0	1.25	3.75	2.00	0.0770	99.92	7.7		
							0.0761	99.92	7.6		
							0.0677	99.92	6.8		
Butanol	0.0144	0.0500	0	1.25	3.75	2.00	0.0770	99.92	7.7		
							0.0761	99.92	7.6		
							0.0677	99.92	6.8		

(b) 0.0481 M 2-<sup>13</sup>C-Acetate and 0.0526 M 1-<sup>13</sup>C-Acetate

Table A.2. Continued.

Competitor	Initial Concentration					Dose Rate		Irradiation Time (h)	Total Dose Mrad	
	[Organic]	[H <sup>13</sup> CO <sub>2</sub> ]	[HCO <sub>2</sub> ]	[NO <sub>2</sub> ]	[NO <sub>3</sub> ]	[OH]	Mrad/h			
dibutyl Phosphate	0.0253	0.0500	0	1.25	3.75	2.00	MH-87-13-1	0.0770	99.92	7.7
-	-	-	-	-	-	-	MH-87-13-2	0.0761	99.92	7.6
-	-	-	-	-	-	-	MH-87-13-3	0.0677	99.92	6.8
-	0	0.0530	0.0501	1.25	3.75	2.02	1-ML-10-1	0.467	8.67	4.0
-	-	-	-	-	-	-	1-ML-10-2	0.467	23.67	11.0
-	-	-	-	-	-	-	1-ML-10-3	0.467	31.67	14.8
-	0	0.0984	0.100	1.25	3.75	2.02	1-ML-11-1	0.467	8.67	4.0
-	-	-	-	-	-	-	1-ML-11-2	0.467	23.67	11.0
-	-	-	-	-	-	-	1-ML-11-3	0.467	31.67	14.8
-	0	0.199	0.204	1.25	3.75	2.02	1-ML-12-1	0.467	23.67	11.0
-	-	-	-	-	-	-	1-ML-12-2	0.467	31.67	14.8
-	-	-	-	-	-	-	1-ML-12-3	0.467	31.67	24.6
-	0	0.404	0.413	1.25	3.75	2.02	1-ML-13-1	0.612	16.00	26.9
-	-	-	-	-	-	-	1-ML-13-2	0.467	57.73	24.6
-	-	-	-	-	-	-	1-ML-13-3	0.467	31.67	40.5
-	0	0.505	0.506	1.25	3.75	2.02	1-ML-14-1	0.612	42.07	24.6
-	-	-	-	-	-	-	1-ML-14-2	0.467	52.73	24.6
-	-	-	-	-	-	-	1-ML-14-3	0.467	31.67	40.5
-	0	0.0992	0	1.25	3.75	2.00	MH-84-0.10	0.612	42.07	40.5
-	-	-	-	-	-	-	MH-84-0.10	0.0657	120.12	7.9
-	-	-	-	-	-	-	MH-84-0.10	0.0646	120.10	7.8
-	0	0.0500	0	1.25	3.75	2.00	MH-84-0.10	0.0670	120.13	8.0
-	-	-	-	-	-	-	MH-84-0.05	0.0657	120.12	7.9
-	-	-	-	-	-	-	MH-84-0.05	0.0646	120.10	7.8
-	-	-	-	-	-	-	MH-84-0.05	0.0670	120.13	8.0

**Table A.3. Conversion of Formate to Carbonate as a Function of  $\gamma$ -Dose/Time**

[Formate] <sub>0</sub>	% <sup>13</sup> C	Time h	Dose Mrad	<sup>13</sup> CO <sub>3</sub> <sup>2-</sup> mM	G(CO <sub>3</sub> <sup>2-</sup> )
0.049	100	120.0	9.60	6.5	0.48
0.049	100	191.7	15.34	12.3	0.57
0.049	100	215.8	17.26	13.7	0.56
0.050	100	120.0	7.89	6.4	0.57
0.050	100	120.0	7.76	6.8	0.62
0.050	100	120.0	8.49	6.9	0.57
0.099	100	120.0	9.60	11.0	0.79
0.099	100	263.9	21.10	24.2	0.81
0.10	100	120.0	7.89	9.3	0.83
0.10	100	120.0	7.76	1.1	1.0
0.10	100	120.0	8.49	1.2	1.0
0.35	28.6	143.9	10.96	5.0	1.1
0.35	28.6	288.9	20.89	9.8	1.2
0.35	28.6	143.9	10.02	6.7	1.6
0.35	28.6	288.9	20.81	9.5	1.1
0.35	28.6	143.9	10.09	5.5	1.3
0.35	28.6	288.9	19.95	1.0	1.3
0.60	16.7	143.9	11.91	3.5	1.2
0.60	16.7	288.9	21.85	6.9	1.3
0.60	16.7	143.9	10.87	6.0	2.3
0.60	16.7	288.9	21.66	7.8	1.5
0.60	16.7	143.9	10.39	3.8	1.5
0.60	16.7	288.9	20.26	7.8	1.6
1.1	9.09	288.9	21.85	4.9	1.7
1.1	9.09	288.9	21.66	5.5	2.0
1.1	9.09	288.9	20.26	5.3	2.0

**Table A.4. Yields of Carbonate(a) from Radiolysis of Formate: Experiment versus Model**

initial [Formate]	time (h)	Dose (Mrad)	[CO <sub>3</sub> <sup>2-</sup> ]		G(CO <sub>3</sub> <sup>2-</sup> ) molecules/100 eV		% conversion	sample identity
			expt	model	expt	model		
0.03 <sup>(b)</sup>	24	2.4	0.0047	0.0064	1.73	2.38	16%	(c)
	48	4.8	0.0111	0.0120	2.07	2.23	37%	(c)
	68	6.8	0.0160	0.0161	2.10	2.12	53%	(c)
0.049 <sup>(d)</sup>	120	6.6	0.0065	0.0066	0.70	0.71	13%	Table A2
	191.7	15.3	0.0123	0.0131	0.57	0.61	25%	Table A2
	215.8	17.3	0.0137	0.0145	0.57	0.60	27%	Table A2
0.1	8.7	4.06	0.0046	0.0046	0.81	0.80	5%	1-ML10-1
	23.7	11.06	0.0112	0.0121	0.72	0.78	11%	1-ML10-2
	31.7	14.79	0.0120	0.0159	0.58	0.77	12%	1-ML10-3
0.2	8.7	4.06	0.0180	0.0072	3.17	1.27	9%	1-ML11-1
	23.7	11.06	0.0200	0.0192	1.29	1.24	10%	1-ML11-2
	31.7	14.79	0.0263	0.0254	1.27	1.23	13%	1-ML11-3
0.4	23.7	11.06	0.0406	0.0259	2.62	1.67	10%	1-ML12-1
	31.7	14.8	0.0354	0.0344	1.71	1.66	9%	1-ML12-2
	31.7,16 <sup>(e)</sup>	24.6	ND					1-ML12-3
0.8	57.7	26.9	0.0719	0.0690	1.91	1.83	9%	1-ML13-1
	31.7,16 <sup>(e)</sup>	24.6	0.0694	0.0675	2.02	1.96	9%	1-ML13-2
	31.7,42 <sup>(e)</sup>	40.56	0.1108	0.1072	1.95	1.89	14%	1-ML13-3
1	57.7	26.9	0.0750	0.0632	1.99	1.68	8%	1-ML14-1
	31.7,16 <sup>(e)</sup>	24.6	0.0638	0.0632	1.85	1.84	6%	1-ML14-2
	31.7,42 <sup>(e)</sup>	40.56	0.1040	0.1033	1.83	1.82	10%	1-ML14-3

(a) In 3.75 M NaNO<sub>3</sub>, 1.25 M NaNO<sub>2</sub>, and 2 M NaOH (ρ = 1.35 g/mL) unless noted.

(b) In 0.1 M NaNO<sub>3</sub>, 0.03 M NaNO<sub>2</sub>, and 1 M NaOH (ρ = 1.08 g/mL).

(c) Lilga et al. 1996.

(d) Dose rate: 0.01 Mrad/h.

(e) Initial dose rate: 0.466 Mrad/h; final dose rate: 0.612 Mrad/h.

Table A.5. Yields of  $^{13}\text{C}$ -labeled Carbonate, Oxalate, and Formate from Radiolysis of  $2\text{-}^{13}\text{C}$ -Glycine: Experiment versus Model

time (h)	Dose (Mrad)	$[2\text{-}^{13}\text{C}\text{-Glycine}]$		$[\text{H}^{13}\text{CO}_2]$		$[^{13}\text{CO}_3^{2-}]$		$[^{13}\text{C}\text{-Oxalate}]$		Glycine conversion		Sample #
		expt	model	expt	model	expt	model	expt	model	%		
9.1 <sup>(e)</sup>	4.7	0.0731	0.0724	0.0066	0.0069	0.0000	0.0002	0.0021	0.0024	11%		2-ML-9-1
15 <sup>(e)</sup>	7.8	0.0663	0.0666	0.0108	0.0109	0.0006	0.0005	0.0042	0.0038	19%		2-ML-9-2
24 <sup>(e)</sup>	14.5	0.0572	0.0584	0.0180	0.0162	0.0016	0.0013	0.0051	0.0058	30%		2-ML-9-3
30 <sup>(e)</sup>	16.8	0.0538	0.0534	0.0190	0.0193	0.0021	0.0020	0.0066	0.0071	34%		2-ML-9-4
8.7 <sup>(e)</sup>	5.4	0.0760	0.0745	0.0042	0.0051	0.0000	0.0001	0.0009	0.0017	8%		1-ML19-1a
15 <sup>(e)</sup>	9.3	0.0696	0.0697	0.0087	0.0086	0.0000	0.0002	0.0031	0.0029	14%		1-ML19-2
29.8 <sup>(e)</sup>	18.4	0.0590	0.0592	0.0155	0.0158	0.0011	0.0009	0.0055	0.0055	27%		1-ML19-1b

(a) In 1.25 M  $\text{NaNO}_2$ , 3.75 M  $\text{NaNO}_3$ , 2 M  $\text{NaOH}$  ( $d=1.35$  g/mL); (b) in 2 M  $\text{NaNO}_2$ , 2 M  $\text{NaNO}_3$ , 2 M  $\text{NaOH}$ , and 0.052 M  $^{12}\text{C}$ -Formate.

**Table A.6. Chemical Shifts of Organic Species Studied**

Compound	<sup>1</sup> H Chemical Shift (ppm) <sup>(a)</sup>	Multiplicity	Assignment
EDTA	2.462	(singlet)	N-CH <sub>2</sub> -CH <sub>2</sub> -N
	3.049	(singlet)	-O <sub>2</sub> C-CH <sub>2</sub> -N
HEDTA	2.513	(singlet)	N-CH <sub>2</sub> -CH <sub>2</sub> -N
	2.567	(triplet)	HO-CH <sub>2</sub> -CH <sub>2</sub> -N
	3.067	(singlet)	N-(CH <sub>2</sub> -CO <sub>2</sub> <sup>-</sup> ) <sub>2</sub>
	3.086	(singlet)	N-CH <sub>2</sub> -CO <sub>2</sub> <sup>-</sup>
	3.616	(triplet)	HO-CH <sub>2</sub> -CH <sub>2</sub> -N
ED3A	2.580	(singlet)	N-CH <sub>2</sub> -CH <sub>2</sub> -N
	3.142	(singlet)	N-(CH <sub>2</sub> -CO <sub>2</sub> <sup>-</sup> ) <sub>2</sub>
	3.182	(singlet)	N-CH <sub>2</sub> -CO <sub>2</sub> <sup>-</sup>
s-EDDA	2.644	(singlet)	N-CH <sub>2</sub> -CH <sub>2</sub> -N
	3.153	(singlet)	N-CH <sub>2</sub> -CO <sub>2</sub> <sup>-</sup>
u-EDDA	2.466	(triplet)	H <sub>2</sub> NCH <sub>2</sub> -CH <sub>2</sub> -N(CH <sub>2</sub> CO <sub>2</sub> <sup>-</sup> ) <sub>2</sub>
	2.652	(triplet)	H <sub>2</sub> NCH <sub>2</sub> -CH <sub>2</sub> -N(CH <sub>2</sub> CO <sub>2</sub> <sup>-</sup> ) <sub>2</sub>
	3.067	(singlet)	N-(CH <sub>2</sub> -CO <sub>2</sub> <sup>-</sup> ) <sub>2</sub>
NTA	3.097	(singlet)	
IDA	3.147	(singlet)	
Glycine	3.185	(singlet)	
Formate	8.438	(singlet)	
Glycolate	3.95	(singlet)	
Acetate	1.896	(singlet)	

(a) Peak positions and shape can change with temperature and concentration.

**Table A.7. Reactivity of EDTA Relative to <sup>13</sup>C-Formate Ion: MH-84 Series**

Sample Name	Concentrations (M)		<i>k</i> <sub>rel</sub>
	<sup>13</sup> C-Formate	EDTA	
MH-84-1	0.0992	0.0200	
MH-84-1-1	0.0912	0.0115	6.6
MH-84-1-2	0.0909	0.0126	5.3
MH-84-1-3	0.0888	0.0111	5.3

**Table A.8. NMR Data for EDTA Aging Experiments: 1-ML-15**

Species	Integral regions	Concentrations from <sup>1</sup> H NMR Spectra of EDTA Aging Experiments				
		1-ML-15	1-ML-15-1a	1-ML-15-2	1-ML-15-3	1-ML-15-1b
<sup>13</sup> C-Formate	8.8-8.7, 8.2-8.0	1.11E-01	9.57E-02	9.74E-02	9.63E-02	9.56E-02
<sup>12</sup> C-Formate	8.45-8.42	1.17E-03	1.03E-02	1.70E-02	2.72E-02	3.22E-02
Glycolate	3.98-3.90	0.00E+00	7.85E-05	1.66E-03	0.00E+00	8.12E-04
(a)	3.58-3.55	0.00E+00	0.00E+00	0.00E+00	1.91E-04	2.02E-05
(a)	3.51-3.49	0.00E+00	2.62E-05	4.26E-04	6.91E-04	5.29E-04
(a)	3.23-3.2	0.00E+00	4.94E-04	1.02E-03	8.80E-04	1.19E-03
(b)	3.18-3.14	0.00E+00	8.06E-03	1.19E-02	1.32E-02	1.84E-02
ED3A	3.14-3.11	0.00E+00	1.78E-03	2.25E-03	2.50E-03	2.03E-03
EDTA	3.08-3.02	4.65E-02	3.02E-02	2.59E-02	2.17E-02	1.97E-02
(a)	2.86-2.84	0.00E+00	3.92E-05	1.20E-03	1.81E-03	1.39E-03
(a)	2.84-2.82	0.00E+00	7.06E-05	3.10E-05	4.55E-04	1.18E-04
(a)	2.79-2.77	0.00E+00	3.92E-05	2.05E-04	0.00E+00	3.97E-04
s-EDDA	2.66-2.64	0.00E+00	7.26E-04	2.73E-03	3.23E-03	3.57E-03
(a)	2.64-2.62	0.00E+00	0.00E+00	0.00E+00	0.00E+00	4.57E-04
ED3A	2.62-2.58	0.00E+00	5.29E-03	7.96E-03	7.44E-03	8.29E-03
EDTA	2.48-2.43	4.35E-02	2.90E-02	2.54E-02	2.12E-02	1.92E-02
Acetate	1.88-1.86	0.00E+00	0.00E+00	0.00E+00	8.67E-05	5.01E-04

(a) Unassigned peaks; nm; not measured. (b) Glycine and/or s-EDDA

**Table A.9. NMR Data for EDTA Aging Experiments: 1-ML-15**

Species	Integral regions	Peak Areas in Proton NMR Spectra of EDTA Aging Experiments				
		1-ML-15	1-ML-15-1a	1-ML-15-2	1-ML-15-3	1-ML-15-1b
<sup>13</sup> C-Formate	8.8-8.7, 8.2-8.0	762.3	609.4	785.1	740.9	789.1
<sup>12</sup> C-Formate	8.45-8.42	8	65.7	137.3	209.5	266.1
DMM	1.27-1.18	227.1	210.9	266.9	254.7	273.3
Glycolate	3.98-3.90		1	26.8	nm	13.4
(a)	3.58-3.55		0	0	8.8	1
(a)	3.51-3.49		1	20.6	31.9	26.2
(a)	3.23-3.2		18.9	49.5	40.6	59.1
(b)	3.18-3.14		154	287.2	305.7	456.9
ED3A	3.14-3.11		204.2	326.2	345.8	301.1
EDTA	3.08-3.02	2552.4	1538.9	1671	1336.3	1303.9
(a)	2.86-2.84		1	38.7	55.6	45.78
(a)	2.84-2.82		1.8	1	14	3.9
(a)	2.79-2.77		1	6.6		13.1
s-EDDA	2.66-2.64		18.5	88.1	99.4	117.8
(a)	2.64-2.62		0	0	0	15.1
ED3A	2.62-2.58		134.7	256.7	229.1	273.9
EDTA	2.48-2.43	1194	739	819.4	651.1	634.79
Acetate	1.88-1.86	0	0	0	2	12.4
DMM	1.27-1.18	227.1	210.9	266.9	254.7	273.3

Table A.10. NMR Data for HEDTA Aging Experiments: 2-ML-1

Species	descriptor	Integral region	Peak Areas in <sup>1</sup> H NMR Spectra of HEDTA Aging Experiments				
			2-ML-1	2-ML-1-1	2-ML-1-2	2-ML-1-3	
<sup>12</sup> C Formate		8.45-8.42	38.3	112.4	148.7	307.8	405.9
<sup>13</sup> C Formate		8.8-8.7, 8.2-8.0	3276	1348.3	1205.1	1047.6	1254.4
Glycolate		3.98-3.90	0	49.91	35.46	42.6	56.9
HEDTA <sup>(a)</sup>	CH <sub>2</sub> -OH	3.68-3.54	2868	912.8	897.82	712.7	825.7
HEDTA <sup>(b)</sup>	CH <sub>2</sub> -CO <sub>2</sub>	3.18-2.95	9178	1987.6	1332.5	868.6	847.7
HEDTA <sup>(a)</sup>	CH <sub>2</sub> -CH <sub>2</sub> OH	2.65-2.54	3370	886.25	588.7	363.9	408.7
HEDTA	N-CH <sub>2</sub> CH <sub>2</sub> -N	2.54-2.42	5695	1405.9	946.1	532.6	544.6
Acetate		1.88-1.86	0	7.37	10.25	19.2	130.6
DMM		1.27-1.18	1186	431.8	429.4	337.3	483.8
Glycine	singlet	3.18-3.16	0	112.01	175.6	117	183.9
EDDA + IDA	singlet	3.16-3.14	0	476.06	621.4	689.4	1000.5
NTA	shoulder	3.10-3.09	0	103.71	94.2	192.7	78.6
(c)	multiplet	2.7-2.62	0	411.73	474.9	639.3	898
EDDA	singlet	2.62-2..59	0	355.34	392.9	342.5	439.1
(c)		2.59-2.57	0	107.2	132.7	109.5	137.6
(c)	multiplet	2.83-2.78	0	0	18.9	45.5	43.5
(c)	singlet	3.27-3.26	0	0	21.3	14.7	13.3
(c)	singlet	3.24-3.22	0	0	21.1	13.2	25.3
(c)	shoulder	3.1-3.09	0	0	145.8	66.7	78.6

(a) During radiolysis a second multiplet (possibly a triplet) grows in coincidental with the CH<sub>2</sub>-OH of HEDTA.

(b) Broad overlapping peaks may hide product resonances.

Table A.11. Concentrations of Species in HEDTA Aging Experiments: 2-ML-1

Species	Descriptor	Integration region	Concentrations (M) of Species in Samples				
			2-ML-1	2-ML-1-1	2-ML-1-2	2-ML-1-3	2-ML-1-4
<sup>13</sup> C Formate		8.45-8.42	1.07E-03	8.62E-03	1.15E-02	3.02E-02	2.78E-02
<sup>13</sup> C Formate		8.8-8.7, 8.18-8.0	9.14E-02	1.03E-01	9.29E-02	1.03E-01	8.58E-02
Glycolate		3.98-3.90	0.00E+00	1.91E-03	1.37E-03	2.09E-03	1.95E-03
HEDTA <sup>(a)</sup>	CH <sub>2</sub> -OH	3.68-3.54	4.00E-02	3.50E-02	3.46E-02	3.50E-02	2.83E-02
HEDTA <sup>(b)</sup>	CH <sub>2</sub> -CO <sub>2</sub>	3.18-2.95	4.27E-02	2.54E-02	1.71E-02	1.42E-02	9.67E-03
HEDTA <sup>(c)</sup>	CH <sub>2</sub> -CH <sub>2</sub> -OH	2.65-2.54	4.70E-02	3.40E-02	2.27E-02	1.79E-02	1.40E-02
HEDTA	N-CH <sub>2</sub> CH <sub>2</sub> -N	2.54-2.42	3.97E-02	2.69E-02	1.82E-02	1.31E-02	9.32E-03
Acetate		1.88-1.86	0.00E+00	1.88E-04	2.63E-04	6.28E-04	2.98E-03
DMM		1.27-1.18	1.84E-03	1.84E-03	1.84E-03	1.84E-03	1.84E-03
Glycine	singlet	3.18-3.16	0.00E+00	4.29E-03	6.77E-03	5.74E-03	6.29E-03
EDDA + IDA	singlet	3.16-3.14	0.00E+00	9.12E-03	1.20E-02	1.69E-02	1.71E-02
NTA	shoulder	3.10-3.09	0.00E+00	1.33E-03	1.21E-03	3.15E-03	8.96E-04
(c)	multiplet	2.7-2.62	0.00E+00	3.16E-02	3.66E-02	6.27E-02	6.14E-02
EDDA	singlet	2.62-2..59	0.00E+00	6.81E-03	7.57E-03	8.40E-03	7.51E-03
(c)		2.59-2.57	0.00E+00	8.22E-03	1.02E-02	1.07E-02	9.42E-03
(c)	multiplet	2.83-2.78	0.00E+00	0.00E+00	1.46E-03	4.47E-03	2.98E-03
(c)	singlet	3.27-3.26	0.00E+00	0.00E+00	1.64E-03	1.44E-03	9.10E-04
(c)	singlet	3.24-3.22	0.00E+00	0.00E+00	1.63E-03	1.30E-03	1.73E-03
(c)	shoulder	3.1-3.09	0.00E+00	0.00E+00	1.12E-02	6.55E-03	5.38E-03

(a) During radiolysis a second multiplet (triplet?) grows in coincidental with the CH<sub>2</sub>-OH of HEDTA. (b) Broad overlapping peaks may hide product resonances. (c) Unassigned peak.

**Table A.12.** Reactivity of HEDTA Relative to  $^{13}\text{C}$ -Formate Ion: MH Samples

Sample Name	Concentrations, (M)			$k_{rel}$
	$^{13}\text{C}$ -Formate	HEDTA	HEDTA (IPC)	
MH-79-2-C	0.0992	0.088	0.105	
MH-79-2-1	0.0930	0.063	0.072	5.53
MH-79-2-2	0.0919	0.057	0.074	6.13
MH-79-2-3	0.0930	0.061	0.076	5.40
MH-84-7-C	0.0992	0.0395		
MH-84-7-1	0.0920	0.0137		13.9
MH-84-7-2	0.0917	0.0100		14.0
MH-84-7-3	0.0899	0.0110		13.1

**Table A.13.**  $^1\text{H}$  NMR Data for s-EDDA Aging Experiments: 1-ML-17

Species	Descriptor	Peak Areas of Species in Samples				
		1-ML-17	1-ML-17-1a	1-ML-17-2	1-ML-17-3	1-ML-17-1b
$^{13}\text{C}$ -Formate		3960.85	2158.05	1908.06	1940.66	1858.04
$^{12}\text{C}$ -Formate		37.34	216.69	350.59	560.89	648.22
DMM		1285.64	716.37	678.23	714.48	710.09
EDDA	$\text{CH}_2\text{-CO}_2$	13427.63	6201.3	5391	4582.16	4263.02
EDDA	$\text{NCH}_2\text{CH}_2\text{N}$	13362.7	5598.72	4582.62	3599.45	3242.73
Glycolate		0	0	7.8	44.7	45.31

**Table A.14.**  $^{13}\text{C}$  NMR Data for s-EDDA Aging Experiments: 1-ML-17

Species	Descriptor	Peak Areas of Species in Samples				
		1-ML-17	1-ML-17-1a	1-ML-17-2	1-ML-17-3	1-ML-17-1b
$^{13}\text{C}$ -Formate		nm	7646.41	7599.28	7261	7228.63
$^{13}\text{C}$ -Carbonate		nm	211.74	357.74	525.44	573.39

**Table A.15.** Concentrations of Species Determined by  $^1\text{H}$  NMR in s-EDDA Aging Experiments: 1-ML-17 Series

Species	Descriptor	Concentrations (M) of Species in Samples				
		1-ML-17	1-ML-17-1a	1-ML-17-2	1-ML-17-3	1-ML-17-1b
$^{13}\text{C}$ -Formate		1.02E-01	9.97E-02	9.31E-02	8.99E-02	8.66E-02
$^{12}\text{C}$ -Formate		9.62E-04	1.00E-02	1.71E-02	2.60E-02	3.02E-02
EDDA	$\text{CH}_2\text{-CO}_2$	8.64E-02	7.16E-02	6.58E-02	5.31E-02	4.97E-02
EDDA	$\text{NCH}_2\text{CH}_2\text{N}$	8.60E-02	6.47E-02	5.59E-02	4.17E-02	3.78E-02
Glycolate		0.00E+00	0.00E+00	1.90E-04	1.04E-03	1.06E-03

**Table A.16. Concentrations of Species Determined by  $^{13}\text{C}$  NMR in s-EDDA Aging Experiments: 1-ML-17 Series**

Species	Concentrations (M) of Species in Samples				
	1-ML-17	1-ML-17-1a	1-ML-17-2	1-ML-17-3	1-ML-17-1b
$^{13}\text{C}$ -Formate	1.02E-01	9.91E-02	9.72E-02	9.49E-02	9.43E-02
$^{13}\text{C}$ -Carbonate	0.00E+00	2.74E-03	4.58E-03	6.87E-03	7.48E-03

**Table A.17. Reactivity of s-EDDA Relative to  $^{13}\text{C}$ -Formate Ion**

Sample Name	Concentrations		$k_{rel}$
	$^{13}\text{C}$ Formate	s-EDDA	
MH-84-6	0.0992	0.0206	
MH-84-6-1	0.0905	0.0068	12.0
MH-84-6-2	0.0924	0.0071	14.9
MH-84-6-3	0.0906	0.0075	11.1

**Table A.18. Reactivity of u-EDDA Relative to  $^{13}\text{C}$ -Formate Ion**

Sample Name	Concentrations		$k_{rel}$
	$^{13}\text{C}$ Formate	u-EDDA	
MH-87-11	0.0901	0.0120	
MH-87-11-1	0.0824	0.0053	12.9
MH-87-11-2	0.0851	0.0040	13.0
MH-87-11-3	0.0930	0.0045	13.4

**Table A.19. NMR Data for NTA Aging Experiments: 1-ML-16**

Species	$^1\text{H}$ -NMR Peak Areas of Species in Samples				
	1-ML-16	1-ML-16-1a	1-ML-16-2	1-ML-16-3	1-ML-16-1b
$^{13}\text{C}$ -Formate	2756.36	3581	3471	2763	2510
$^{12}\text{C}$ -Formate	0	283	443	586	725
DMM	852	1161	1176	1044	915
NTA	10337	11121	9930	7969	6081
IDA	0	1270.75	1854.4	2878.35	1822.2
Glycine	0	167.9	(a)	(a)	(a)
Glycolate	0	77.39	98.87	169.46	274.82

$^{13}\text{C}$ -NMR Areas					
$^{13}\text{C}$ -Formate	(b)	7468	7577	6999	7120
$^{13}\text{C}$ -Carbonate	(b)	226	287	575	690

(a) Glycine was an unintegratable shoulder on IDA peak. (b) Not measured.

**Table A.20. Concentrations of Species in NTA Aging Experiments: 1-ML-16**

Species	Concentrations (M) in Samples by <sup>1</sup> H-NMR				
	1-ML-16	1-ML-16-1a	1-ML-16-2	1-ML-16-3	1-ML-16-1b
<sup>13</sup> C-Formate	1.07E-01	1.02E-01	9.77E-02	8.76E-02	9.09E-02
<sup>12</sup> C-Formate	0.00E+00	8.07E-03	1.25E-02	1.86E-02	2.63E-02
NTA	6.69E-02	5.29E-02	4.66E-02	4.21E-02	3.67E-02
IDA	0.00E+00	9.06E-03	1.31E-02	2.28E-02	1.65E-02
Glycolate	0	1.10E-03	1.39E-03	2.69E-03	4.97E-03

Species	Concentrations (M) in Samples by <sup>13</sup> C-NMR				
	1-ML-16	1-ML-16-1a	1-ML-16-2	1-ML-16-3	1-ML-16-1b
<sup>13</sup> C-Formate	1.02E-01	9.88E-02	9.81E-02	9.41E-02	9.28E-02
<sup>13</sup> C-Carbonate	0.00E+00	2.99E-03	3.71E-03	7.73E-03	9.00E-03

**Table A.21. Reactivity of NTA Relative to <sup>13</sup>C-Formate Ion: MH Series**

Sample Name	Concentrations		
	<sup>13</sup> C Formate	NTA	<i>k</i> <sub>rel</sub>
MH-84-4	0.0992	0.0164	
MH-84-4-1	0.0911	0.0074	9.3
MH-84-4-2	0.0872	0.0044	10.2
MH-84-4-3	0.0901	0.0063	9.9

**Table A.22. NMR Data for IDA Aging Experiments: 1-ML-18**

Species	<sup>1</sup> H-NMR Peak Areas of Species in Samples				
	1-ML-18	1-ML-18-1a	1-ML-18-2	1-ML-18-3	1-ML-18-1b
<sup>13</sup> C-Formate	2231.38	794.71	538.03	770.07	747.21
<sup>12</sup> C-Formate	12.57	89.45	393.8	212.95	250.87
DMM	732.19	256.85	250.92	253.48	257.7
IDA	6631.15	1640.09	1410.75	1064.81	995.3
Glycine	0	367.29	352.17	469.13	366.23
Glycolate	0	53.11	56.57	88.66	100.55
"3.1 ppm peak"	0	0.96	24.14	26.14	32.66

	<sup>13</sup> C-NMR Areas				
	(a)				
<sup>13</sup> C-Formate	(a)	7742.6	7565.18	7593.93	7206.67
<sup>13</sup> C-Carbonate	(a)	241.2	445.76	597.09	621.62

**Table A.23. Concentrations of Species in IDA Aging Experiments: 1-ML-18**

Species	Concentrations (M) in Samples by <sup>1</sup> H-NMR				
	1-ML-18	1-ML-18-1a	1-ML-18-2	1-ML-18-3	1-ML-18-1b
<sup>13</sup> C-Formate	1.01E-01	1.02E-01	7.10E-02	1.01E-01	9.60E-02
<sup>12</sup> C-Formate	5.68E-04	1.15E-02	5.20E-02	2.78E-02	3.22E-02
IDA	7.50E-02	5.28E-02	4.65E-02	3.48E-02	3.20E-02
Glycine	0.00E+00	2.37E-02	2.32E-02	3.06E-02	2.35E-02
Glycolate	0.00E+00	3.42E-03	3.73E-03	5.79E-03	6.46E-03
3.1 ppm	0.00E+00	2.06E-05	5.31E-04	5.69E-04	6.99E-04

**Table A.24. Concentrations of Species in IDA Aging Experiments: 1-ML-18**

Species	Concentrations (M) in Samples by <sup>13</sup> C-NMR				
	1-ML-18	1-ML-18-1a	1-ML-18-2	1-ML-18-3	1-ML-18-1b
<sup>13</sup> C-Formate	1.02E-01	9.87E-02	9.61E-02	9.44E-02	9.37E-02
<sup>13</sup> C-Carbonate	0.00E+00	3.08E-03	5.66E-03	7.42E-03	8.08E-03

**Table A.25. Reactivity of IDA Relative to <sup>13</sup>C-Formate Ion**

Sample Name	Concentrations (M)		<i>k</i> <sub>rel</sub>
	<sup>13</sup> C-Formate	IDA	
MH-84-5	0.0992	0.0363	
MH-84-5-1	0.0929	0.0163	15.7
MH-84-5-2	0.0904	0.0155	12.3
MH-84-5-3	0.0905	0.0153	9.1

**Table A.26. NMR Data for Glycine Aging Experiments: 2-ML-11**

Species	Peak Areas in <sup>1</sup> H-NMR Spectra of Samples		
	2-ML-11-2	2-ML-11-3	2-ML-11-4
<sup>13</sup> C-Formate	383.98	454.68	487.92
<sup>12</sup> C-Formate	11.84	9.45	9.46
DMM	2496.71	2456.3	2365.62
Total Glycine	5229.13	2232.81	1871.96
2- <sup>12</sup> C-Glycine	86	40	64
2- <sup>13</sup> C-Glycine	5143.13	2192.81	1807.96

	<sup>13</sup> C-NMR Areas		
	2-ML-11-2	2-ML-11-3	2-ML-11-4
Oxalate	284.17	642.32	652.36
Formate	690.4	901.79	835.01
Carbonate	82.7	356.68	398.31
2- <sup>13</sup> C-Glycine	3036.13	1260.98	1097.76

**Table A.27. NMR Data for Glycine Aging Experiments: 2-ML-9**

Species	Peak Areas in <sup>1</sup> H-NMR Spectra of Samples			
	2-ML-9-1	2-ML-9-2	2-ML-9-3	2-ML-9-4
<sup>13</sup> C-Formate	92.88	148.27	237.62	325.11
<sup>12</sup> C-Formate	0.83	3.51	5.13	5.84
DMM	568.85	539.62	507.27	655.15
Total Glycine	2210.67	2046.23	1442.9	1860.91
2- <sup>12</sup> C-Glycine	17.63	13.74	18.85	9.33
2- <sup>13</sup> C-Glycine	2193.04	2032.49	1424.05	1851.58

	<sup>13</sup> C-NMR Areas			
	2-ML-9-1	2-ML-9-2	2-ML-9-3	2-ML-9-4
Oxalate	168.21	308.23	332.45	447.16
Formate	526.25	782.07	1173.28	1314.52
Carbonate	trace	45.21	103.19	143.46
2- <sup>13</sup> C-Glycine	5787.78	4819.43	3723.91	3638.87

**Table A.28. NMR Data for Glycine Aging Experiments: 2-ML-7**

Species	Peak Areas in $^1\text{H-NMR}$ Spectra of Samples	
	2-ML-7	2-ML-7-4
$^{13}\text{C-Formate}$	0	29.65
$^{12}\text{C-Formate}$	0	0.92
DMM	690.69	67.13
Total Glycine	2874.87	237.7
1- $^{13}\text{C-Glycine}$	2854.54	235.23
2- $^{13}\text{C-Glycine}$	20.33	2.47

$^{13}\text{C-NMR}$ Areas		
Oxalate	(a)	365.32
Formate	(a)	1075.05
Carbonate	(a)	86.03
1- $^{13}\text{C-Glycine}$	(a)	0
2- $^{13}\text{C-Glycine}$	(a)	4162.57

(a) Not measured

**Table A.29. NMR Data for Glycine Aging Experiments: 2-ML-5**

Species	Peak Areas in $^1\text{H-NMR}$ Spectra of Samples			
	2-ML-5	2-ML-5-1	2-ML-5-2	2-ML-5-3
$^{13}\text{C-Formate}$	0	35.8	6.86	18.81
$^{12}\text{C-Formate}$	8.42	37.11	6.86	18.73
DMM	69.96	671.95	71.35	91.32
Total Glycine	2398.09	280.93	348.71	0
1- $^{13}\text{C-Glycine}$	153.01	1139.6	138.04	169.51
2- $^{13}\text{C-Glycine}$	160.04	1258.49	142.89	179.2

$^{13}\text{C-NMR}$ Areas				
Oxalate	0	112.61	196.64	(a)
Formate	0	146.37	285.12	(a)
Carbonate	0	101.09	170.15	(a)
1- $^{13}\text{C-Glycine}$	2377.92	2125.33	1955.81	(a)
2- $^{13}\text{C-Glycine}$	2697.88	2891.85	2311.34	(a)

(a) Not measured

**Table A.30. Reactivity of Glycine Relative to  $^{13}\text{C-Formate}$  Ion: MH-84-3 Series**

Sample Name	Concentrations		$k_{rel}$
	$^{13}\text{C}$ Formate	Glycine	
MH-84-3	0.0992	0.0496	
MH-84-3-1	0.0083	0.0253	7.8
MH-84-3-2	0.0084	0.0249	9.0
MH-84-3-3	0.0083	0.0243	8.1

**Table A.31. Reactivity of Glycine Relative to <sup>13</sup>C-Formate: MH-79-1 Series**

Sample Name	Concentrations		<i>k</i> <sub>rel</sub>
	<sup>13</sup> C Formate	Glycolate	
MH-79-1	0.1000	0.1200	
MH-79-1-1	0.0935	0.0843	4.7
MH-79-1-2	0.0900	0.0812	2.9
MH-79-1-3	0.0920	0.0747	6.2
MH-84-2	0.1007	0.0401	
MH-84-2-1	0.0723	0.0138	3.2
MH-84-2-2	0.0849	0.0148	5.8
MH-84-2-3	0.0910	0.0212	6.3

**Table A.32. NMR Data for Species in Citrate Ion Aging Experiments: ML Series<sup>(a)</sup>**

Species	<sup>1</sup> H-NMR Peak Areas of Species in Samples			
	1-ML-21	1-ML-21-2	1-ML-21-3	1-ML-21-1b
<sup>13</sup> C-Formate	432.22	791.77	341.78	348.7
<sup>12</sup> C-Formate	3.2	19.21	10.1	14.84
DMM	258.82	532.02	228.45	272.24
Citrate (a)	254.2	404.28	241.77	240.13
Citrate (b)	531.27	1080.03	496.52	516.34
Citrate (c)	445.41	755.44	371.04	422.45
Citrate (d)	226.63	554.48	216.39	231.5
	<sup>13</sup> C-NMR Areas			
<sup>13</sup> C-Formate	(a)	3990.85	3744.6	3203.36
<sup>13</sup> C-Carbonate	(a)	167.52	387.79	350.94

(a) Citrate proton NMR is a second order spectrum with four peaks labelled a, b, c, and d. The "b" peak was used for the calculations due to the strongest signal. The concentrations are based on the "b" peak being 37.3% of the total signal from citrate.

**Table A.33. Concentrations of Species in Citrate Ion Aging Experiments: ML Series**

Species	Concentrations (M) From <sup>1</sup> H-NMR			
	1-ML-21	1-ML-21-2	1-ML-21-3	1-ML-21-1b
<sup>13</sup> C-Formate	5.53E-02	4.93E-02	4.95E-02	4.24E-02
<sup>12</sup> C-Formate	4.09E-04	1.20E-03	1.46E-03	1.80E-03
Citrate (b)	4.55E-02	4.50E-02	4.82E-02	4.21E-02
Species	Concentrations (M) From <sup>13</sup> C-NMR			
<sup>13</sup> C-Formate	5.26E-02	4.86E-02	4.69E-02	4.64E-02
<sup>13</sup> C-Carbonate	0.00E+00	4.01E-03	5.74E-03	6.24E-03

**Table A.34. Reactivity of Citrate Ion Relative to <sup>13</sup>C-Formate Ion: MH Series**

Sample Name	Concentrations		<i>k</i> <sub>rel</sub>
	<sup>13</sup> C Formate	Citrate	
MH-79-3	0.0670	0.0047	
MH-79-3-1	0.0567	0.0044	0.44
MH-79-3-2	0.0542	0.0041	0.69
MH-79-3-3	0.0537	0.0046	0.11
MH-84-8	0.0670	0.0052	
MH-84-8-1	0.0307	0.0027	0.82
MH-84-8-2	0.0388	0.0037	0.64
MH-84-8-3	0.0347	0.0033	0.70

**Table A.35. NMR Data for Acetate Ion Aging Experiments: 2-ML-6**

Species	Peak Areas in <sup>1</sup> H-NMR Spectra of Samples	
	2-ML-6-3	2-ML-6-4
<sup>13</sup> C-Formate	19.12	1.65
<sup>12</sup> C-Formate	24.99	2.34
DMM	667.02	62.27
Total Acetate	4773.78	549.01
1- <sup>13</sup> C-Acetate	2479.73	261
2- <sup>13</sup> C-Acetate	290.35	288.01

	<sup>13</sup> C-NMR Areas	
	2-ML-6-3	2-ML-6-4
Oxalate	0	0
Formate	77.95	68.26
Carbonate	75.68	84.22
1- <sup>13</sup> C-Acetate	2652.89	2694.63
2- <sup>13</sup> C-Acetate	3628.32	3661.01

**Table A.36. NMR Data and Concentrations for Acetate Aging Experiments: 1-ML-22**

Species	Peak Areas in <sup>1</sup> H-NMR Spectra of Samples				
	1-ML-22	1-ML-22-1a	1-ML-22-2	1-ML-22-3	1-ML-22-1b
<sup>13</sup> C-Formate	447.48	788.56	801.75	683.99	371.25
<sup>12</sup> C-Formate	3.1	8.81	21.8	17.27	10.95
DMM	257.83	498.69	510.09	490.84	256.56
Acetate	1211.41	2109.56	2247.08	2093.22	1188.21

<sup>13</sup> C-NMR Areas					
<sup>13</sup> C-Formate	(a)	3990.85	3744.6	3203.36	3534.62
<sup>13</sup> C-Carbonate	(a)	167.52	387.79	350.94	602.63

Concentrations (M) From <sup>1</sup> H-NMR					
<sup>13</sup> C-Formate	5.75E-02	5.23E-02	5.20E-02	4.61E-02	4.79E-02
<sup>12</sup> C-Formate	3.98E-04	5.85E-04	1.41E-03	1.16E-03	1.41E-03
Acetate	5.18E-02	4.67E-02	4.86E-02	4.71E-02	5.11E-02

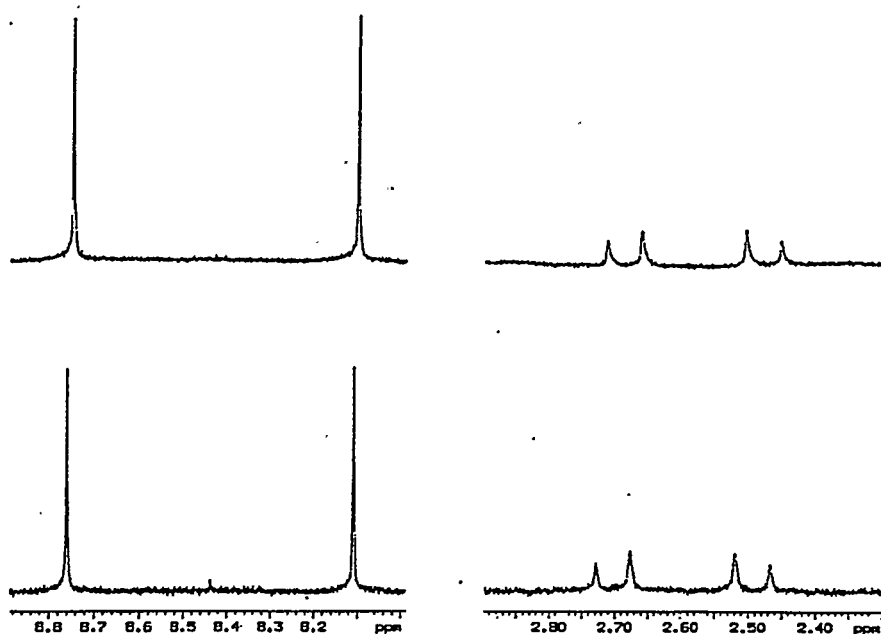
Concentrations (M) From <sup>13</sup> C-NMR					
<sup>13</sup> C-Formate	5.06E-02	4.86E-02	4.59E-02	4.56E-02	4.32E-02
<sup>13</sup> C-Carbonate	0.00E+00	2.04E-03	4.75E-03	5.00E-03	7.37E-03

**Table A.37. Reactivity of Acetate Ion Relative to <sup>13</sup>C-Formate Ion: MH Series**

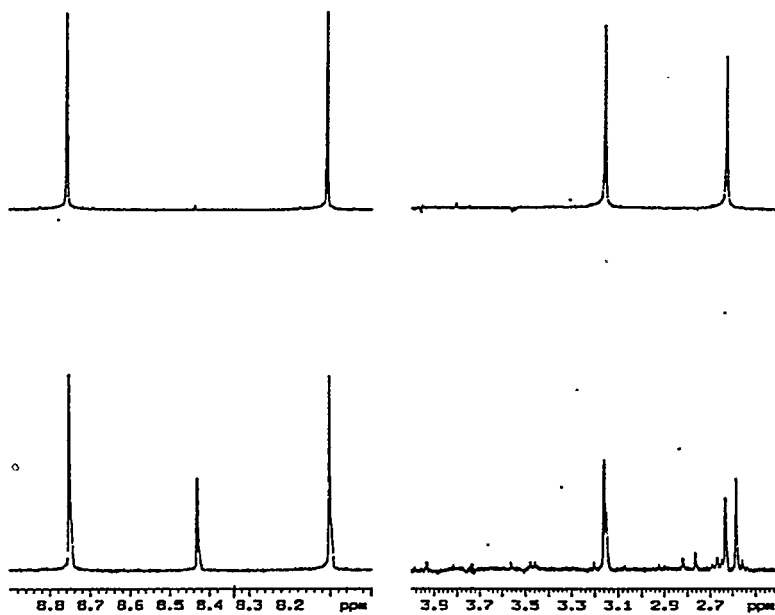
Sample Name	Concentrations		<i>k</i> <sub>rel</sub>
	<sup>13</sup> C Formate	Acetate	
MH-84-9	0.0995	0.0078	
MH-84-9-1	0.0846	0.0079	
MH-84-9-2	0.0495	0.0047	0.72
MH-84-9-3	0.0770	0.0073	0.28

MH-84-9-1b	0.0316	0.0032	0.77
MH-84-9-2b	0.0198	0.0024	0.73
MH-84-9-3b	0.0279	0.0033	0.66



**Figure A.1.** NMR Spectra of Citrate and Formate-<sup>13</sup>C Solution before(top) and after (bottom)  $\gamma$  Irradiation at 20°C



**Figure A.2.** NMR Spectra of s-EDDA and Formate-<sup>13</sup>C Solution before (top) and after (bottom)  $\gamma$  Irradiation at 20°C

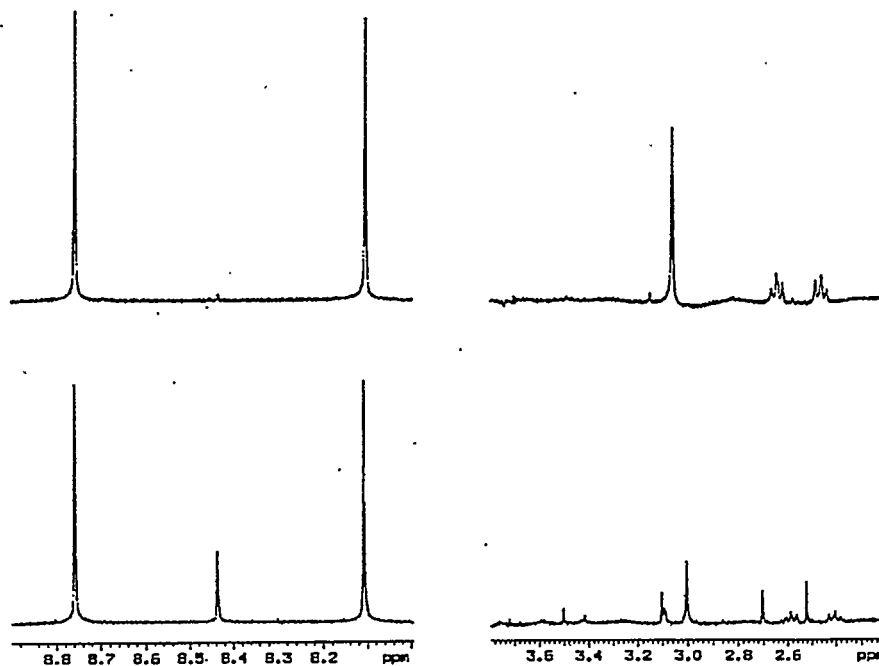


**Figure A.3.** NMR Spectra of u-EDDA and Formate-<sup>13</sup>C Solution before (top) and after (bottom)  $\gamma$  Irradiation at 20°C

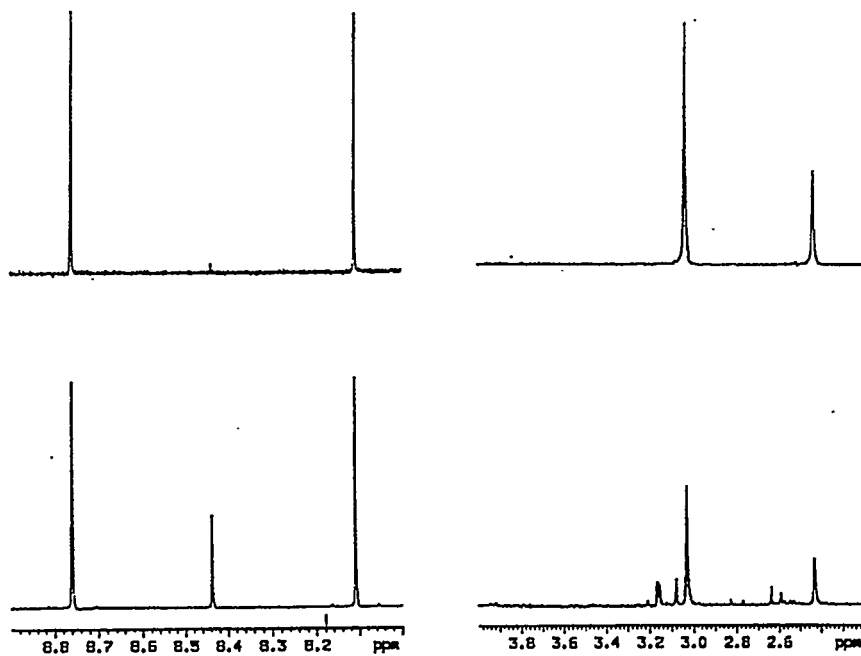


**Figure A.4.** NMR Spectra of EDTA and Formate-<sup>13</sup>C Solution before (top) and after (bottom)  $\gamma$  Irradiation at 20°C

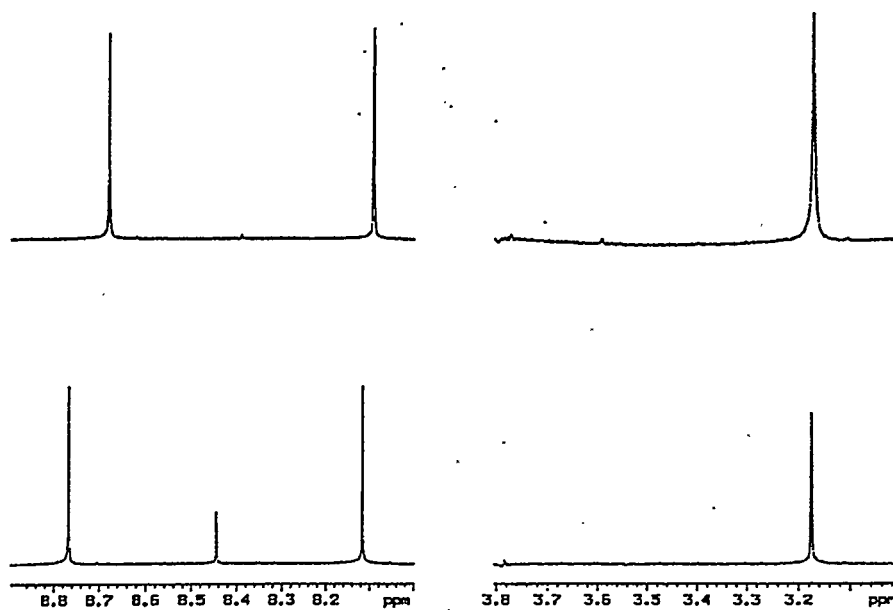


**Figure A.5.** NMR Spectra of Glycine and Formate-<sup>13</sup>C Solution before (top) and after (bottom)  $\gamma$  Irradiation at 20°C

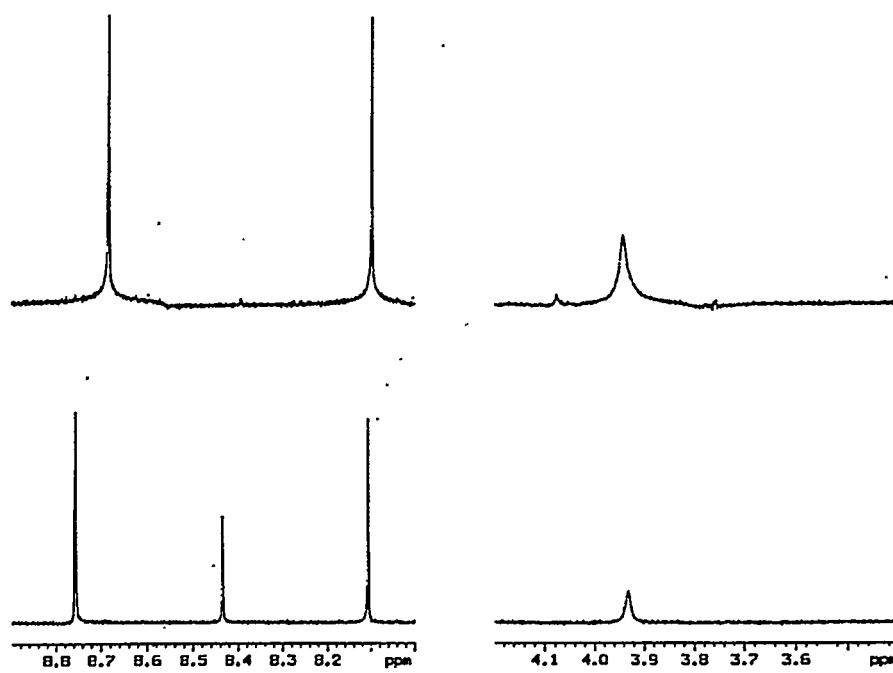


**Figure A.6.** NMR Spectra of Glycolate and Formate-<sup>13</sup>C Solution before (top) and after (bottom)  $\gamma$  Irradiation at 20°C

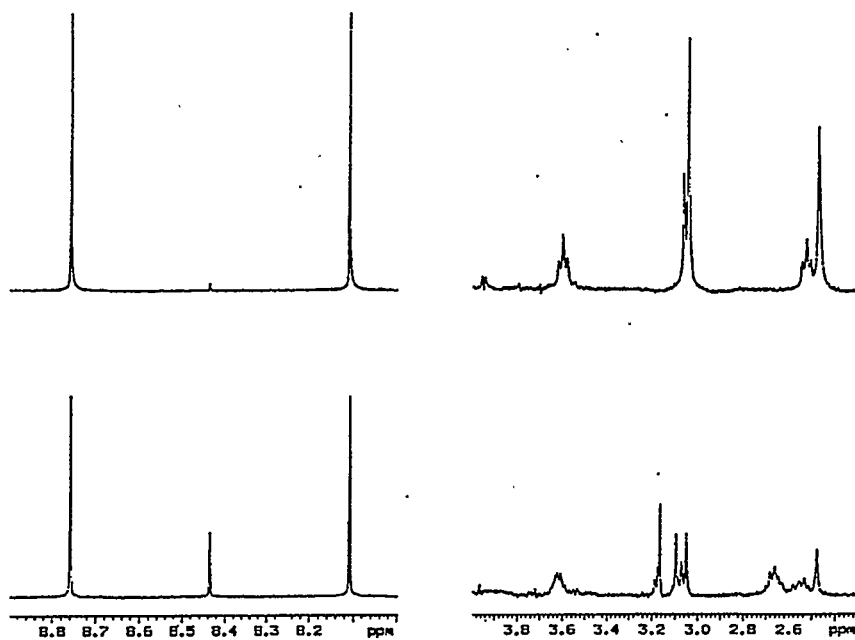


**Figure A.7.** Spectra of HEDTA and Formate-<sup>13</sup>C Solution before (top) and after (bottom)  $\gamma$  Irradiation at 20°C

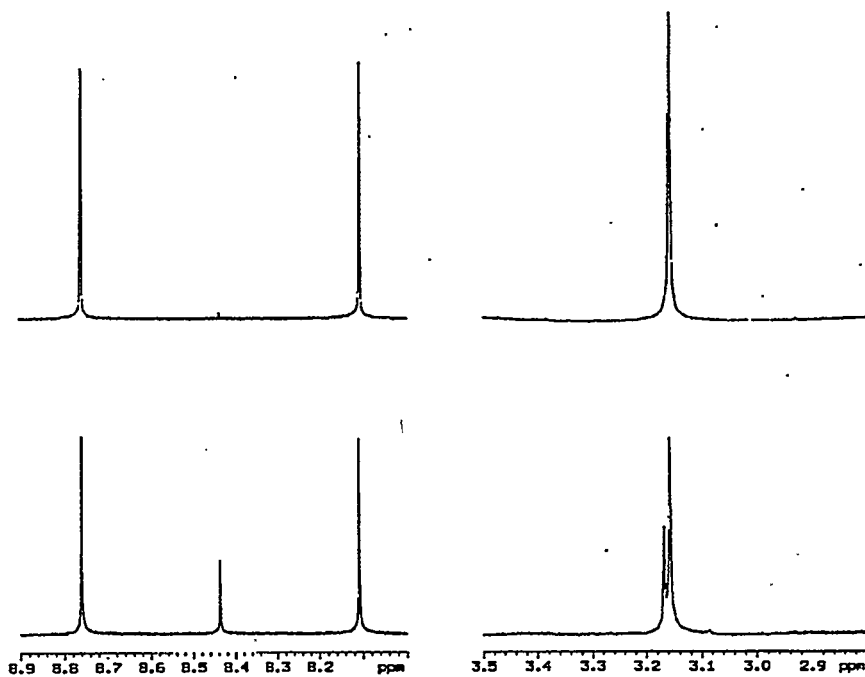


**Figure A.8.** NMR Spectra of IDA and Formate-<sup>13</sup>C Solution before (top) and after (bottom)  $\gamma$  Irradiation at 20°C

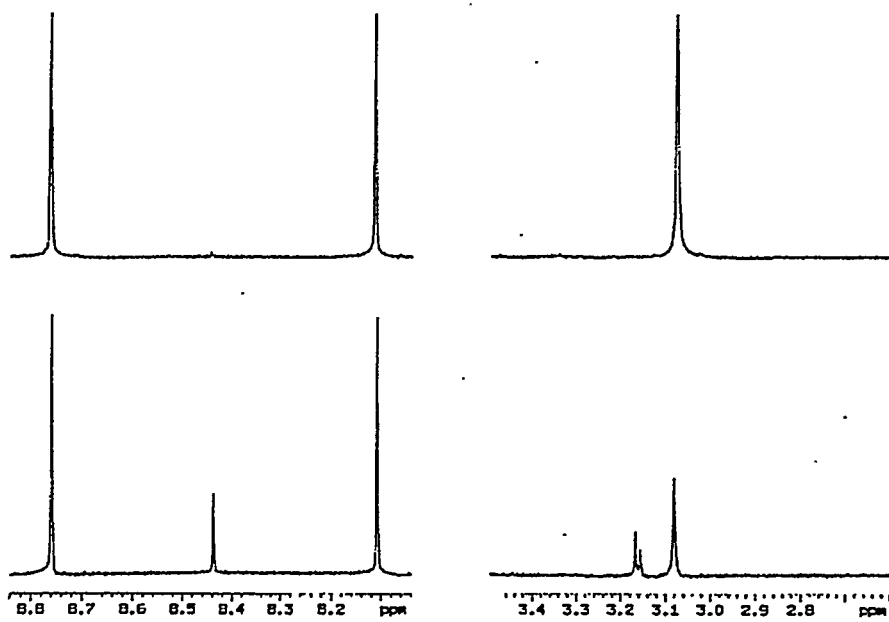


**Figure A.9.** NMR Spectra of NTA and Formate-<sup>13</sup>C Solution before (top) and after (bottom)  $\gamma$  Irradiation at 20°C

## **Appendix B**

### **Data for SIM-PAS-95-1 Aging Studies**

Table B.1. Effects of Radiation on PAS-95 Simulants at 40, 70, and 90°C(a)

Dose Mrad	Reactants/Products, M											Sample Number	
	Formate	Oxalate	Glycolate	Citrate	HEDTA	EDTA	Succinate	Acetate	CO <sub>3</sub> <sup>2-</sup>	NO <sub>2</sub> <sup>-</sup>	NO <sub>3</sub> <sup>-</sup>		NH <sub>3</sub>
90 °C													
0	0.000	0.000	0.195	0.098	0.057	0.0068	0.0000	0.0000	0.011	1.21	2.48	0.000	99-2:1
22	0.001	0.005	0.186	0.102	0.041	0.0058	0.0035	0.0000	0.076	1.19	2.17	0.000	98-1:1
50	0.055	0.055	0.143	0.100	0.028	0.0040	0.0130	0.0000	0.154	1.09	1.83	0.000	99-1:1
114	0.066	0.068	0.119	0.070	0.012	0.0018	0.0232	0.0031	0.367	1.42	1.89	0.067	99-4:1
146	0.111	0.075	0.122	0.071	0.003	0.0014	0.0237	0.0035	0.515	1.50	1.70	0.076	100-2:1
70 °C													
0	0.000	0.000	0.139	0.102	0.069	0.0136	0.0000	0.006	0.028	1.01	2.07		97-1
30	0.022	0.024	0.126	0.098	0.040	0.0090	0.0011	0.011	0.089	1.09	1.97		84-3:1
50	0.048	0.040	0.113	0.091	0.023	0.0055	0.0031	0.013	0.130	1.15	1.89		90-5:1
100	0.070	0.050	0.099	0.083	0.010	0.0038	0.0117	0.015	0.264	1.27	1.69		93-1:1
150	0.124	0.074	0.088	0.075	0.004	0.0010	0.0192	0.017	0.338	0.57	1.67		96-1:1
40 °C													
0	0.000	0.000	0.195	0.098	0.057	0.0068	0.0000	0.0000	0.017	1.38	2.52	0.000	104-2:1
28	0.008	0.001	0.183	0.095	0.037	0.0061	0.0068	0.0000	0.077	0.52	2.43	0.004	101-1:1
43	0.015	0.018	0.177	0.084	0.020	0.0039	0.0186	0.0000	0.118	1.18	2.58	0.008	107-2:2
65	0.077	0.016	0.145	0.084	0.014	0.0039	0.0384	0.0000	0.175	1.18	2.29	0.008	111-1:1

(a) Starting composition of cover gas is 80/20 Ar/O<sub>2</sub>

**Table B.2. Effects of O<sub>2</sub> in Cover Gas and Iron on Radiolytic Aging of PAS-95-1d Simulant at 70°**

Dose Mrad	Reactants/Products, M											Sample Number
	Formate	Oxalate	Glycolate	Citrate	HEDTA	EDTA	Succinate	CO <sub>3</sub> <sup>2-</sup>	NO <sub>2</sub> <sup>-</sup>	NO <sub>3</sub> <sup>-</sup>	NH <sub>3</sub>	
0	0.000	0.000	0.195	0.098	0.057	0.0068	0.0000	0.011	1.26	2.93	0.000	110-2:1
47 <sup>(a)</sup>	0.027	0.030	0.174	0.100	0.018	0.0044	0.0317	0.137	1.16	2.25	0.020	107-3:1
48 <sup>(a)</sup>	0.016	0.033	0.176	0.077	0.019	0.0036	0.0112	0.089	0.53	1.81	0.007	104-3:1
47.6 <sup>(b)</sup>	0.016	0.023	0.179	0.090	0.020	0.0038	0.0291	0.111	1.07	2.09	0.005	105-1:1
45.6 <sup>(b)</sup>	0.034	0.021	0.185	0.090	0.023	0.0042	0.0287	0.096	1.00	1.80	0.001	108-1:1
46.2 <sup>(a),(c)</sup>	0.042	0.020	0.183	0.089	0.025	0.0034	0.0244	0.127	0.92	2.34	0.003	110-1:1

(a) 20/80 O<sub>2</sub>/Ar; (b) 100% Ar; (c) 20/80 O<sub>2</sub>/Ar, no Fe.

**Table B.3. Thermal Aging of PAS-95-1d Simulant at 90°C in Presence and Absence of O<sub>2</sub> in Cover Gas**

Cover Gas	Reactants/Products, M											Sample Number		
	Time, h	Formate	Oxalate	Glycolate	Citrate	HEDTA	EDTA	Succinate	Acetate	CO <sub>3</sub> <sup>2-</sup>	NO <sub>2</sub> <sup>-</sup>		NO <sub>3</sub> <sup>-</sup>	NH <sub>3</sub>
20/80 O <sub>2</sub> /Ar	0	0.000	0.000	0.195	0.098	0.057	0.0068	0.0000	0.0000	0.011	1.21	2.48	0.000	99-2:1
	335	0.000	0.026	0.160	0.099	0.060	0.0081	0.0000	0.0000	0.041	1.01	1.76	0.004	99-3:1
	675	0.000	0.010	0.159	0.092	0.053	0.0085	0.0081	0.0037	0.065	0.95	1.71	0.009	100-1:1
	1329	0.015	0.027	0.154	0.077	0.047	0.0089	0.0099	0.0075	0.117	1.17	2.03	0.028	100-3:1
	2880	0.052	0.032	0.147	0.077	0.039	0.0084	0.0250	0.0598	0.199	0.59	1.71	0.027	111-4:1
100% Ar	0	0.000	0.000	0.195	0.098	0.057	0.0068	0.0000	0.0000	0.011	1.21	2.48	0.000	99-2:1
	336	0.000	0.000	0.201	0.097	0.061	0.0090	0.0055	0.0045	0.023	0.44	2.36	0.006	101-2:1
	666	0.000	0.006	0.201	0.089	0.057	0.0088	0.0057	0.0042	0.032	0.32	2.60	0.009	104-1:1
	1338	0.000	0.019	0.170	0.086	0.052	0.0092	0.0328	0.0038	0.055	0.41	2.47	0.024	107-1:1

**Table B.4. Effects of Radiation on PAS-95 Simulants at 40, 70, and 90°C:(a) Concentrations of Analytes (mg C/g) and Nitrate Reaction Enthalpies**

Dose, Mrad	Reactants/Products, mg C/g											Tot. Org. C wt% <sup>(a)</sup>	$\Delta H_r$ , J/g soln <sup>(b)</sup>	Sample Number	
	Formate	Oxalate	Glycolate	Citrate	HEDTA	EDTA	Succinate	Acetate	CO <sub>3</sub> <sup>2-</sup>	CO <sub>2</sub>	CO				
PAS-95-1c, 90 °C															
0	0.00	0.00	3.68	5.58	5.43	0.64	0.00	0.00	0.12	1.53	447	99-2:1			
22	0.01	0.10	3.51	5.79	3.89	0.55	0.13	0.00	0.71	1.47	419	98-1:1			
50	0.52	1.04	2.71	5.67	2.61	0.37	0.49	0.00	1.46	1.40	367	99-1:1			
114	0.62	1.29	2.25	3.97	1.09	0.17	0.88	0.06	3.47	1.20	303	99-4:1			
146	1.04	1.41	2.30	4.00	0.24	0.13	0.90	0.07	4.87	1.06	246	100-2:1			
PAS-95-1c, 70 °C															
0	0.00	0.00	2.63	5.76	6.51	1.28	0.00	0.11	0.27	1.63	487	97-1			
30	0.20	0.46	2.38	5.58	3.75	0.85	0.04	0.20	0.84	1.57	449	84-3:1			
50	0.45	0.76	2.14	5.17	2.19	0.52	0.12	0.24	1.23	1.53	426	90-5:1			
100	0.66	0.94	1.87	4.69	0.92	0.36	0.44	0.28	2.50	1.41	376	93-1:1			
150	1.17	1.39	1.67	4.25	0.42	0.09	0.72	0.32	3.19	1.34	338	96-1:1			
PAS-95-1c, 40 °C															
0	0.00	0.00	3.68	5.58	5.42	0.64	0.00	0.00	0.17	1.53	446	104-2:1			
28	0.07	0.02	3.46	5.37	3.50	0.57	0.26	0.00	0.73	1.47	421	101-1:1			
43	0.14	0.34	3.34	4.74	1.88	0.37	0.70	0.00	1.12	1.44	398	107-2:2			
65	0.73	0.31	2.73	4.74	1.32	0.37	1.45	0.00	1.65	1.38	369	111-1:1			

(a) Starting composition of cover gas is 80/20 Ar/O<sub>2</sub>. (b) Calculated as the  $\sum OC_i + (TC_o - TC_d)$  where  $OC_i$  is concentration of organic species in mg C/g,  $TC_o$  is total concentration of organic and carbonate carbon at start of irradiation, and  $TC_d$  is the total concentration of organic and carbonate carbon after having absorbed dose d. (c) Calculated as  $\sum OC_i \times \Delta H_i$  where  $\Delta H_i$  is enthalpy (kJ) for reaction of a quantity of specie i that contains 1 g of carbon with excess nitrate, e.g., specie,  $\Delta H$  (kJ/gC): formate, -17.9; Oxalate, -11.2; glycolate, -25.5; citrate, -25.1; Na<sub>3</sub>HEDTA, -35.4; Na<sub>4</sub>EDTA, -32.1; succinate, -24.7; acetate, -30.7; unidentified products, -32.1, average of Na<sub>3</sub>ED3A, Na<sub>3</sub>NTA, Na<sub>2</sub>IDA, Na<sub>2</sub>EDDA, and glycine (see Table 4.4).

**Table B.5.** Effects of O<sub>2</sub> in Cover Gas and Iron on Radiolytic Aging of PAS-95-1d Simulant at 70°:  
Concentrations of Analytes (mgC/g) and Nitrate Reaction Enthalpies

Dose Mrad	Reactants/Products, mg C/g										Tot. Org. C wt% <sup>(a)</sup>	$\Delta H_r$ J/g soln <sup>(a)</sup>	Sample Number
	Formate	Oxalate	Glycolate	Citrate	HEDTA	EDTA	Succinate	CO <sub>3</sub> <sup>2-</sup>	Org. C wt% <sup>(a)</sup>	$\Delta H_r$ J/g soln <sup>(a)</sup>			
0	0.00	0.00	3.68	5.58	5.42	0.64	0.00	0.10	1.53	446	110-2:1		
47 <sup>(b)</sup>	0.26	0.57	3.29	5.66	1.69	0.42	1.20	1.30	1.40	371	107-3:1		
48 <sup>(b)</sup>	0.15	0.62	3.33	4.36	1.76	0.34	0.42	0.84	1.45	400	104-3:1		
47.6 <sup>(c)</sup>	0.15	0.43	3.38	5.12	1.89	0.36	1.10	1.05	1.43	388	105-1:1		
45.6 <sup>(c)</sup>	0.32	0.40	3.49	5.12	2.20	0.39	1.08	0.91	1.44	391	108-1:1		
46.2 <sup>(b)(d)</sup>	0.40	0.38	3.47	5.03	2.33	0.32	0.92	1.20	1.41	383	110-1:1		

(a) See notes in Table B.4. (b) 20/80 O<sub>2</sub>/Ar. (c) 100% Ar. (d) 20/80 O<sub>2</sub>/Ar, no Fe.

**Table B.6.** Thermal Aging of PAS-95-1d Simulant at 90°C in Presence and Absence of O<sub>2</sub> in Cover Gas: Concentrations of  
Analytes (mgC/g) and Nitrate Reaction Enthalpies

Time h.	Reactants/Products, mg C/g										Tot. Org. C wt% <sup>(a)</sup>	$\Delta H_r$ J/g soln <sup>(a)</sup>	Sample Number
	Formate	Oxalate	Glycolate	Citrate	HEDTA	EDTA	Succinate	Acetate	CO <sub>3</sub> <sup>2-</sup>	Org. C wt% <sup>(a)</sup>			
20/80 O <sub>2</sub> /Ar													
0	0.00	0.00	3.68	5.58	5.43	0.64	0.00	0.00	0.11	1.53	447	99-2:1	
335	0.00	0.49	3.03	5.62	5.66	0.76	0.00	0.00	0.38	1.51	430	99-3:1	
675	0.00	0.19	3.01	5.20	5.05	0.80	0.31	0.07	0.61	1.48	427	100-1:1	
1329	0.14	0.51	2.90	4.37	4.48	0.84	0.37	0.14	1.10	1.43	407	100-3:1	
2880	0.50	0.60	2.78	4.38	3.68	0.80	0.95	1.13	1.88	1.36	367	111-4:1	
100 % Ar													
0	0.00	0.00	3.68	5.58	5.42	0.64	0.00	0.00	0.104	1.53	446	99-2:1	
336	0.00	0.00	3.79	5.50	5.73	0.85	0.21	0.08	0.220	1.52	445	101-2:1	
666	0.00	0.12	3.81	5.06	5.37	0.84	0.21	0.08	0.302	1.51	444	104-1:1	
1338	0.00	0.35	3.22	4.85	4.96	0.87	1.24	0.07	0.519	1.49	435	107-1:1	

(a) See notes in Table B.4.

**Table B.7. Headspace Gas Composition (mol%) versus Radiolytic Dose, Temperature, and O<sub>2</sub> in Cover Gas (PAS-95-1d simulant)**

Starting Headspace Gas	20/80 O <sub>2</sub> /Ar						Ar	
	40°		70°		90°		70°	
Dose/Time, Mrad (h)	47.2 (143)	64.9 (251)	47 (167)	146 (428)	47.6 (169)	45.6 (170)	46.2 (175.5)	70°
Ar	74.8	75.3	73.5	65.4	90.40	90.55	77.2	
O <sub>2</sub>	15.6	13.1	13.6	2.17	0.07	0.078	11.9	
H <sub>2</sub>	1.48	2.38	2.74	12.6	3.14	2.9	4.6	
N <sub>2</sub> O	6.9	8.2	8.6	16.5	4.33	4.8	5.2	
N <sub>2</sub>	1.13	1.08	1.57	3.29	2.01	1.66	1.04	
CH <sub>4</sub>	0.004	0.003	0.009	0.035	0.06	0.047	0.005	
NO <sub>x</sub>	0.005	0.05	0.005	0.019	0.01	0.005	0.05	

Cover gas volume is 378 mL, of which 7.8 mL is tubing between the gas manifold and reactor. Starting gas pressure was 1 atm at 292K.

**Table B.8.** Radiolytic Yield (G) of Gas from Simulant PAS-95-1d in a  $10^5$  rad/h  $\gamma$  Field

Gas	Radiolytic Yield (G) vs. Temp and Starting Headspace Composition				
	40 °C, O <sub>2</sub> /Ar <sup>(a)</sup>	70 °C, O <sub>2</sub> /Ar <sup>(b)</sup>	70 °C, Ar <sup>(c)</sup>	90 °C, O <sub>2</sub> /Ar <sup>(d)</sup>	70 °C, O <sub>2</sub> /Ar <sup>(e)</sup>
O <sub>2</sub>	-0.086	-0.11	0.001	-0.11	-0.17
H <sub>2</sub>	0.033	0.058	0.058	0.097	0.095
N <sub>2</sub> O	0.13	0.18	0.088	0.13	0.11
N <sub>2</sub>	0.020	0.033	0.036	0.025	0.021

(a) Average of 47 Mrad and 65 Mrad doses (Table B.1). (b) 46 Mrad dose (Table B.2).

(c) Average of 46 Mrad and 48 Mrad doses (Table B.1). (d) 146 Mrad dose (Table B.1).

(e) Simulant without Fe; 46 Mrad dose (Table B.2).

**Table B.9.** Rates of Production of Gas from Simulant PAS-95-1d at 90°C without Irradiation<sup>(a)</sup>

Gas	Rate of Disappearance/Production		
	Starting with 20/80 O <sub>2</sub> /Ar	Starting with Ar	
	mmol/1000 h	mmol/1000 h	mmol/2000 h
O <sub>2</sub>	-0.14	0.0036	0.049
H <sub>2</sub>	0.22	0.21	0.71
N <sub>2</sub> O	0.22	0.30	0.88
N <sub>2</sub>	0.022	0.019	0.050
Total Products	0.46	0.52	1.69

(a) Derived from Table B.10.

**Table B.10.** Headspace Gas Composition vs Heating Time at 90°C: Effect of O<sub>2</sub><sup>(a)</sup>

Rxn time, h	Headspace Gas Composition mole %				
	0	1338	2184	0	1239
Ar	100	62.9	44.5	80	59.8
Oxygen	0	0.26	0.127	20	4.44
Hydrogen	0	14.5	23.8	0	17.0
N <sub>2</sub> O	0	21.0	28.5	0	17.1
Nitrogen	0	1.31	3	0	1.69
Methane	00	0.004	0.001	0	0.008

(a) Cover gas volume is 25 mL, of which 7.8 mL is tubing between the gas manifold and reactor. Starting gas pressure was 1 atm at 292K.

**Table B.11.** Approximate Compositions of Solutions Used to Prepare SIM-PAS-95-1 Simulants

Component	Mol. Wt (g/mol)	Mass (g)	Conc. (M)
<u>Solution 1</u>			
NaOH	40	142	3.55
Al(NO <sub>3</sub> ) <sub>3</sub> •9H <sub>2</sub> O	375.13	32	0.085
Na <sub>2</sub> SiO <sub>3</sub> •9H <sub>2</sub> O	284.2	0.9	0.003
NaNO <sub>3</sub>	84.99	187	2.20
NaF	41.99	4.4	0.10
Na <sub>2</sub> SO <sub>4</sub>	142.04	1.2	0.01
Na <sub>3</sub> PO <sub>4</sub> •12H <sub>2</sub> O	380.13	3.1	0.01
Na <sub>3</sub> HEDTA•2H <sub>2</sub> O	344.18	36.2	0.11
Na <sub>4</sub> EDTA•3H <sub>2</sub> O	380.2	8.79	0.02
Na <sub>3</sub> Citrate	294	35.8	0.12
Glycolic acid	76	23	0.30
H <sub>2</sub> O	18	735	40.8
<u>Solution 2</u>			
Fe(NO <sub>3</sub> ) <sub>3</sub> •9H <sub>2</sub> O	404	29.1	0.72
H <sub>2</sub> O	18	64.8	36.00
<u>Solution 3</u>			
NaNO <sub>2</sub>	69	87.3	6.33
Cr(NO <sub>3</sub> ) <sub>3</sub> •9H <sub>2</sub> O	400.15	0.5	0.01
Ni(NO <sub>3</sub> ) <sub>2</sub> •6H <sub>2</sub> O	290.81	0.8	0.01
Mn(NO <sub>3</sub> ) <sub>2</sub>	178.95	0.3	0.01
KNO <sub>3</sub>	101.1	0.4	0.02
Pd(NO <sub>3</sub> ) <sub>2</sub>	230.41	0.012	0.0003
RuCl <sub>4</sub> •5H <sub>2</sub> O	332.96	0.02	0.0003
Rh(NO <sub>3</sub> ) <sub>3</sub> •2H <sub>2</sub> O	324.93	0.019	0.0003
Ce(NO <sub>3</sub> ) <sub>3</sub> •6H <sub>2</sub> O	434.23	1.8	0.02
Bi(NO <sub>3</sub> ) <sub>3</sub> •5H <sub>2</sub> O	485.07	1.5	0.02
Pb(NO <sub>3</sub> ) <sub>2</sub>	331.23	2.6	0.04
H <sub>2</sub> O	18	162.5	45.1

**Table B.12. Procedure for Irradiating the Simulant and Collecting Gas Samples**

---

1. Close vent, open purge valves, and turn on headspace gas mixture for 10 minutes
  2. Close purge valves and turn off gas
  3. Open vent
  4. Hook up vessels; close vent
  5. Open gas (oxygen/argon) inlet (2.7 atm)
  6. Slowly open purge valves; let the vessel sit for 5 to 10 minutes; leak-check fittings on the lid with leak detector solution
  7. Take readings of temperature and pressure; close purge valves; open vent; let the vessel sit for 30 to 60 minutes
  8. Take pressure readings to verify that the vessel does not leak
  9. Slowly open each purge valve until bubbles are gone; close purge valves
  10. Turn gas on and vent manifold; close vent
  11. Slowly open purge valves; let the vessel sit for 5 to 10 minutes
  12. Close purge valves; close gas inlet
  13. Open vent
  14. Repeat steps 6 to 10
  15. Repeat 6; take readings, including pressure
  16. Repeat 7 and continue at step 17
  17. Open purge valves slowly and wait until the pressure reaches ~2.7 atm; let the vessel sit for 5 to 10 minutes
  18. Take readings; close purge valves
  19. Close gas supply; open vent. Shut off regulator
  20. Leave vessel at pressure overnight
  21. Check pressures
  22. If pressures are OK, then open vent; slowly open each purge valve until bubbles are gone
  23. Close purge valves
  24. Connect thermocouple and heat tape to temperature controller; place vessel in the irradiator, if irradiating
  25. Bring vessel up to temperature slowly; stabilize at temperature for 1 to 2 hours
  26. Take readings and start data logging
  27. Record time and pressure prior to discontinuing heating and removal of vessel from  $\gamma$  irradiator.
  28. Collect headspace gas sample after reactor has cooled to ambient temperature (~25°C)
  29. Close reactor valve and disconnect from the gas manifold
  30. Remove solution and solids from the reactor and clean the vessel
-

**Table B.13. Columns and Conditions Used for IPC Analyses of EDTA and HEDTA**

---

Guard column: Adsorbosphere® C-8 cartridge  
Analytical Column: Adsorbosphere® C-8 (25 cm x 4.6 mm, 5- $\mu$ m particle size)  
Flow: 1.5 mL/min  
Sample Volume: 5  $\mu$ L  
Detection: UV, 280 nm, as copper complex  
Mobile phase: 0.002 M dodecyltrimethylammonium bromide and 0.05 M potassium dihydrogen phosphate, pH 6.5

---

**Table B.14. AS-11 IC Analysis Conditions**

---

Guard column: Dionex AG11  
Analytical Column: Dionex AS11  
Anion Suppressor: ASRS-I, 4mm  
Flow: 2.0 mL/min  
Sample Volume: 25  $\mu$ L  
Column Temperature: Ambient  
Detection: Conductivity

---

**Table B.15. AS-11 Analysis Mobile Phase Gradient**

---

Time (minutes)	% Water	5 mM NaOH	100 mM NaOH
0.0	90	10	0
2.9	90	10	0
6.4	0	100	0
18.4	0	65	35

---

**Table B.16. AS-6 Analysis Conditions**

---

Guard column:	None
Analytical Column:	Dionex ICE-IonPac AS6 (9x250 mm)
Flow:	1.0 mL/min
Sample Volume:	25 $\mu$ L
Mobile phase:	0.4 mM heptafluorobutyric acid
Detection:	Conductivity
Suppressor:	AMMS-ICE
Suppression eluant:	5 mM tetrabutylammonium hydroxide
Suppression eluant flow	3 mL/min
Column Temperature	Ambient

---

## **Appendix C**

### **The Energy Content of Intermediate Organic Compounds**

# The Energy Content of Intermediate Organic Compounds

Leon M. Stock  
August 11, 1998

The chemical reaction sequences discussed in this report and in other reports indicate that a variety of intermediate compounds are produced during the conversion of the original complexants into remnants, oxalate, formate, and carbonate ion. Concerns have often been expressed about the energy contents of the intermediates formed during these reactions and especially about the possibility that one or another of the intermediates might be more energetic than the original complexants.

Some chemical transformations of the original complexants proceed directly to form the observed products. But, in other cases, the chemical transformations of the original complexants proceed indirectly through more highly functionalized intermediates containing additional hydroxyl, nitroso, C- or O-nitro groups. Intermediates containing carbonyl, amido, and cyano groups also participate in the chemical transformations that eventually lead to the observed remnants and oxidized products.

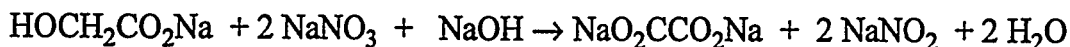
The well-known concept that the molecular behavior of a complex molecule can be described as the additive sum of the contributions of its functional groups has been used to estimate changes in the thermodynamic heats of the nitrate-ion oxidation of the intermediates and the original complexants. The results indicate the substitution of a hydrogen atom in a complexant by a hydroxyl, C-nitro, O-nitro, or nitroso group either has no effect or decreases the thermodynamic heat of nitrate ion-oxidation. The conversion of a carbon atom in a waste molecule into an aldehyde, keto, amido, or cyano group should lower the thermodynamic heat of the nitrate ion-oxidation reaction. Generally, the results of this assessment indicate that the heats of the nitrate-ion oxidation of these intermediate compounds should be the same or smaller than the heats of reaction of the original complexants. The fuel content of the waste is systematically decreased during the aging process as the less-energetic intermediates, remnant molecules, oxalate, formate, and carbonate ion form.

## C.1 Introduction

The chemical reaction sequences discussed in this report and in Stock and Pederson (1997) indicate that a variety of intermediate compounds are produced during conversion of the original complexants into remnant molecules such as ED3A, ED2A, NTA, and IDA, and acetate, oxalate, and formate ion. The thermodynamic heats of the nitrate ion-oxidation reactions of the original complexants and the elementary carboxylic acids have been established (Burger 1995). However, the heats of oxidation for many of the intermediate compounds have not been examined. Because information about the energy contents of the different organic waste constituents is needed for the confident discussion of the energetics and the evaluation of risks (Hunter et al. 1997), this aspect of the chemistry is examined in this appendix. The chemistry of aging is briefly outlined in Section C.2, and energy changes associated with aging are examined in Section C.3.

## C.2 The Chemistry of Intermediate Compounds

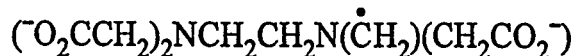
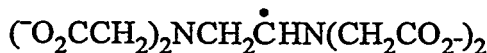
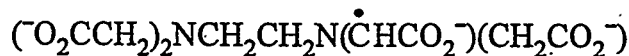
The investigations of pure compounds, mixtures of waste simulants, and the wastes have shown the chemistry is more subtle than implied by equations showing, for example, the oxidation of glycolate ion to oxalate ion and the reduction of nitrate ion to nitrite ion::



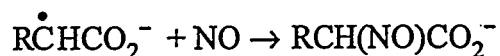
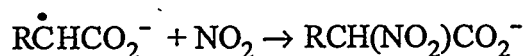
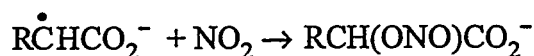
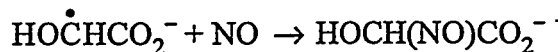
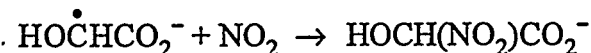
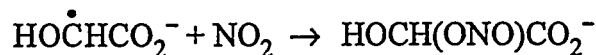
because the oxidation proceeds through several different intermediates and the inorganic oxidant becomes enmeshed in a reaction cascade leading to NO, NO-, N<sub>2</sub>O, N<sub>2</sub>, NH<sub>2</sub>OH, and NH<sub>3</sub>.

As already discussed in the main report, the chemistry begins with the radiolysis of the waste to provide H, OH, O<sup>-</sup>, electrons, NO<sub>3</sub><sup>2-</sup>, NO and NO<sub>2</sub>. The organic oxidation reactions proceed by several different pathways. In one, the oxidation begins with reactions in which one of the reactive radicals produced during radiolysis or thermolysis abstracts a hydrogen atom from the complexant, and that reaction is followed by recombination reactions to produce a substituted molecule. In another pathway, the complexant undergoes an electron transfer reaction in the initial step, and that reaction is followed by chemical transformations that lead to oxidized intermediates.

Elaboration of this chemistry begins with the recognition that the family of reactive radicals is rather restricted, with most of the chemical processes dictated by the reactions with nitric oxide and nitrogen dioxide. The family of organic radicals is much broader because of the array of different hydrogen atoms in the complexants and intermediates. The abstraction reactions of glycolate and citrate ions each produce one free radical. EDTA provides two free radicals. HEDTA provides four radicals closely related to the substances formed from EDTA, and another radical with a distinctive structure. The electron transfer reactions and decarboxylation of EDTA and HEDTA provide primary radicals:



The recombination reactions of these radicals with the inorganic radicals lead to substitution products as illustrated for the radical from glycolate and for one of the EDTA radicals [R = (O<sub>2</sub>CCH<sub>2</sub>)<sub>2</sub>NCH<sub>2</sub>CH<sub>2</sub>NCH<sub>2</sub>CO<sub>2</sub><sup>-</sup>].



Inspection of the structures of the products shown in these equations and consideration of the broad family of reactions of the other radicals shown above and the related radicals produced from the remnants reveal that the recombination reactions lead to the replacement of a hydrogen atom in the original complexant by a group with an electronegative oxygen or nitrogen. The reactions of the different radicals provide new substances with an additional C-nitro, O-nitro, or nitroso group.

The products from these initial reactions are transformed into other substances in the alkaline waste solutions discussed in Stock and Pederson (1997). Some processes are quite elementary. For example, the O-nitro group, a nitrite ester, is converted into a hydroxyl group by hydrolysis and the products from the original complexants with two electronegative functional groups bonded to one carbon atom are hydrolyzed to molecules with carbonyl groups yielding aldehydes, ketones, and amides. The chemistry of the molecules with C-nitroso and C-nitro groups is somewhat more complex. The compounds with C-nitroso groups rearrange to oximes or oximates, which are subsequently converted into carbonyl compounds or carboxylates, and the C-nitro compounds are either converted into carbonyl compounds or oxidized by additional reactions with the inorganic nitrogen oxides.

In summary, the oxidation reactions of the complexants that are initiated by free radicals lead to hydrogen atom removal or decarboxylation and to the introduction of an electronegative hydroxyl, C-nitroso, C- or O-nitro group into the molecule. These oxidized molecules are converted into carbonyl compounds, including aldehydes, amides, and carboxylates. These functionalized intermediate substances are not stable in the aqueous alkaline wastes and are converted into the more stable remnant molecules including ED3A, NTA and IDA and formate, and oxalate and carbonate ions.

### C.3 The Energy Content of the Intermediate Molecules

Burger (1995) calculated the thermodynamic heats of reaction for the oxidation of the organic complexants, selected remnants, and the simple carboxylate ions by sodium nitrite and sodium nitrate in alkaline solution. His approach could not be used for the evaluation of the heats of reaction of intermediates because the required thermodynamic data are not available for these somewhat unusual substances.

Fortunately, there is an alternative approach based upon the concept that molecular properties can be treated additively to provide approximate but reliable estimates of the expected changes in the energy contents of the intermediates. Linear free energy relationships and group increment approaches have been used for many years to evaluate the physical and chemical properties of substituted organic molecules (Lowry and Richardson 1987; March 1992). For example, the group increment heats of formation data tabulated by Benson (Benson 1975; Lowry and Richardson 1987) have been widely used to estimate the heats of formation of chemical compounds for which the thermodynamic information has not been obtained.

The well-known concept asserts that the molecular properties of molecules can be regarded as the additive sum of the contributions of their functional groups. This approach has been used here in an elementary form to estimate the change in the thermodynamic heats of reaction resulting from the replacement of a hydrogen atom in a complexant by the groups discussed in Section C.2 to determine whether the intermediate organic compounds have increased or decreased energy contents.

Specifically, it is postulated that the difference in the heat content of an intermediate and the compound from which it was formed can be estimated with sufficient accuracy by comparing the difference in the heat content resulting from the introduction of the same substituent group into a simple molecule for which accurate data are available. To illustrate, the difference in the heat of oxidation of glycolate ion and the nitroglycolate ion is equated to the difference in the heats of reaction of methane and nitromethane or ethane and nitroethane:

$$\{[\text{heat of oxidation of HOCH}_2\text{CO}_2^-] - [\text{heat of oxidation of HOCH}(\text{NO}_2)\text{CO}_2^-]\}$$

is approximately equal to

$$\{[\text{heat of oxidation of CH}_4] - [\text{heat of oxidation of CH}_3\text{NO}_2]\}$$

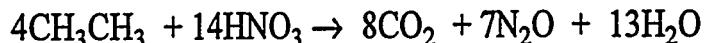
and to

$$\{[\text{heat of oxidation of CH}_3\text{CH}_3] - [\text{heat of oxidation of CH}_3\text{CH}_2\text{NO}_2]\}$$

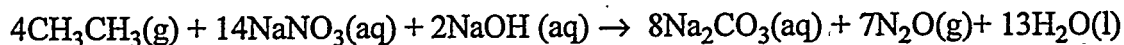
The approach is most suitable when the structural change is modest, as it is for substitution reactions where, as in this illustration, a nitro group is substituted for a hydrogen atom in each case.

In addition, it is necessary to select molecular fragments for which the heats of formation are known. Fortunately, there are many heat of formation data for methanes and ethanes with the

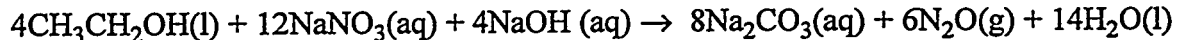
desired functional groups. Unfortunately, the heats of solution of these substances are not all known. This difficulty was circumvented by adopting the gas phase oxidation with nitric acid. The heats of formation of the requisite molecules are available, and the reaction leading to carbon dioxide and nitrous oxide was employed to represent the nitrate-ion oxidation.



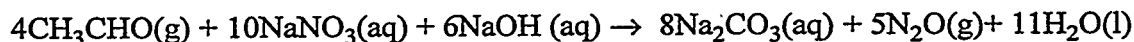
The accuracy of the approach was examined in several ways. First, it was noted that Camaioni et al. 1994; Camaioni and Samuels (1995) and their colleagues had shown that the heats of nitrate-ion oxidation of the organic complexants in alkaline solution evaluated by Burger were linearly related with the heats of oxidation of the same substances with oxygen in the gas phase. Next, the heats of oxidation of ethane by nitric acid for the reaction shown in the equation were compared with the heat of reaction for the same reaction with nitrate ion in alkaline solution.



The results indicate the heat of oxidation is -1216 kJ/mole for the liquid phase reaction compared with -1246 kJ/mole for the gas phase reaction. Similarly, the heats of the oxidation reactions of ethanol and acetaldehyde in alkaline aqueous systems with sodium nitrate and in the gas phase with nitric acid were compared:



Heat of oxidation is -1104 kJ/mole compared to -1113 kJ/mole for the gas phase reaction.



Heat of oxidation is -906 kJ/mole compared to -958 kJ/mole for the gas phase reaction.

These observations indicate there are no significant differences between the heats of reaction of ethane and ethanol in the gas and liquid phases and that the difference for acetaldehyde is small, about 50 kJ/mole, compared with the difference in the heat of oxidation of ethanol and acetaldehyde, 150 to 200 kJ/mole. Differences of this kind would not compromise the conclusions of the analysis presented in the remainder of this section.

The observations for the family of different derivatives of methane and ethane are assembled in Tables C.1 through C.3. The results in Table C.1 reaffirm the generally agreed-upon viewpoint that oxidation reduces the energy content of organic substances in a systematic manner. The heat content of the organic molecule is reduced by more than 100 kJ/mole by oxidation of the hydrocarbon to the alcohol and by oxidation of the alcohol to the aldehyde, and by even larger amounts by oxidation of the aldehyde to the acid and the acid to carbon dioxide.

**Table C.1.** Heats of Nitric Acid Oxidation of Methane and Ethane and Their Oxidized Derivatives in kJ/Mole at 300K in the Gas Phase

Compound	Heat	Compound	Heat
Methane	-693	Ethane	-1246
Methanol	-594	Ethanol	-1113
Methanal	-472	Ethanal	-858
Formic Acid	-230	Acetic Acid	-727
		Oxalic Acid	-269
Carbon Dioxide	0	Carbon Dioxide	0

**Table C.2.** Heats of Nitric Acid Oxidation of Methane and Ethane and the Nitrate Ester, Nitrite Ester, Nitroso and Nitro Compounds in kJ/Mole at 300K in the Gas Phase

Compound	Heat	Compound	Heat
Methane	-693	Ethane	-1246
Nitrosomethane	-700	Nitrosoethane	-1233
Nitromethane	-586		
Trinitromethane	-521		
Tetranitromethane	-460		
Methyl Nitrite	-595		
Methyl Nitrate	-570		

**Table C.3.** Heats of Nitric Acid Oxidation of Methane and Ethane and Related Oxides, Amides, Nitriles and Amines in kJ/Mole at 300K in the Gas Phase

Compound	Heat	Compound	Heat
Methane	-693	Ethane	-1246
		Dimethyl ether	-1165
Methyl hydroperoxide	-691	Dimethyl peroxide	-1253
Hydrogen cyanide	-527	Acetonitrile	-1032
Formamide	-447		
Methyl amine	-798	Dimethyl amine	-1354

The influences of the substitution of an electronegative hydroxyl, C-nitro, O-nitro or nitroso group for a hydrogen atom are explored in Table C.2. The heats of oxidation of the nitroso compounds are unchanged from the heats of oxidation of the parent hydrocarbons. In contrast, the heats of oxidation of the inorganic esters, i.e., the O-nitro compound and the related ester of nitric acid, are smaller than the heats of oxidation of the unsubstituted compound. The C-nitro compound also has a smaller heat of oxidation than the unsubstituted compound. These

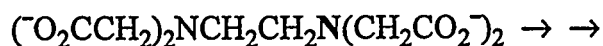
reductions in the heat content of the organic intermediates are anticipated because of the oxidative nature of the process in which a fuel-rich carbon-hydrogen unit is replaced by a relatively fuel-poor carbon-oxygen or carbon-nitrogen unit.

The ongoing interest in the role of C-nitro compounds in the waste prompted the comparison of the consequences of the systematic substitution of all of the carbon-hydrogen sites with nitro groups. The heats of oxidation for the compounds with one, three and four C-nitro groups in Table C.2 show the successive replacement of hydrogen systematically decreases the fuel value of these compounds. Nitromethane and its derivatives are not energetic molecules in the environment of the waste for two reasons. First, as already mentioned, the replacement of a hydrogen atom by an electronegative nitro group decreases the energy content of the molecule, and second, because it is inconsequential whether the oxidizing agent is provided intermolecularly or intramolecularly in the oxidant rich environment of the waste.

Results for several other substances are assembled in Table C.3. Hydroperoxides are anticipated intermediates in the reactions of oxygen generated during radiolysis with the organic waste molecules. The results in the table suggest that the heats of oxidation of the molecules formed by the replacement of hydrogen with a hydroperoxy group and the related ethers and peroxides, which are considered for completeness, should have energy contents comparable with the energy content of the compounds from which they are formed.

The heats of oxidation of amides and nitriles were examined since molecules with these structural components are anticipated intermediates. These substances, in which carbon is in the same oxidation state as the carbon in a carboxylic acid or carboxylate ion, have considerably smaller heats of oxidation than the molecules from which they would have been formed as expected on the basis of the results displayed in Table C.3.

The results in Table C.3 indicate the replacement of a hydrogen atom by an amino group to form an alkyl amine would lead to an increase in the energy content of the molecule as a consequence of the introduction of the additional, energetic nitrogen-hydrogen bonds. However, amines do not form by substitution reactions because chemistry of this kind is precluded by the oxidative nature of the reaction system. Rather, the organic molecules with primary amino groups such as glycinate ion and secondary amino groups such as IDA are produced after rather long reaction sequences. The changing energy contents are illustrated by the conversion of EDTA into an amide and the conversion of the amide into NTA and IDA.



The secondary amino group of IDA (bold type) is derived from the nitrogen (also shown in bold type) in EDTA and the amide formed from it. The heat of oxidation of the amide with an oxidized methylene group is considerably smaller than the heat of oxidation of EDTA. Hydrolysis of the intermediate amide provides NTA and IDA. The heat of oxidation per carbon of IDA, which has a secondary amino group and a nitrogen-hydrogen bond, is somewhat greater than the

heat of oxidation per carbon of NTA. However, the sum of the heats of oxidation of NTA and IDA is much less than the heat of oxidation of EDTA. As before, the oxidation reactions systematically decrease the energy content of the reaction system.

In summary, an additivity approach has been used to estimate the changes in the thermodynamic heats of the nitrate-ion oxidation of the intermediates and the original complexants. Some of the reactions involving the substitution of a hydrogen atom in a complexant by a hydroxyl, C-nitro, O-nitro, or nitroso group yield intermediates with the same energy content as the original complexant, but most reactions provide intermediates with lower thermodynamic heats of oxidation. The conversion of a carbon atom in a waste molecule into an aldehyde, keto, amido, or cyano group should similarly lower the thermodynamic heat of the nitrate ion-oxidation reaction. When molecules fragment, as discussed for the conversion of EDTA to NTA and IDA, the energy content of the system is both reduced and redistributed. Quite generally, the results indicate that the heats of the nitrate-ion oxidation of intermediate compounds should be the same or smaller than the heats of reaction of the original complexants. The fuel content of the waste is systematically decreased during the aging process as the less energetic intermediates, remnant molecules, oxalate, formate, and carbonate ion form.

#### C.4 References

Benson SW. 1976. *Thermochemical Kinetics*, Second Edition, John Wiley and Sons, New York.

Burger LL. 1995. *Calculation of Reaction Energies and Adiabatic Temperatures for Waste Tank Reactions*. PNL-8557 Rev 1, Pacific Northwest Laboratory, Richland, Washington.

Camaioni DM and WD Samuels. 1995. "Origin and Subsequent Aging of Organic Chemicals in Hanford Tank Farms." In Webb et al. 1995, *Preliminary Safety Criteria for Organic Watch List Tanks at the Hanford Site*, WHC-SD-WM-SARR-033 Rev. 0, Westinghouse Hanford Company, Richland, Washington.

Hunter VL, SD Colson, T Ferryman, RE Gephart, P Heasler, and RD Scheele. 1997. *Applications of the Risk-Based Strategy to the Hanford Tank Waste Organic-Nitrate Safety Issue*. PNNL-11798, Pacific Northwest National Laboratory, Richland, Washington.

Lowry TH and KS Richardson. 1987. *Mechanism and Theory in Organic Chemistry*, Third Edition. Harper and Row, New York.

March J. 1992. *Advanced Organic Chemistry: Reactions, Mechanisms, and Structure*, Fourth Edition. John Wiley and Sons, New York.

Samuels WD, DM Camaioni, LL Burger, and H Babad. 1994. "Effects of Aging on the Energy Content of Organic Compounds in the Hanford Tanks." *Symposia on Scientific Issues Related to Safety and Treatment of Hanford Waste Tanks*, 208th American Chemical Society Meeting, August 21-25, 1994. PNL-SA-24067, Pacific Northwest Laboratory, Richland, Washington.

Stock LM and LR Pederson. 1997. *Chemical Pathways for the Formation of Ammonia in Hanford Waste*. PNNL-11702, Pacific Northwest National Laboratory, Richland, Washington.